

DESIGN, CONSTRUCTION AND PERFORMANCE EVALUATION OF A
SUBMERSIBLE PUMP WITH NUMERICAL EXPERIMENTATION

A THESIS SUBMITTED TO
THE GRADUATE SCHOOL OF NATURAL AND APPLIED SCIENCES
OF
MIDDLE EAST TECHNICAL UNIVERSITY

BY

ERTAN ENGİN

IN PARTIAL FULFILLMENT OF THE REQUIREMENTS
FOR
THE DEGREE OF MASTER OF SCIENCE
IN
MECHANICAL ENGINEERING

SEPTEMBER 2005

Approval of the Graduate School of Natural and Applied Sciences

Prof. Dr. Canan ÖZGEN
Director

I certify that this thesis satisfies all the requirements as a thesis for the degree of Master of Science.

Prof. Dr. S. Kemal İDER
Head of Department

This is to certify that we have read this thesis and that in our opinion it is fully adequate, in scope and quality, as a thesis for the degree of Master of Science.

Prof. Dr. Kahraman ALBAYRAK
Supervisor

Examining Committee Members

Prof. Dr. O. Cahit ERALP	(METU, ME)	_____
Prof. Dr. Kahraman ALBAYRAK	(METU, ME)	_____
Assoc. Prof. Dr. Cemil YAMALI	(METU, ME)	_____
Dr. Tahsin A. ÇETİNKAYA	(METU, ME)	_____
M. Sc. Onur KONURALP	(Layne Bowler)	_____

I hereby declare that all information in this document has been obtained and presented in accordance with academic rules and ethical conduct. I also declare that, as required by these rules and conduct, I have fully cited and referenced all material and results that are not original to this work.

Name, Last name : Ertan Engin

Signature :

ABSTRACT

DESIGN, CONSTRUCTION AND PERFORMANCE EVALUATION OF A SUBMERSIBLE PUMP WITH NUMERICAL EXPERIMENTATION

Engin, Ertan

M. S., Department of Mechanical Engineering

Supervisor : Prof. Dr. Kahraman Albayrak

September 2005, 103 pages

Due to the increasing demand, nonclog type sewage pumps are designed and manufactured in large amounts all over the world. However, a methodology on the design of these special duty pumps is not encountered in the literature. Therefore, the manufacturers tend to develop their own empirical methodologies.

In this thesis, a nonclog pump is designed and constructed on the basis of suitable approaches of known centrifugal pump design methods. In this frame, a nonclog type submersible pump that is capable of handling solids, up to a diameter of 80 mm is aimed to be designed. The designed pump delivers 100 l/s flow rate against a head of 24 m. The rotational speed of the pump is 1000 rpm. Design procedure and the important points that differ nonclog pump design from standard centrifugal pump designs are given.

In addition, hydraulic characteristics of two nonclog pumps, one of which is the pump designed in this study, are investigated by means of computational fluid dynamics (CFD) code.

The designed pump is manufactured and tested in Layne Bowler Pump Company Inc. The test result indicates that design point is reached with a deviation in the limits of the related standard. Wire to water total best efficiency obtained by the test is 60%.

Close agreement between results of actual test and numerical experimentation performed by CFD code shows that CFD analysis is a quite useful tool in predicting the hydraulic characteristics of nonclog pumps.

Moreover, the pump is tested at 750 rpm and the test results are found to be in good agreement with the similitude analysis results.

Keywords: Submersible centrifugal sewage pumps, nonclog pump design, CFD analysis, pump construction, pump performance test

ÖZ

SAYISAL DENEYİ İLE BİRLİKTE BİR DALGIÇ POMPANIN TASARIMI, ÜRETİMİ VE ÇALIŞMA KOŞULLARININ BELİRLENMESİ

Engin, Ertan

Yüksek Lisans, Makina Mühendisliği Bölümü

Tez Yöneticisi : Prof. Dr. Kahraman Albayrak

Eylül 2005, 103 sayfa

Artan talebe bağlı olarak tüm dünyada çok sayıda tıkanmaz tip atık su pompası tasarlanmakta ve üretilmektedir. Ancak kaynaklarda, bu özel pompaların tasarımına yönelik bir metoda rastlanmamıştır. Bu yüzden üreticiler kendi ampirik temelli yöntemlerini geliştirme eğilimindedirler.

Bu tezde, bilinen santrifüj pompa tasarım yöntemlerinin uygun yaklaşımları temel alınarak bir tıkanmaz pompa tasarlanmış ve üretilmiştir. Bu kapsamda, çapı 80 mm'ye kadar olan katı parçacıkları basabilen bir tıkanmaz tip dalgıç pompa tasarlanması hedeflenmiştir. Tasarlanan pompanın debisi 100 l/s, basma yüksekliği 24 m, dönüş hızı 1000 d/d'dır. Tasarım prosedürü, tıkanmaz pompa tasarımını standard santrifüj pompa tasarımlarından ayıran önemli noktalarla birlikte verilmiştir.

Ayrıca, biri bu çalışma kapsamında tasarlanan pompa olmak üzere iki tıkanmaz pompanın hidrolik karakteristikleri, hesaplamalı akışkanlar dinamiği (HAD) yazılımı ile incelenmiştir.

Tasarlanan pompa, Layne Bowler Pompa Sanayi ve Ticaret A.Ş.'de üretilmiş ve test edilmiştir. Deney sonucu, tasarım noktasına, ilgili standardda belirtilen sınırlamaların içinde kalan bir sapmayla yaklaşıldığını göstermiştir. Deney sonucunda elde edilen telden suya sistem en iyi verimi %60'tır.

Gerçek ve HAD programı ile yapılan sayısal deney sonuçlarının birbirlerine yakınlığı, HAD çözümünün, tıkanmaz pompaların hidrolik karakteristiklerinin önceden tahmin edilebilmesi konusunda çok yararlı bir araç olduğunu göstermiştir.

Ayrıca, pompa 750 d/d'lık dönüş hızı ile test edilmiş ve test sonuçlarının benzeşim sonuçları ile uygun olduğu görülmüştür.

Anahtar Kelimeler: Dalgıç santrifüj atık su pompaları, tıkanmaz pompa tasarımı, HAD çözümü, pompa üretimi, pompa performans deneyi

ACKNOWLEDGEMENTS

The author wishes to express sincere appreciation to his supervisor Prof. Dr. Kahraman Albayrak for his guidance, advice and encouragement throughout this study.

This thesis is based on the project supported by TÜBİTAK – TİDEB, which was proposed by Layne Bowler Pump Company Inc. The support of Mr. Kutlu Karavelioğlu, general manager of Layne Bowler, is gratefully acknowledged. The author wishes to express his deepest gratitude to Mr. Onur Konuralp, manager of Layne Bowler Project and Quality Control Department, for his insight and invaluable assistance in theoretical and practical aspects. The author would like to thank his colleagues Mr. Ramazan Özcan for his kind technical help and Mr. Onur Özgen for his altruistic contribution in numerical analyses. The author also wishes to thank Mr. Kayhan Cengiz, technical drawer, for his contribution in technical drawing and solid modelling.

Special thanks go to Miss Selin Akyol for her invaluable patience, insight and encouragement throughout the hard days of this study. This thesis would not be completed without her sincere support.

Finally, the author wishes to offer deepest thanks to his beloved parents Samiye and İsmail Engin and his sister Zeynep Engin for their never-ending patience, love, encouragement and sacrifice.

TABLE OF CONTENTS

PLAGIARISM.....	iii
ABSTRACT.....	iv
ÖZ.....	vi
ACKNOWLEDGEMENTS.....	viii
TABLE OF CONTENTS.....	ix
LIST OF TABLES.....	xi
LIST OF FIGURES.....	xii
LIST OF SYMBOLS.....	xv
CHAPTER	
1. INTRODUCTION.....	1
1.1 General Layout of the Thesis.....	1
1.2 General Information on Submersible Sewage Pumps.....	1
1.2.1 Historical Background, Definition and Types of Submersible Sewage Pumps.....	2
1.2.2 Area of Usage and Installation Types of Submersible Sewage Pumps.....	5
1.2.3 Inner Structure and Working Principle of Submersible Sewage Pumps.....	7
2. HYDRAULIC, MECHANICAL DESIGN AND PRODUCTION OF THE PUMP.....	10
2.1 Design Parameters.....	10
2.2 Hydraulic Design of the Pump.....	11
2.2.1 Impeller Design.....	11
2.2.2 Volute Design.....	23
2.3 Mechanical and Structural Design of the Pump.....	27
2.3.1 Shaft Design.....	28
2.3.2 Assembly Design and Selection of Auxiliary Parts.....	30

2.3.2.1	Structural Forming.....	30
2.3.2.2	Selection of Electric Motor.....	32
2.3.2.3	Selection of Bearings.....	33
2.3.2.4	Selection of Mechanical Seals.....	34
2.3.2.5	Selection of O-rings.....	34
2.3.3	Critical Speed Check.....	35
2.4	Preparation of Drawings and Production of the Pump.....	37
2.4.1	Preparation of Pattern and Machining Drawings.....	37
2.4.2	Casting and Machining.....	38
3.	CFD ANALYSES AND RESULTS.....	39
3.1	General Information on CFD Analyses and Software.....	39
3.2	Steps of the Analyses.....	40
3.2.1	Preparation of Solid Models.....	40
3.2.2	Meshing.....	41
3.2.3	Definition of Boundary Conditions.....	41
3.3	Analysis and Results of Case 1.....	42
3.4	Analysis and Results of Case 2.....	54
4.	EXPERIMENTAL SETUP AND PROCEDURE.....	70
4.1	Test Stand.....	70
4.2	Test Setups.....	73
4.3	Test Procedure and Calculations	78
4.3.1	Test Procedure.....	78
4.3.2	Processing the Test Data and Calculations.....	79
5.	RESULTS AND CONCLUSION.....	82
	REFERENCES.....	90
APPENDICES		
A.	SAMPLE PATTERN, CORE BOX, CORE AND CAST PART PHOTOGRAPHS OF THE SUBMERSIBLE PUMP.....	92
B.	SAMPLE UNCERTAINTY CALCULATION.....	98

LIST OF TABLES

TABLES

Table B.1 – Test data for the best efficiency point.....	98
Table B.2 – Values of random uncertainty for each reading.....	99
Table B.3 – Values of systematic uncertainty for each reading.....	99
Table B.4 – Values of total uncertainty for each reading.....	100
Table B.5 – Comparison of total uncertainty percentages and their limits in the regarding standard.....	103

LIST OF FIGURES

FIGURES

Figure 1.1 – Sample pictures of sewage pump impellers of type; a) vortex, b) cutter-grinder, c) nonclog.....	3
Figure 1.2 – Installation types of submersible sewage pumps; a) portable wet, b) vertical stationary dry, c) horizontal stationary dry, d) stationary wet installations.....	6
Figure 2.1 – Meridional view of a typical centrifugal pump impeller showing the main geometrical parameters.....	12
Figure 2.2 – Design chart giving the relation between width number (b_2 / d_2) and specific speed in SI units.....	18
Figure 2.3 – Cross - sectional view of a volute with trapezoidal profile showing the main geometrical parameters.....	24
Figure 2.4 – Cross-sectional view of the final product.....	31
Figure 3.1 – Solid model of the volute (case 1).....	42
Figure 3.2 – Solid model of the impeller (case 1).....	43
Figure 3.3 – Solid model of rotating region (case 1).....	43
Figure 3.4 – Exploded view of solid model assembly (case 1)	44
Figure 3.5 – Final view of solid model assembly (case 1).....	44
Figure 3.6 – Mesh used in the solution (view-1) (case 1).....	45
Figure 3.7 – Mesh used in the solution (view-2) (case 1).....	46
Figure 3.8 – Mesh used in the solution (view-3) (case 1).....	47
Figure 3.9 – Convergence monitor (case 1).....	48
Figure 3.10 – Absolute velocity vectors inside the pump on a vertical cut plane coincident with the axis of rotation (case 1)	49

Figure 3.11 – Absolute velocity vectors inside the pump on cut plane perpendicular to the axis of rotation and coincident to the midplane between the hub and shroud (case 1).....	50
Figure 3.12 – Relative velocity vectors on the midplane of the impeller (view 1) (case 1).....	51
Figure 3.13 – Relative velocity vectors on the midplane of the impeller (view 2) (case 1).....	52
Figure 3.14 – Static pressure distribution in the pump for different positions of impeller blades (case 1).....	53
Figure 3.15 – Solid model of the volute (case 2).....	54
Figure 3.16 – Solid model of the impeller attached to the shaft together with mechanical seal pair (case 2).....	55
Figure 3.17 – Solid model of suction flange of the base (case 2).....	56
Figure 3.18 – Solid model of rotating region (case 2).....	56
Figure 3.19 – Exploded view of solid model assembly (case 2).....	57
Figure 3.20 – Final view of solid model assembly (case 2).....	57
Figure 3.21 – Mesh used in the solution (view-1) (case 2).....	58
Figure 3.22 – Mesh used in the solution (view-2) (case 2).....	59
Figure 3.23 – Mesh used in the solution (view-3) (case 2).....	60
Figure 3.24 – Sample convergence monitor (case 2).....	61
Figure 3.25 – Absolute velocity vectors inside the pump on a vertical cut plane coincident with the axis of rotation (case 2).....	62
Figure 3.26 – Absolute velocity vectors inside the pump on cut plane perpendicular to the axis of rotation and coincident to the midplane between the hub and shroud (case 2).....	64
Figure 3.27 – Relative velocity vectors on the midplane of the impeller (view 1) (case 2).....	65
Figure 3.28 – Relative velocity vectors on the midplane of the impeller (view 2) (case 2).....	65
Figure 3.29 – Static pressure distribution in the pump for different positions of impeller blades (case 2).....	66

Figure 3.30 – Isosurface formed by the fluid having an absolute velocity of 0.3 m/s (case 2).....	67
Figure 3.31 – Head versus flow rate and efficiency versus flow rate curves of the pump that are obtained by CFD analysis (case 2).....	68
Figure 4.1 – Test stand.....	71
Figure 4.2 – Test setup-1.....	73
Figure 4.3 – Cross-sectional view of lower part of test setup-1.....	74
Figure 4.4 – Test setup-2.....	75
Figure 5.1 – Head versus flow rate and efficiency versus flow rate curves that are obtained by testing the designed nonclog type submersible sewage pump.....	83
Figure 5.2 – Comparison of results of the performance test and CFD analysis for case 1.....	85
Figure 5.3 – Comparison of pump characteristic curves obtained by performance test and CFD analysis of case 2.....	87
Figure 5.4 – Comparison of head versus flow rate curves of the designed pump that are obtained by performance test and similarity formulas at a rotational speed of 750 rpm.....	88
Figure A.1 – Photograph of impeller pattern.....	92
Figure A.2 – Photograph of volute core box.....	92
Figure A.3 – Photograph of volute core.....	93
Figure A.4 – Photograph of volute pattern.....	93
Figure A.5 – Photograph of motor core box.....	94
Figure A.6 – Photograph of motor pattern.....	94
Figure A.7 – Photograph of top cover pattern.....	95
Figure A.8 – Photograph of oil case cover pattern.....	95
Figure A.9 – Photograph of base pattern.....	96
Figure A.10 – Photograph of impeller before machining.....	96
Figure A.11 – Photograph of volute before machining.....	97
Figure A.12 – Photograph of motor case before machining.....	97

LIST OF SYMBOLS

SYMBOLS

a	distance to the inlet of the volute
b	breadth
d	diameter
e	length of central streamline
g	gravitational acceleration
k	constant (see equation 2.19)
l	length
m	parameter (see equations 2.13, 2.14), mass
n	rotating speed, factor, number of readings
r	radius
s	blade thickness, standard deviation
t	thickness
u	tangential component of velocity
v	velocity
w	rotational speed
x	value of test reading
\bar{x}	average of test readings
y	deflection
z	number of blades
A	area
C	velocity, correction factor due to slip, parameter (see equations 2.13, 2.15), experimental coefficient (see equation 2.31)
F	force
H	pump head
K	empirical coefficient (see equation 2.21)

N	specific speed
P	power
Q	flow rate
S	strength
T	torque
U	uncertainty
V	volume
α	fluid angle
β	blade angle
δ	angle of divergence
η	efficiency
θ	central angle
π	pi number
ρ	density of pumping fluid
τ	permissible stress
Φ	diameter of the solid particle

INDICES

0	inlet of the impeller
1	inlet of the blade
2	exit of the blade
3	inlet of the volute
4	rounded inlet of the volute
cr	critical
cv	velocity in the volute
dyn	dynamic
h	hydraulic
m	meridional, manometer, mass, mean
max	maximum

mec	mechanical
min	minimum
mot	motor
n	number of readings
nom	nominal
op	outlet pipe
p	Pfleiderer, pump
pf	pumped fluid
s	shaft, centroid of central streamline
safety	safety
sp	submersible pump
sy	shear
t	total
th	theoretical
tors	torsional
u	tangential direction, unbalance
v	volumetric, volute
vpf	velocity of pumped fluid
w	weight
y	yield
H _{dyn}	dynamic water level
H _m	head measured by manometer
H _t	total head
P	power
Q	flow rate
R	random
S	systematic
T	total
V	volume

η_{sp}	efficiency of submersible pump
θ	central angle
ρ	density of pumping fluid
∞	infinite number of blades

CHAPTER 1

INTRODUCTION

1.1 General Layout of the Thesis

In this study, a nonclog type submersible sewage pump, which is closed-coupled with an asynchronous electric motor, is aimed to be designed and manufactured. Testing the pump and making a comparison between the results of actual test and numerical experimentation are also defined as the objectives of this study. In addition, making a similitude analysis on rotational speed of the manufactured pump is another objective.

In this thesis, the terms “submersible pump” and “submersible sewage pump” are referred to the system, in which the pump, being the hydraulic component, is closed-coupled with the electric motor by a single shaft.

General information on submersible sewage pumps is given in the following part of Chapter 1. Then, in Chapter 2, design and manufacturing procedures of a nonclog type submersible sewage pump are explained. The steps and results of numerical experimentation of the designed pump are given in Chapter 3. In Chapter 4, setups and procedure of the pump tests are stated. Finally, in Chapter 5, the results of actual and numerical experiments are compared and the conclusions drawn from this study are discussed.

1.2 General Information on Submersible Sewage Pumps

General information on submersible sewage pumps is given below stating the historical background, definition and types. Then, the usage areas of submersible

sewage pumps and installation types suitable for these areas are mentioned. Finally, their inner structure and working principle are stated below.

1.2.1 Historical Background, Definition and Types of Submersible Sewage Pumps

In the early times, sewerage systems of the residential areas were so simple that transporting the sewage was not a requirement. However, with the growing population, big cities and complex sewerage systems were built. As a result, transporting the sewerage became compulsory. “One of the earliest sewage pumping systems (steam-driven) was designed and constructed as part of Boston's main drainage works in 1884”, [1]. Among the widespread types of pumps that were used in sewerage systems, centrifugal ones became favourable then, [1]. With the development on leak-proof designs, submersible pump arrangements began to be used in wastewater pumping. Especially with the industrialization, wastewater disposal amount has significantly increased. Also, the physical properties of the solid content have varied a lot. Depending on these facts, an increasing demand on submersible sewage pumps is being observed for the last few decades.

“A submersible pump is a pump with an asynchronous motor with the external motor housing designed to be submerged, so that the motor can be cooled by the surrounding liquid handled”, [2]. In some types, the pump can also be operated without submerging into the pumping fluid due to the special cooling system that the pump is equipped with.

On the other hand, a sewage pump is defined to be “ a centrifugal pump, designed for handling contaminated water (often containing solids), the chemical analysis of which can widely vary”, [2].

On this basis, a submersible sewage pump can be defined as a centrifugal pump coupled with an electric motor in a compact structure, that is designed and

manufactured to pump a large variety of fluids containing solid particles (as mentioned below) without any trouble such as clogging and can be operated by submerging into the pumping fluid.

The submersible sewage pumps can be divided into three groups, depending on the type of impeller that they are equipped with; vortex, cutter-grinder and nonclog, which are given in Figure 1.1 a), b) and c), respectively. Each of these has a different approach to cope with the clogging problem, which is very likely to happen when pumping fluids containing solids.

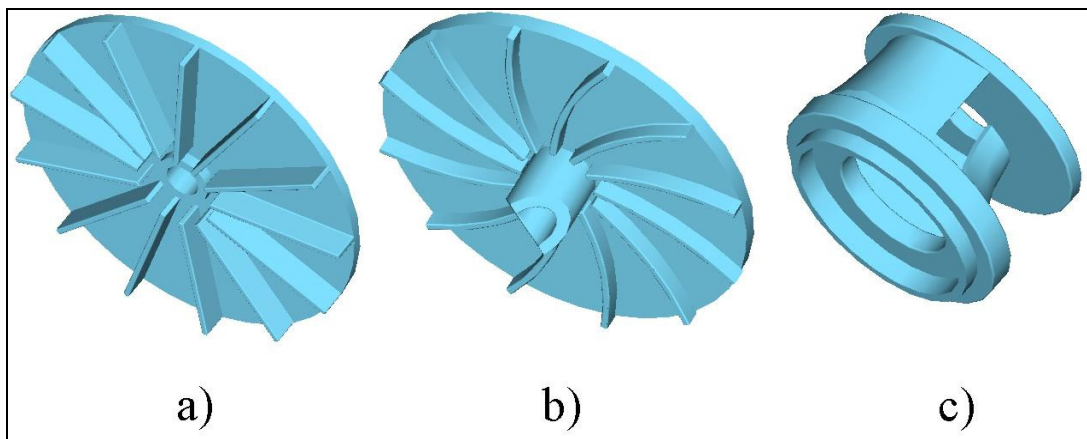


Figure 1.1 – Sample pictures of sewage pump impellers of type;
a) vortex, b) cutter-grinder, c) nonclog

Vortex type sewage pumps have casings with constant peripheral flow area instead of the volute, which has a gradually increasing peripheral flow area. At the upper wall of this casing, impeller is located. When the casing dimensions of vortex type sewage pumps are considered with respect to the dimensions of the impeller, it can be seen that casing is quite wide and high. The reason of employing a comparatively small impeller is to maximize the flow passage area and minimize the possibility of direct interaction between the impeller blades and the solid particles that pumping fluid may contain. In some designs, the impeller is totally

embedded into a cavity on the upper wall of the casing for the same purpose. Obviously, especially in this type of pumps, the centrifugal impelling action of the impeller is significantly diminished. Despite, the fluid is pumped by the pressure difference through the vortex formed in the casing. With such a working principle, vortex pumps can be used to deliver flow rates up to 90 l/s, [3], and heads up to 130 m, [4]. Also handling solid particles having a maximum diameter of 100 mm is possible by vortex type sewage pumps, [3] and [4].

The main working principle of cutter-grinder type sewage pumps is not different than vortex type sewage pumps. The extra precaution taken for clogging is cutting or grinding the solid particles in the pumping fluid into very small pieces that cause no problems in pumping. This is done just before the fluid enters the impeller passages. A cutting edge is placed at the eye of the impeller to form a very small clearance with the suction of the pump. When the pump is driven, the cutting edge is rotated together with the impeller. In this way, the solid particles that are big enough to cause clogging are cut into tiny pieces and then pumped with the fluid. Cutter-grinder type of sewage pumps that can deliver flow rates up to 13 l/s and heads up to 50 m are present in the market, [4]. The sizes of the solid particles in the pumped fluid can be as small as 5 x 15 mm when cutter-grinder type sewage pumps are employed, [4].

Different than the two types of sewage pumps mentioned above, nonclog type sewage pumps are nothing but centrifugal pumps that are modified to prevent clogging. They have “comparatively large openings between vanes of their impellers, which are well rounded at their entrance ends, to prevent clogging with strings, rags and solids when handling sewage or other liquids containing matter that tends to clog the impeller”, [5]. To maximize the passage area, their blade numbers are reduced as much as possible. Therefore, they have impellers having at most three blades. Nonclog type sewage pumps can deliver flow rates up to 500 l/s and heads up to 80 m, [4]. The maximum diameter of solids to be handled by a nonclog pump can be as large as 190 mm, [4].

Sewage pumps can be used in a large variety of cases. Other than being used for pumping sewage, they can be employed in pre and post treatment of domestic wastewater, mine dewatering, construction, industrial processes [6], and in the removal of sludge and storm water, [2]. With special material selection, pressurizing the seawater and solid containing chemicals is possible by sewage pumps, [7]. A rather different usage area of sewage pumps is based on transporting the solid particles inside the fluid instead of the fluid itself. In food industry, sewage pumps are being used for transporting fruits and vegetables like orange or potato.

1.2.2 Area of Usage and Installation Types of Submersible Sewage Pumps

Submersible sewage pumps can be installed to the working site in different installation types by means of different accessories. Mainly, these installation types can be divided into four; portable wet, vertical stationary dry, horizontal stationary dry and stationary wet installations. These installation types are shown in Figure 1.2 a), b), c) and d), respectively.

The first installation type, being the portable wet installation, is the simplest among the others, since it does not require a construction or arrangement in the working site. The pump is submerged into the fluid to be pumped, with a hose attached at the exit. Optionally, an elbow may be used between the pump and the hose. Since the pump does not require to be fixed to the ground, a quite flexible operation can be obtained by this type of installation. Especially in the construction sites, submersible sewage pumps are installed in this way, since they have to be operated at different locations depending on the accumulation rates and locations of groundwater.

The vertical and horizontal stationary dry installations are basically the same, except that the accessories used differ from each other due to the positioning of the pump. In both installations, the pump and the fluid to be pumped are in different compartments. Since the pump is not submerged, these installation types are

recalled as dry installations. The main advantage of dry installations is to enable reaching to the pump for service or maintenance purposes without dismantling the pipe connections. The reason for using a submersible pump in such a dry installation is to achieve a “completely flood-proof” pumping system, [8]. However, dry installation of the pump reduces cooling rate of the motor by free convection from the casing considerably. Therefore, the pump has to be equipped with special motor cooling systems, as stated below, in order to be used in a dry installation application. These installation types are generally used in pumping stations or water treatment plants.

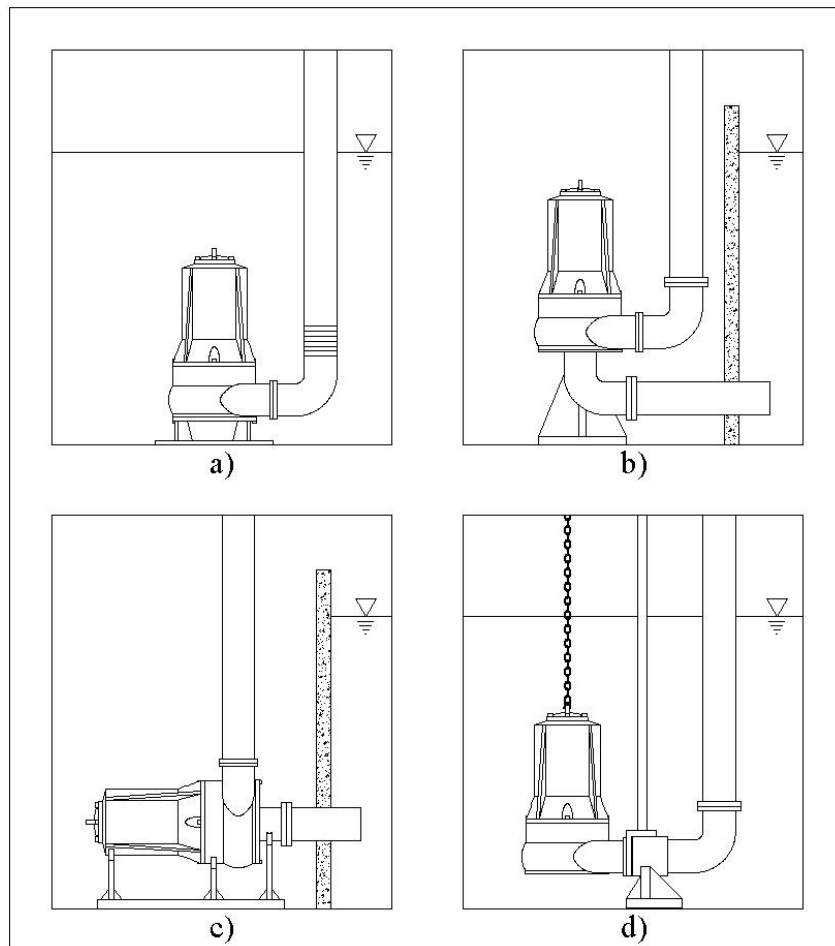


Figure 1.2 – Installation types of submersible sewage pumps; a) portable wet, b) vertical stationary dry, c) horizontal stationary dry, d) stationary wet installations, [7]

Stationary wet installation, on the other hand, collects most of the advantages offered by the other installation types on it. No special cooling systems are required for the motor, since the pump is submerged into the pumping fluid. However, the pump can easily be dismantled from the outlet pipe when required. This installation type is composed of a stationary outlet pipe and guiding rails wrapped by the fitting, that is attached to the exit flange of the pump. Just by lowering the pump through the guide rails, it is automatically coupled to the outlet pipe. Similarly, when the pump is pulled up, it is easily uncoupled from the pumping system. A discharge, aligned with the centreline of the pump, is desirable for this type of installation, since it provides better slip along the guide rails. Stationary wet installations of submersible sewage pumps are mostly used in the same places with stationary dry installations.

1.2.3 Inner Structure and Working Principle of Submersible Sewage Pumps

The literature survey made on submersible sewage pumps and the examined submersible pumps in the market have shown that, there is not a significant difference in the inner structure and so in the working principle of the submersible pumps, depending on the type of the impeller used or the manufacturer.

The power is transferred from the electric motor, which is located in the casing, to the impeller in the volute by means of a vertically mounted shaft and a key. The shaft is generally aligned by two bearings, one at the upper end and the other below the electric motor. The lower bearing also balances the axial load acting on the rotating components of the pump. The shaft length is kept as small as possible to minimize torsional deflection and bending, [7] and [8]. “This results in low vibration, longer seal and bearing lifetime and silent operation”, [8]. At the upper wall of the volute, a mechanical seal pair is used in order to prevent leakage of pumping fluid through the gap between the shaft and the volute. “Mechanical seal pairs provide a leakproof design with low power losses for a wide range of fluids, such as corrosive acids and gritty or inflammable liquids”, [5]. For this reason, they

are suitable for sewage pumps that may be used for pressurizing highly corrosive and / or abrasive fluids. A mechanical seal pair is composed of two parts, each having “polished surfaces running on each other” [5]. The materials of the surfaces vary in a wide range depending on the media that mechanical seal works in. These sealing surfaces, which are “held in continual contact by springs, form a fluid-tight seal”, [5], between rotating and stationary members, that are shaft and volute in this case. An oil case is located on top of the volute. However, the oil inside the case is not used for lubrication. It is insurance for the electric motor in a possible failure of the mechanical seal pair below the oil case. In such a case, the pressurized fluid enters the oil case instead of the region that electric motor is located. When the area of usage of sewage pumps is considered, it can be seen that the fluid to be pumped has a larger density than the oil. Therefore, the pressurized leaking fluid does not pass to the motor side, but forces the oil upwards. Even if the second mechanical seal pair, which is located on top of the oil case, fails, oil that is a nonconductor fluid and so harmless to the electric motor passes to the motor side. This is an effective system for preventing the motor. Also, in some designs, oil is used as a media for the humidity sensor, which is located in the oil case. This sensor detects the leakage of the pumping fluid to the oil case and transmits a signal to the relay on the control panel. Then the relay opens the circuit that feeds the electric motor and so stops the pump. Generally, the part that forms the upper wall of the oil case is also designed to be housing for the lower bearing. Similarly, the cover on top of the motor is used as the housing of the upper bearing. The cover also carries all the weight and has a hole on it for lifting the submersible pump.

Submersible sewage pumps are classified in two groups depending on their motor cooling mechanisms. In the first group of pumps, the electric motor in the casing is cooled by free convection of the fluid that the pump is submerged in. In some submersible pumps, the electric motor runs in oil to have better convection. However, no special parts or systems are used in order to prevent overheating of the electric motor except the casing itself, which is designed to have finlike shapes on its outer surface in some pumps. In this manner, the submergence level for the

pumps mentioned above is vital. Hence, most manufacturers define a “minimum submergence level” in the catalogues of their pumps, [3], [4] and [7]. The second group of pumps has an extra cover, which is named as “cooling jacket”, surrounding the outer surface of the submersible pump and having a gap in between. The pumping fluid flows between the casing and the cooling jacket over the whole periphery. In this way, the heat is transferred from the motor casing by forced convection. The flow around the casing is obtained either by a closed circuit of pumping fluid, or by directing the pumped fluid through the gap, towards the discharge of the pump that is located at the top. In case of closed circuit usage, some amount of the pressurized fluid cools the motor and turns back to the volute. In some designs, an extra impeller, which is coupled to the same shaft with the impeller of the pump, is employed for this circulation.

CHAPTER 2

HYDRAULIC, MECHANICAL DESIGN AND PRODUCTION OF THE PUMP

2.1 Design Parameters

The pump that is designed in this study is a nonclog type submersible centrifugal pump. Therefore, it is expected to operate in solid particle containing fluids without clogging. In this frame, the specification of the solid particles becomes a primary design parameter for the pump to be designed. However, defining a variable (or a group of variables), which enables the description of all physical properties of the solid particles affecting the clogging potential, is quite difficult due to the excessively large usage area of nonclog pumps, as mentioned in Chapter 1. Also, no research, that intends to define some variables and so, classify the physical properties of solid particles in the pumping fluid, is encountered during the literature survey. Instead, the general tendency of nonclog pump industry on this subject is to minimize the obstacles on the flow pattern and maximize the passage area as much as possible without paying an effort on classification of solid particles. The only variable arising from this tendency is solid size. For the purpose of simplification, diameter of the largest spherical solid particle in the pumping fluid that can be handled by the pump without clogging, is being used to specify the minimum passage area of the pump by the manufacturers, [3], [7] and [8].

On this basis, “a nonclog pump specification should designate the maximum diameter of the solid expected to pass through the pump without clogging”, [6]. Therefore, maximum diameter of the solid particle, Φ_{max} , in the fluid to be pumped becomes the fourth cornerstone of the design after rotating speed, n , desired head, H , and desired flow rate, Q , of the pump.

Similar to all design procedures, firstly a market search is made in order to determine the demand on the nonclog pumps. Then, the pumps of the firms in the market, which satisfy the most demanded specifications, are determined. Finally, analysing the expected economical benefits, the design parameters are determined.

On the basis of research results, a nonclog type submersible pump, that is capable of handling solids, having a maximum diameter of 80 mm, and can deliver 100 l/s flow rate against a head of 24 m, with a rotational speed of 1000 rpm, is decided to be designed and manufactured. Then, the design and construction steps given below are followed to finish with a submersible pump having the desired specifications.

2.2 Hydraulic Design of the Pump

Being special purpose pumps as stated in Chapter 1, the design procedure of a nonclog pump is different than standard centrifugal pump design procedures. Therefore, the centrifugal pump design methods in the literature cannot be used directly to design a nonclog pump. However, no method regarding nonclog pump design is encountered during the literature survey. For this reason, it is aimed to develop a special method on nonclog pump design using suitable approaches of known centrifugal pump design methods. The design procedure is given below together with the important points that differ nonclog pump design from standard centrifugal pump designs.

2.2.1 Impeller Design

Starting with the impeller, due to small number of blades, the geometrical variable that determines the maximum diameter of solid particle is the vertical distance between hub and shroud of the impeller, except that the ratio of outer diameter to the inner is very low. In this frame, the standard centrifugal impeller form indicates the variable b_2 , being the breadth of impeller at exit, as critical, since the minimum gap between hub and shroud is at the exit of the impeller (Figure 2.1). This form is

a result of the assumption of ratio of the meridional velocity at the exit, to the one at the inlet, C_{m2}/C_{m1} , being in the order of 0.7 to 0.75, [9], and the increasing peripheral area from inlet to the exit of the impeller. Coming to the conclusion, the value b_2 is one of the outputs of the standard centrifugal pump design procedure, whereas it must be taken as an input constraint in the design of a nonclog pump. A similar approach in determining the value b_1 should be followed in case the maximum solid diameter, as a design constraint, is taken to be large when compared to the hub to shroud distance at the inlet that is calculated from the standard centrifugal pump design methods. Having an extra factor affecting on the geometry of the impeller other than hydraulic respects, some empiric approaches on geometrical values of the impeller, obviously, do not hold for nonclog impeller design. Inlet and exit velocity coefficients may be counted as examples of this inconsistency.

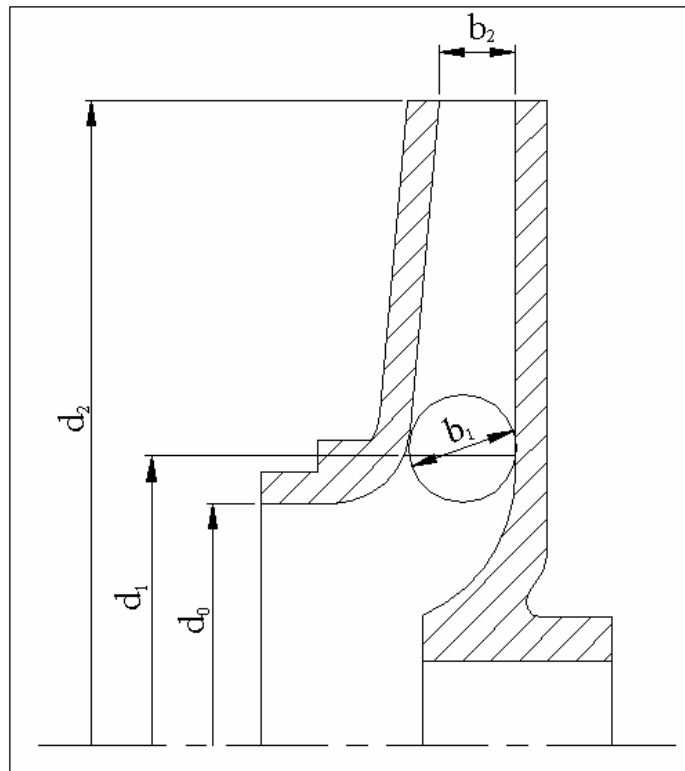


Figure 2.1 – Meridional view of a typical centrifugal pump impeller showing the main geometrical parameters

When the area of usage of the nonclog pumps is recalled, it can be seen that taking only the maximum diameter of solid particles in the fluid to be pumped into consideration, and setting the minimum passage area in the flow pattern accordingly, is not sufficient to prevent clogging in the impeller. The reason is that, the pumping fluid may include stringy material, which may cause clogging, as well. “A nonclog pump that is designed to pass 3 inch diameter solid can not be expected to pass a 12 inch long by 3 inch wide rag simply because it has little thickness. Because the rag will likely wrap around the impeller blade tips at the inlet”, [6]. In this frame, reducing the number of blades, the “opportunity for rags catching on the blades” is also reduced, [6]. Similarly, this situation is an extra factor affecting the determination of number of blades of the impeller, other than hydraulic respects. Therefore, the blade number check that is given as verification of the assumed value by an iterative procedure in Reference [9] may not be considered as an indispensable approach in the design steps.

“A large eye minimizes clogging and net positive suction head required (NPSHR) and maximizes solid size capability”, [6]. Considering this, the eye diameter of the impeller is kept as large as possible. On the other hand, enlarging the eye diameter, some increase in the axial load and impingement velocity at the blade tips are accepted, [6]. Also, since the pump designed is a single-stage one, impeller hub is not extended into the eye to minimize the restriction of the inlet by the hub, [9].

Firstly, the non-dimensional specific speed, N , of the pump to be designed is calculated:

$$N = \frac{nQ^{1/2}}{(gH)^{3/4}} \quad (2.1)$$

Where, n is in rad/s, Q is in m^3/s , g is in m/s^2 and H is in m. “Impellers with blades of single curvature are among the simplest and used in pumps with low specific speeds ($N < 0.57$) and discharges of up to ~ 140 l/s”, [9]. Since the specific speed of

the pump to be designed (0.55) is below the given limit, a blade of single curvature is decided to be designed due to its easiness in manufacturing. Different from the standard centrifugal pump design methods, the design is started by setting the blade inlet and outlet breadth values, b_1 and b_2 , according to the predetermined maximum diameter of the solids to be handled. Next, volumetric efficiency of the pump, η_v , is estimated. This estimation is kept below the recommended range, being 95% - 99%, [10], since the clearance between the impeller and the volute must be larger when compared with standard centrifugal pumps. Need for larger clearance arises due to the area of application of nonclog pumps, including sandy fluids, which cause considerable wear at the close surfaces of impeller and volute. Also, too small clearance may increase the risk of clogging. Then, the flow rate passing through the impeller, Q' , is calculated as:

$$Q' = \frac{Q}{\eta_v} \quad (2.2)$$

The wear effect of solid particles in the pumping fluid becomes considerably significant when the velocity of the flow inside the pump is high. Therefore, an impeller inlet velocity, C_0 , that is not too high and in the recommended range, being 1.5 to 6 m/s, [9], is selected. Since the hub of the impeller was not extended to the eye, the inlet diameter of the impeller, d_0 , is calculated from the equation:

$$d_0 = \sqrt{\frac{4Q'}{\pi C_0}} \quad (2.3)$$

The calculated inlet diameter of the impeller is then compared with the recommended value, being two times the maximum solid diameter, [11], and the difference in between is tried to be kept low. Then, d_0 is changed to the nearest standard pipe diameter in order to have the opportunity to use an inlet pipe that can be required in some installation types which are explained in Chapter 1. Next, the assumed value of C_0 is revised for the new impeller inlet diameter.

Then the diameter of the blade inlet is determined, taking the aim of maximization of passage area into consideration. In order to calculate the area, A_1 , and so the meridional velocity, C_{m1} at the blade inlet, the number of blades, z , and blade thickness at the tangential direction at the inlet, s_{u1} , have to be estimated. “Minimizing the number of vanes increases the potential solid rating by increasing the distance between blades and reducing the impeller eye blockage”, [6]. Therefore, an impeller with a single blade is the most advantageous alternative in the respect of clogging potential considerations. However, a previous study on a nonclog type sewage pump having an impeller of single blade showed that these type of impellers cause serious balancing problems. Although the impeller and the other rotating parts of the pump were balanced within the limits given in the regarding standard [12], rubbing was observed between the impeller and suction flange at a certain location of impeller. When the system was solved by a CFD (computational fluid dynamics) code (Chapter 3, case-1), it was observed that the direction of the calculated radial force acting on the impeller during operation was matching the rubbing location with a deviation of 3° , which can be explained by measurement errors. The reason is that, although it is a matter of technical capabilities, the impellers are mostly balanced in air. Instead, the working media of the impellers is much more dense than the air. This discrepancy results in higher action – reaction forces acting on the impeller, when compared with the ones occurring during the balancing process. Since these forces cannot be balanced by forces acting on symmetrical blade or blades in reverse direction, a significant unbalance occurs even if the impeller is perfectly balanced in air, in case of single blade impeller usage. In other words, “if the impeller is in balance dry, it will be out of balance in operation”, [6]. “Some manufacturers purposefully balance their single vane impellers with a specific imbalance designed to counteract the off shaft centre of gravity of the impeller water mass”, [6]. As a result, balancing an impeller having single blade is not as easy as balancing an impeller having more than one blade. Therefore, the blade number is decided to be 2. In the last steps of impeller design, blade number check formula given in Reference [9] is employed for the purpose of comparison.

Obviously, constriction effect of the blades on the inlet area in a nonclog pump is not as significant as it is in a standard centrifugal pump due to the relatively small number of blades. The thickness of the blade in tangential direction at the inlet, s_{u1} , is defined to be, [9]:

$$s_{u1} = \frac{s_1}{\sin \beta_1} \quad (2.4)$$

Where s_1 and β_1 are blade thickness and blade angle at the inlet respectively. The blade thickness is selected to be smallest value that can be obtained by the manufacturing capabilities as it is done in design example in Reference [10]. Also, the recommended minimum blade thickness for castability, which is given as impeller outer diameter dependent in Reference [13], is examined in order to have an idea about the order of magnitude.

When compared with the standard centrifugal impellers, nonclog impellers have larger impeller and blade inlet diameters, resulting from the aim of maximizing the passage area. Therefore, the tangential component of the velocity is larger with respect to the one in standard centrifugal pumps. Also, resulting from the same purpose, b_1 value is larger, which leads to lower meridional velocities in nonclog pumps. Both changes in the magnitudes of velocity components result in smaller inlet blade angle. Keeping this fact in mind, the estimation of the inlet blade angle is made reasonably lower than the range, being $15^\circ - 45^\circ$, that is given as a generalization in Reference [9]. Also, the blade inlet angles of the examined nonclog pumps in the market are found to be in agreement with the estimation made.

These two estimations are corrected in the progressing steps of the design. On the basis of estimated values, the blade thickness in tangential direction at the inlet is calculated using Equation (2.4). Then, the area at the blade inlet, A_1 , is calculated by the equation:

$$A_1 = (\pi d_1 - z s_{m1}) b_1 \quad (2.5)$$

Next, the meridional velocity at the blade inlet, C_{m1} , is calculated using the A_1 value obtained from Equation (2.5):

$$C_{m1} = \frac{Q}{A_1} \quad (2.6)$$

Then, the tangential component of the velocity at the blade inlet, u_1 , is calculated by the formula, [9]:

$$u_1 = \frac{\pi d_1 n}{60} \quad (2.7)$$

Since the fluid enters the impeller freely, inclination of the absolute velocity of the fluid particles with respect to peripheral velocity, α_0 , equals to 90° leading to, [9]:

$$\beta_1 = \tan^{-1} \left(\frac{C_{m1}}{u_1} \right) \quad (2.8)$$

Using the calculated blade angle at the inlet, A_1 value is revised using Equation (2.5). Then the calculations are repeated until β_1 is determined as a result of this iterative solution.

Going on with the blade exit calculations, firstly, the diameter of the impeller, d_2 (Figure 2.1), is determined. Due to the dimensional discrepancies of nonclog type pumps, impeller diameter determining procedures used in the design of standard centrifugal pumps cannot be employed in designing a nonclog type pump. Therefore, the design chart given in Figure 2.2 is used to determine the impeller diameter, [14]. This chart has two different curves for standard pumps and wastewater pumps that enable determination of “width number”, being b_2 / d_2 ratio, depending on the specific speed of the pump to be designed in SI units. The value

of “width number” corresponding to the specific speed of the designed pump is indicated on the chart by a cross (Figure 2.2). Since the value of breadth at impeller exit was determined previously, the diameter of the impeller is obtained.

As it is stated above, the gap between hub and shroud of a standard centrifugal impeller is minimum at the outer diameter. However, determining b_2 by considering the maximum solid diameter in the pumping fluid, deviation from the standard profile becomes more significant when compared with the variable b_1 in nonclog impeller. As a result, magnitude of the meridional velocity, C_{m2} , and so blade angle at the exit, β_2 , of nonclog pumps become smaller. This fact is also observed on the examined nonclog impellers. In this frame, to be corrected later, the value of β_2 is estimated to be reasonably lower than the range based on generalization, being $20^\circ - 40^\circ$ in Reference [10], as an initial value.

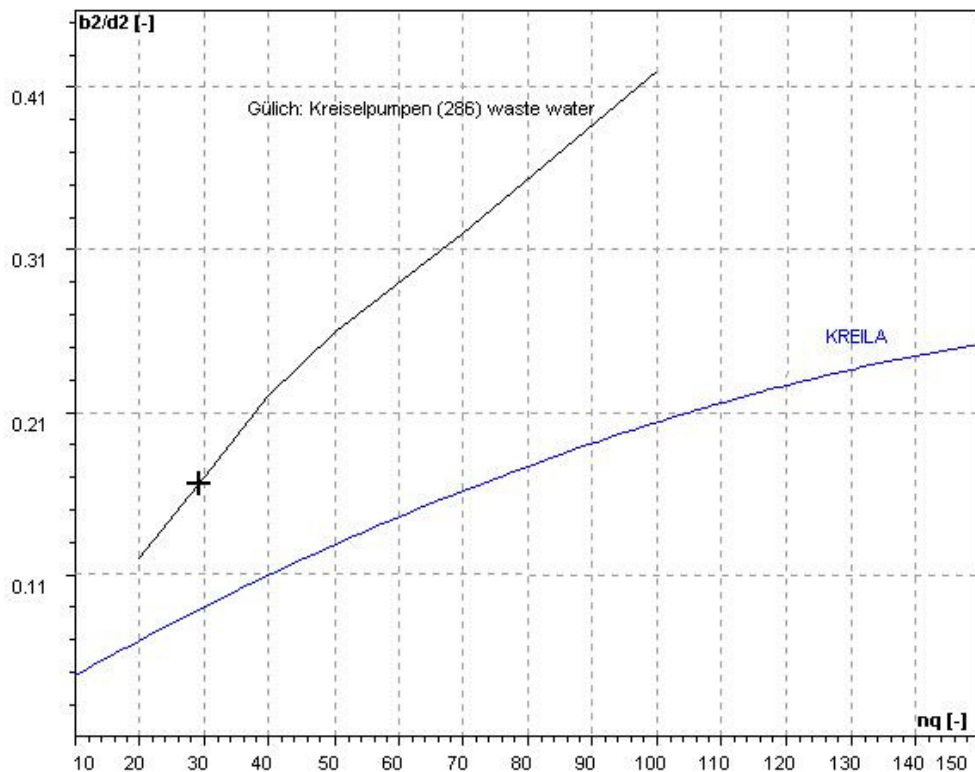


Figure 2.2 – Design chart giving the relation between width number (b_2 / d_2) and specific speed in SI units, [14]

Blade thickness at the inlet, s_2 , is estimated in the same manner as it is done for inlet. Then, A_2 , being the area at the blade exit is calculated:

$$A_2 = (\pi d_2 - z s_{u2}) b_2 \quad (2.9)$$

Where, the blade thickness in tangential direction at the exit, s_{u2} , in Equation (2.9) is given as, [9]:

$$s_{u2} = \frac{s_2}{\sin \beta_2} \quad (2.10)$$

Using the area at the blade exit, the meridional velocity at the blade exit, C_{m2} , is calculated by using the equation:

$$C_{m2} = \frac{Q}{A_2} \quad (2.11)$$

Similar to the calculation made for blade inlet, tangential component of the velocity, u_2 , at the blade exit is calculated by the formula, [9]:

$$u_2 = \frac{\pi d_2 n}{60} \quad (2.12)$$

Blade angle at the exit, β_2 , is given in Reference [15] as:

$$\beta_2 = \tan^{-1} \left[\frac{C_{m2}}{u_2 \left[1 - \left(\frac{52.9 m C}{N} \cdot \frac{C_{m2}}{u_2} \right)^{4/3} \right]} \right] \quad (2.13)$$

Where m and C are parameters defined by Equations (2.14) and (2.15), [15]:

$$m = \sqrt{\frac{b_2 u_2}{d_2 C_{m2}}} \quad (2.14)$$

$$C = \frac{60 g^{3/4}}{\pi^{1/2} \left(\frac{H}{H_{H\infty}} \right)^{3/4}} \left(\frac{\pi d_2 - z S_{u2}}{\pi d_2} \right)^{1/2} \quad (2.15)$$

Where g is the gravitational acceleration.

On the basis of experimental data of pumps that have specific speeds varying from 0.15 to 0.85, the range of parameter m is given as 0.50 – 0.54 in Reference [15]. However, having a larger value of b_2 , and so, small C_{m2} , parameter m for nonclog pumps may increase up to 8 times the standard. Knowing the values of variables on the right hand side of Equation (2.14), parameter m is calculated.

In order to calculate parameter C , the efficiency of the pump, η_p , has to be estimated. The modifications made on the nonclog pumps in order to pressurize fluids containing solid particles inside without clogging, cost in significant decrease in efficiency of the pump when compared with standard centrifugal pumps. The survey made on the catalogues of the nonclog pumps in the market and performance tests performed on them pointed a range of pump efficiency of about 40 – 70 %. Therefore, a pump efficiency in the given range is estimated. The pump efficiency is defined as, [9]:

$$\eta_p = \eta_v \eta_h \eta_{mec} \quad (2.16)$$

Where, η_p , η_v , η_h and η_{mec} designating pump, volumetric, hydraulic and mechanic efficiencies respectively. The mechanical efficiency is assumed to be 94% due to the usage of two mechanical seal pairs together with one ball and one roller bearing to support the shaft. Then the hydraulic efficiency is calculated from Equation (2.16). The definition of η_h is given as, [9]:

$$\eta_h = \frac{H}{H_{th}} \quad (2.17)$$

Where “ H_{th} is the theoretical head, which the pump could generate, if there were no losses due to hydraulic resistance or mechanical friction during flow through the pump”, [9]. Knowing the values of other two parameters in Equation (2.17), theoretical head is calculated. The theoretical head for an infinite number of blades, $H_{th\infty}$, is given in Reference [9] as:

$$H_{th\infty} = H_{th}(1 + C_p) \quad (2.18)$$

Parameter C_p in Equation (2.18) stands for Pfleiderer’s correction factor. The determination of C_p requires iterative solution with β_2 in the standard centrifugal pump design methods on the basis of an initial estimation. The formula for the C_p check is a semi-empirical one and given in Reference [9]. In this formula, Pfleiderer’s correction factor is dependent on the diameters of blade inlet and exit, blade angle at the exit, number of blades and static moment of the central streamline on the blade. However, during the design step of the nonclog pump, it is seen that the convergence of the estimated and calculated values of C_p cannot be achieved for a positive value of blade angle at the exit. This is a physically meaningless case due to conservation of mass throughout the impeller. The successive trials to follow this iterative solution on the C_p and blade angle at the exit led to a conclusion that, the diameter of the impeller has to be several times larger in order to match the estimated and calculated values of C_p . On this basis, it is seen that the semi-empirical formula given for C_p check in Reference [9] does not hold for the nonclog pump to be designed.

In this respect, a reasonable estimation of C_p is required in order to come up with a nonclog pump satisfying the desired head and flow rate. Nonclog impellers, having the lowest number of blades (1 to 3) among the centrifugal pumps, are at the extreme edge of being far away from infinite number of blades assumption.

Therefore, the value of Pfleiderer's correction factor for nonclog pumps is larger than the one for standard centrifugal pumps. The design examples given in Reference [9] and previous design experiences point a range of 0.25 – 0.40 as the value of C_p for impellers having 4 to 7 blades. Also, the C_p value for a previously designed nonclog pump having single blade impeller is calculated on the basis of test results and estimations of volumetric and mechanical efficiencies. Although determining the exact value is not possible due to the estimations, it is seen that the value of C_p is in the range of 0.55 – 0.60. In the presence of these data, a Pfleiderer's correction factor of 0.50, being a value between the two ranges given above, is assumed, since the blade number is taken to be 2. With this assumption, $H_{th\infty}$ is found from Equation (2.18).

Knowing the value of $H_{th\infty}$, parameter C is calculated from Equation (2.15). Next, the blade angle at the exit, β_2 , is calculated using Equation (2.13). For the calculated β_2 , blade exit calculations are repeated resulting in a further iterative procedure to obtain final values of all variables related with the blade exit.

As it is stated above, hydraulic considerations are not the only factors affecting the determination of blade number in nonclog pumps. Purpose of maximizing the flow passages results in decreasing the number of blades. However, the blade check formula given in Reference [9] is employed in order to have an idea of deviation from the standard centrifugal pump design procedures:

$$z = 2k \frac{r_s}{e} \sin \beta_m \quad (2.19)$$

Where k is given to be 6.5 for centrifugal pumps in Reference [9], r_s is the radius of the centroid of the central streamline, e is the length of central streamline in meridional view and β_m is the mean blade angle. An approximation of β_m is given as, [9]:

$$\beta_m = \frac{\beta_1 + \beta_2}{2} \quad (2.20)$$

The blade number is calculated to be 1.52 from Equation (2.19). In this respect, the blade number that was assumed to be 2 at the beginning of the impeller design is confirmed.

After calculating all the variables related with the impeller geometry, blade shape is determined. At this stage, in order to stick to the aim of maximizing the passage area, the overlap angle has to be considered particularly. Overlap angle is defined to be the central angle between the trailing edge of one blade and the leading edge of the subsequent one, [9]. However, for a single blade impeller, overlap may occur between the two edges of the same blade. To set the overlap angle to zero, the central angle that a blade shades from inlet to the exit is decided to be $360^\circ/z$. This approach is also observed at the nonclog pump impellers in the market. However, due to very small inlet and exit blade angles, blades obtained by “point by point” and “conformal representation” methods, [9], does not meet the zero overlap angle requirement for the pump to be designed. Therefore, “two-arc method”, [9], being the simplest among the other two, is used to determine the blade shape. Usage of this method also provides great easiness in making the foundry pattern for the impeller, [9]. Determining the blade shape, impeller design is finished.

2.2.2 Volute Design

Going on with volute design, firstly, the areas of the volute cross-sections are calculated on the basis of constant mean velocity through the volute by the procedure given below. The empirical coefficient, K_{cv} , corresponding to the specific speed of the pump to be designed, is determined from the graph given in Reference [9]. Then, the velocity of flow in the volute, C_v , is calculated by the formula, [9]:

$$C_v = K_{cv} \sqrt{2gH} \quad (2.21)$$

Assuming constant flow rate on the perimeter of the impeller, the volumetric amount of fluid passing through each cross-section of the volute can be related to the central angle shaded with reference to the beginning of the spiral of volute. Therefore, at any central angle, θ in degrees, area of the volute cross-section, $A_{v\theta}$, is calculated to be, [9]:

$$A_{v\theta} = \frac{Q}{C_v} \cdot \frac{\theta}{360} \quad (2.22)$$

Then, the profiles of the volute cross-sections are determined. “For specific speeds above 0.22, the efficiency of the circular volute designs will be 95% of that possible with conventional volute designs”, [13]. Having a higher specific speed than the limiting value, profiles of the volute cross-sections are chosen to be in trapezoidal form (Figure 2.3).

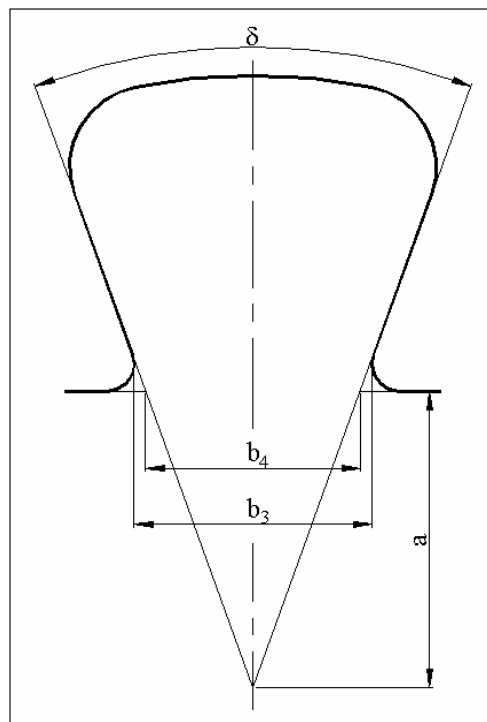


Figure 2.3 – Cross - sectional view of a volute with trapezoidal profile showing the main geometrical parameters

A constant angle of divergence is recommended in Reference [13] due to the good results obtained so far and low pattern costs together with manufacturing time saving. For a fixed cross-sectional area, a large angle of divergence leads to smaller difference between the diameters of the impeller and the wall of the volute, when compared with the difference formed by usage of small angle of divergence. In this manner, to preserve the passage area constituted in the impeller, a small angle of divergence for the volute is desirable. Therefore, an angle of 30° is decided as angle of divergence, δ (Figure 2.3).

Despite the considerable reduction it offers on the radial load, [13] and [16], a double volute is not preferred since putting a splitter on the flow pattern may result in clogging.

The inlet breadth, b_3 (Figure 2.3), is assumed to be 1.75 times the impeller breadth at outlet, b_2 , as it is recommended depending on the specific speed in Reference [13]. Then, the sharp edges of volute entrance are rounded off, giving a new breadth, b_4 (Figure 2.3). Next, the distance between the centre of the arcs forming the outer edges of volute cross-sections and the volute inlet, a (Figure 2.3), is calculated using the formula, [9]:

$$a = \frac{b_4}{2 \tan\left(\frac{\delta}{2}\right)} \quad (2.23)$$

Knowing the location of the centre points, the outer arcs of cross-sections are drawn providing that the net flow area equals to area of the volute at that cross-section. Then, the sharp edges that are formed by the intersections of outer arcs and two sides of the volute segments are rounded. Since the solid particles in the pumping fluid are to be transported by the drag force in the volute, corners, which lead in leakage of the flow around the solid particle, are not desired. Therefore, the radii of rounded corners are chosen to be as large as possible. Rounding off the corners, areas of the volute cross-sections are reduced. To compensate the reductions in the

areas, the radii of the outer arcs of volute cross-sections are increased. Then, the cutwater diameter of the volute is determined as 1.06 times the outer diameter of the impeller considering the recommended values given as specific speed dependent in Reference [13]. As a result, a volute of constant flow velocity, C_v , in all cross-sections is obtained.

Then, taking the maximum diameter of solids to be handled into consideration, the cross-sectional profile of the volute outlet is checked. Since the volute outlet is determined by considering only the flow velocity in the standard centrifugal pump design, the minimum clearance required for a nonclog pump may not be obtained. For this reason, a further adjustment is made on the cross-sectional areas by multiplying them with a constant that is sufficient to enlarge the outlet to give the desired clearance. Obviously, this compulsory enlargement results in reduction of C_v that was calculated previously. In this respect, it is evident that the empirical coefficient, K_{cv} , that is determined for the standard centrifugal pumps in Reference [9], may or may not be employed in the calculation of flow velocity in a nonclog pump volute, depending on the maximum diameter of the solids to be handled. Then, the magnitudes of the area reduction for each cross-section due to rounding the edges are calculated once more and further adjustment is made on the volute profiles. Making these adjustments, design of the volute is finished.

In a standard centrifugal pump, at the exit of the volute a diffusion chamber is present, where the velocity of the pumped fluid is decreased and its static pressure is increased by increasing flow area. In the design of the diffusion chamber, firstly, a standard outlet flange diameter, that is suitable for the flow rate of the pump is selected, [9]. Then, the angle of taper of the diffuser is determined depending on the velocity magnitude of flow in the volute, [9]. Finally, the length of the diffuser is calculated using these two variables, [9].

On the other hand, for a nonclog type centrifugal pump, the volute area calculated by standard centrifugal pump design methods would probably be increased by the

designer, considering the maximum solid diameter, as it is mentioned above. This compulsory change in the flow area results in considerable decrease in the velocity of the flow in the volute. Placing a diffusion chamber at the exit of the volute causes further decrease in the flow velocity. This case is not desirable for two reasons: Firstly, it requires an excessively large outlet flange that is not useful for practical purposes. Secondly, the pumped fluid may become too slow for transporting the solid particles since drag force decreases with decreasing fluid velocity.

In this frame, it is decided not to use a diffuser at the exit of the volute. Instead, the flow is directed through an outlet guide after the volute. A suitable standard outlet flange diameter is selected considering the two important points mentioned above. The flow area of the selected outlet is slightly smaller than the volute outlet area. However, the flow velocity exiting the outlet guide is not higher than it would be, if the standard centrifugal pump design methods were followed throughout the volute and diffusion chamber design steps. Although the reduction in area through it is small, the length of the outlet guide is kept as long as possible.

When the area of usage and installation types of the submersible nonclog pumps are considered (Chapter 1), it can be seen that a discharge, aligned with the centreline of the pump, is quite advantageous. Therefore, the outlet guide is bend with a radius as large as possible, to have a centred outlet. So, the hydraulic design is finished.

2.3 Mechanical and Structural Design of the Pump

After determining shapes and dimensions of the impeller and the volute of the pump, firstly the shaft, being the most critical component of the pump in the respect of strength considerations, is designed. Then, dimensions of all the other components and the inner structure of the pump are determined. Finally, the design is finished with critical speed check as it is mentioned below in sequence.

2.3.1 Shaft Design

In order to determine the diameter of the shaft and the motor to be employed, firstly shaft power required for pump to operate, P_s , is calculated using the equation below, [10]:

$$P_s = \frac{\rho g H Q}{\eta_p} \quad (2.24)$$

The pump efficiency used in this equation was estimated in the hydraulic design. Motor margin values depending on the motor ratings are given in the standard [17]. Adding a suitable motor margin on the shaft power, nominal power of the motor to be employed, $P_{\text{mot_nom}}$ is determined. The motor margin becomes critical in case of instantaneous sudden loadings and pumping a fluid of non-uniform or higher density when compared with the density assumed in Equation (2.24). Therefore, on the basis of determined motor margin, the density of the fluid to be pumped is limited to be at most 1200 kg/m^3 . Also, some rise in the required power may be seen when the pump is not operated in the vicinity of design point. However, due to the usage of a norm electric motor, having extra margin of 25%, which is declared by the manufacturer, keeps the design on the safe side. Thus, the maximum power to be transmitted by the shaft, P_{s_max} , is estimated to be 1.25 times $P_{\text{mot_nom}}$. Then, the minimum shaft diameter, d_{s_min} in m, is calculated by the equation, [9]:

$$d_{s_min} \approx \sqrt[3]{\frac{3.1 \times 10^{-3} P_{s_max}}{\tau_{tors} n}} \quad (2.25)$$

Where, P_{s_max} is the maximum power to be transmitted by the shaft in W, τ_{tors} is permissible torsional stress for the shaft material in MPa and n is the rotational speed of the pump in rpm. The material of the shaft is chosen to be X20Cr13 steel as it is mentioned in the standard [17]. The smallest diameter of the shaft is designed to be inside the coupling of the impeller as it is the most common case,

[9]. The power transmission from the shaft to the impeller is decided to be obtained by means of a key. Therefore, the shaft should satisfy the minimum diameter calculated above, at the location where keyway is placed. Choosing a 3/8" thick square type key, the value of d_{s_min} is increased. Key material is chosen to be SAE 1020 steel. In order to determine the length of the key, firstly torque transmitted by the key, T , is calculated using the formula, [18]:

$$T = \frac{P_{s_max}}{n \frac{\pi}{30}} \quad (2.26)$$

Where, T is in Nm, P_{s_max} is in W and n is in rpm. Then the corresponding force to constitute the calculated torque, F , is determined as, [18]:

$$F = \frac{2T}{d_{s_min}} \quad (2.27)$$

By the distortion energy theory, the shear strength, S_{sy} in kpsi, is calculated using the formula, [18]:

$$S_{,sy} = 0.577 S_y \quad (2.28)$$

Where S_y is the yield strength of key material. Finally, the length of the key, l , is calculated by substituting the values calculated from Equations (2.27) and (2.28), in the Equation (2.29), [18]:

$$l = \frac{Fn_{safety}}{S_{,sy} t} \quad (2.29)$$

Where, t is the key thickness and n_{safety} is the safety factor that is taken to be 2.

Determining the length of key, all critical dimensions regarding the assembly settlement of the submersible pump are obtained.

2.3.2 Assembly Design and Selection of Auxiliary Parts

Starting from the impeller, volute and inlet flange, a complete assembly of the designed pump is formed next. Firstly, the main structure of the pump is obtained and then, the suitable auxiliary parts required are selected from the standard alternatives.

2.3.2.1 Structural Forming

The inner structure of the submersible pump is decided to be similar to the common structure explained in Chapter 1. The structural design considerations mentioned below can be observed on Figure 2.4.

The shaft diameter is increased at three locations to have steps for basing the impeller, lower bearing and the rotor of the electric motor. However, it is preferred to keep the increase in shaft diameter as small as possible since the costs of mechanical seals and bearings generally rise with the diameter of the shaft that they are mounted on.

To be sure about having a leakproof structure, two o-rings are used between the motor casing and the cover on top of it. Also, three o-rings are used between volute, oil case and motor cover. By this arrangement, at least two o-rings have to fail for a leakage to occur.

Height of the base that carries the submersible pump is also important in two respects. Firstly, it should provide a wide enough gap for the pumping fluid and the solid particles in it to pass through. In this frame, a high base is desirable for hydraulic purposes. However, being the second important consideration, a high base

results in increase of the total height and the minimum submergence level of the submersible pump. Large dimensions put the submersible pump into a disadvantageous position among its alternatives at the market. Therefore, an optimisation is made in order to determine the base height of the submersible pump.

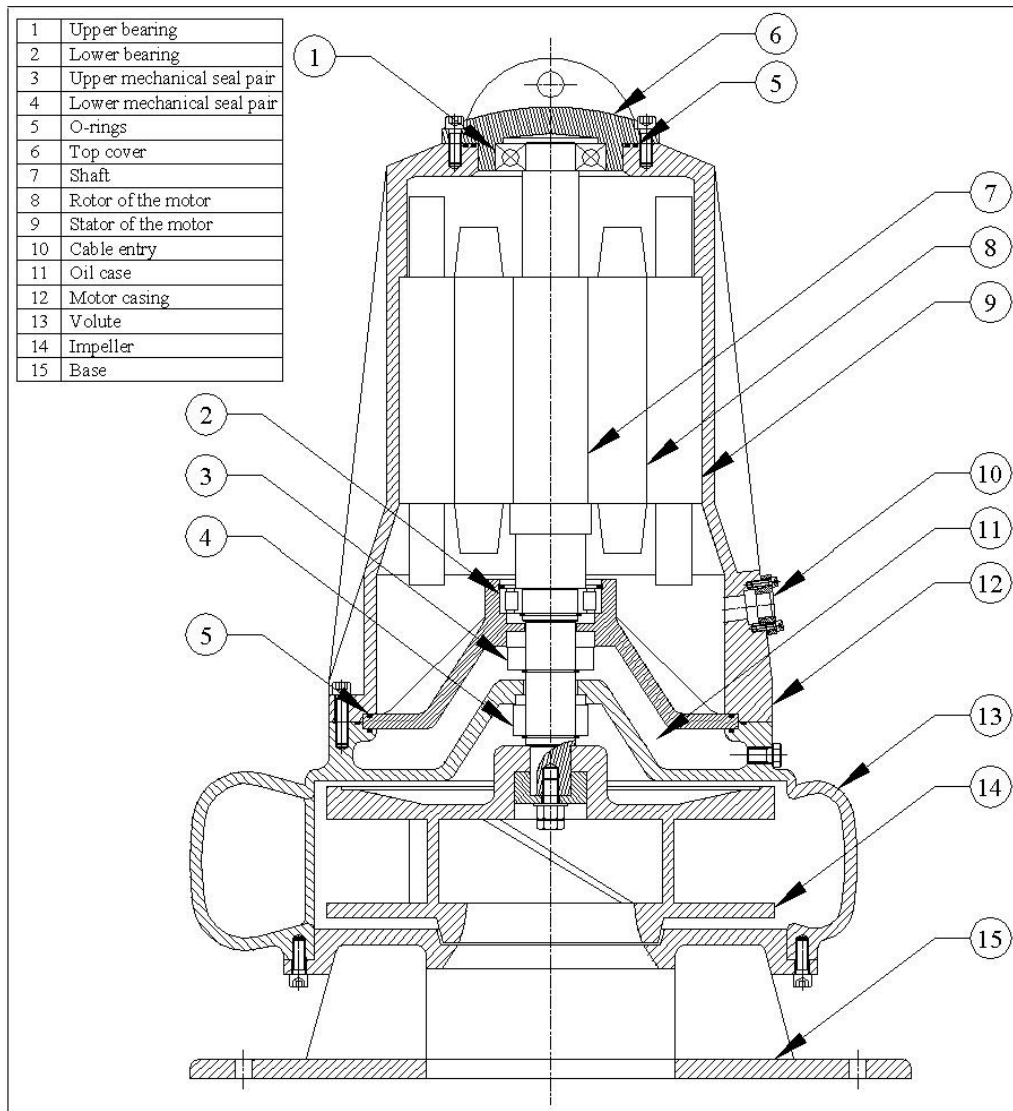


Figure 2.4 – Cross-sectional view of the final product

As a general consideration for the structural forming stage, the main objective is taken to be obtaining a structure, easy to assemble and dismantle. The bolts used are chosen to have same diameter as far as possible. Also, the past experiences on the prototypes of other sewage pumps have shown that, mounting the lower mechanical seal pair correctly is very important to provide a leakproof system. However, if the cavity that the mechanical seal pair is located has a diameter just enough for the seal, mounting becomes very hard. Moreover, mounting process may result in breaking the polished surfaces of the mechanical seal pair since these surfaces are quite fragile. Therefore, the cavity that mechanical seal pair is located is designed to have enough width to provide easy mounting. Having a wide cavity also resulted in better cooling of the mechanical seal pair by convection from the lateral surfaces.

Also, taking the requirements of the market into consideration, the outer dimensions of the submersible pump is aimed to be kept at minimum possible values. Minimizing the dimensions is also needed for minimizing the weight and so, the cost of the submersible pump. However, considering the easiness of production, some deviations from these goals has to be accepted. Similarly, some parts are revised in order to be used together with the auxiliary parts that are bought such as mechanical seals, o-rings or bearings. Also, some modification on the outer structure is made for aesthetical purposes.

2.3.2.2 Selection of Electric Motor

The rotational speed of the electric motor is one of the design parameters, which were decided before the design step. Also, the nominal power of the motor to be employed, $P_{\text{mot_nom}}$, was determined at the shaft design step. A norm type electric motor, satisfying these requirements is selected from the catalogue of the manufacturer, [19]. Then, the required inner dimensions of the motor are asked from the manufacturer, in order to determine the final structure of the submersible pump. Also, some modifications are required in the inner structure of the electric motor, like bearing types and locations, shaft dimensions and cable entries to the

motor casing. These modifications and special usage conditions of the submersible pump are discussed with the motor manufacturer and an agreement is established. Moreover, some requirements of the motor manufacturer resulting from the manufacturing techniques used are taken into consideration and the structure of the submersible pump is modified.

2.3.2.3 Selection of Bearings

The number of bearings and their locations are decided to be the same as it is mentioned under “Inner Structure and Working Principle of Submersible Sewage Pumps” title in Chapter 1; one, in the cover on top of the motor, and the other, over the oil case.

Selection of the lower bearing is quite important, since the entire axial load acting on the rotating parts of the submersible pump is to be carried by this bearing. In this frame, the selected bearing should be capable of carrying axial load together with the radial load. Moreover, the location of the rotating parts in the axial direction has to be fixed by the lower bearing also. Therefore, the selected bearing should not be from the types having length compensation within itself. The lower bearing, on the other side, is not subjected to axial loading but has to carry some amount of radial load. Apart from these practical requirements, both bearings have to be easily accessible and reliable.

Sticking to the considerations stated above, alternatives of bearing types satisfying the required conditions are determined from manufacturer’s catalogue [20]. Then, making a comparison between costs of the alternatives, a deep groove ball bearing and a NUP type cylindrical roller bearing are selected as upper and lower bearings of the submersible pump, respectively. Finally, the bearing selection procedure given in Reference [20] is followed and the dimensions of the bearings to be used are determined as results of calculations based on 2 years of 24 hours/day operation with quite high safety factors.

After determining the bearings to be used in the submersible pump, their assembly dimensions are taken from the catalogue of the manufacturer [20]. Then, these assembly dimensions are used to determine the dimensions and the manufacturing tolerances of the shaft at the points where bearings are located.

2.3.2.4 Selection of Mechanical Seals

The dimensional selection of the mechanical seals is based on the shaft diameter at the locations that mechanical seals are mounted on. To determine the materials of the bellows, rotational and stationary parts of the mechanical seals, the information given in the catalogue of the manufacturer is used [21].

The lower mechanical seal pair is selected as PG5 type since, these mechanical seals are recommended for usage in centrifugal water and sewage pumps in the catalogue of the manufacturer [21]. This type of mechanical seals is “balanced, independent of direction of rotation and self cleaning”, [21]. The materials of the sealing surfaces are SiC. For the upper mechanical seal pair, P40 type, which has carbon – ceramic sealing surfaces, is selected due to the usage in oil case. These mentioned materials are selected to be the standard materials for mechanical seal pairs. However, for the submersible pumps to be operated under special conditions, these materials are decided to be changed accordingly.

Selecting the suitable mechanical seal pairs, all dimensions and machining tolerances of the shaft are determined since; the assembly dimensions of mechanical seal pairs are given in the catalogue of the manufacturer [21].

2.3.2.5 Selection of O-rings

The last items of auxiliary parts to be selected are o-rings since they have a wide variety of standard dimensions that offer at least a few suitable alternatives for the structure they will be inserted in. Taking the operating media into consideration, the

standard material for the o-rings is selected as polychloroprene, from the catalogue of the manufacturer, [22]. Also, ethylene-propylene and nitril-butadiene are determined to be alternatives for o-ring material to be used in special operating conditions. After making some small revisions on the parts that would serve as housings for the o-rings, the final structure and dimensions of all the parts forming the submersible pump assembly are obtained.

2.3.3 Critical Speed Check

When the complete assembly is obtained, the general form and dimensions of the shaft are achieved. On this basis, the maximum deflection and critical speed checks are made as follows.

The shaft of the submersible pump has two bearings and an overhung impeller attached on it. Since the pump can be installed both horizontally and vertically, maximum deflection and critical speed checks has to be made for each installation type, separately.

When the pump is installed vertically, the weight of the rotating parts has no effect on the shaft in the respect of deflection. Therefore, only unbalance of the rotating parts is taken into consideration. However, if horizontal installation is the case, the weights of the rotating parts become quite significant on the deflection of the shaft. In this respect, the total deflection is found by superimposing the deflections caused by the weight and unbalance of the rotating parts.

Firstly, the solid model of the impeller is created and its weight is calculated by using Mechanical Desktop 2006 program. Then, the shear force and bending moment diagrams of the shaft are drawn. Next, using the “moment area method” given in Reference [23], deflection of the shaft, due to weights of rotating parts, at the location of the impeller, y_w , is calculated.

The maximum deflection due to unbalance of rotating parts is limited with G 6.3 quality degree for pumps in the related standard [12]. Since the manufacturing of the pump is to be based on this standard, the maximum deflection due to unbalance, y_u , is taken to be equal to the given limit that corresponds to the rotating speed of the pump, being 40 μm .

Superimposing the deflections for the horizontal installation, the total deflection of the shaft, y_t , is calculated, [9]:

$$y_t = y_w + y_u \quad (2.30)$$

For vertical installation, the total deflection is equalized to the maximum deflection due to unbalance. Next, the smallest distance between rotating and stationary parts of the pump, being the clearance between impeller and suction flange, is determined considering both total deflection of the shaft and the particles that pumping fluid may contain.

Then, the critical speed of the pump in rad/s, w_{cr} , is calculated using the approximate formula given in Reference [9]:

$$w_{cr} = C \cdot \sqrt{\frac{g}{y_t}} \quad (2.31)$$

Where, C is an experimental coefficient varying from 1 to 1.268, [9]. Since the common fraction or multiples of critical the speeds calculated by Equation (2.31) for both vertical and horizontal installations are far away from the operating speed, no revising on the shaft form is required.

2.4 Preparation of Drawings and Production of the Pump

Finalizing the forms and dimensions of all parts in the submersible pump assembly, the design step is finished. Next, the pattern and machining drawings are prepared and then, the designed nonclog type submersible pump is produced, as stated below.

2.4.1 Preparation of Pattern and Machining Drawings

All parts of the submersible pump other than the shaft are to be manufactured from cast parts. Therefore, their pattern drawings are to be prepared. Firstly, the surfaces of the parts that have to be machined are determined. Then, machining thicknesses are added to these surfaces. Next, the drawings of the parts are scaled up in the amount that casting material requires, due to shrinkage. Finally, the taper angles are given to necessary surfaces depending on the direction that pattern would be taken out. For the patterns that have simple geometries, the drawings that are prepared in the way explained above are sufficient. However, for the parts having complex geometries, like the impeller and volute, determining the required dimensions at each point on the surfaces and showing them on the drawings are not possible. Therefore, cross-sectional views of the solid models that are created for the CFD analysis, as mentioned in Chapter 3, are obtained in CAD program. Then, one to one scaled printouts of these cross-sections are used to give the required shape to the wooden tablet at the corresponding layer of the part. When the tablets are piled up and stuck together, the three dimensional complex forms of the surfaces, that are critical in the respect of hydraulic characteristics and efficiency of the pump, are obtained.

The final shapes and dimensions of each part of the submersible pump were already determined in the structural forming step. The machining tolerances at the locations of auxiliary parts were also determined from the catalogues of these parts. For the rest, machining tolerances, that are suitable to the assembly structure, are determined in the range that manufacturing techniques allow. Then, sticking to the

reference surfaces required for machining, the dimensions and their tolerances are given and machining drawings of the parts are prepared.

2.4.2 Casting and Machining

The first step in production of the designed submersible pump is manufacturing the patterns using the prepared drawings. Then, these patterns are used for sand casting. Then, the cast parts are obtained. Sample pattern, core box, core and cast part photographs of the designed pump are given in Appendix A, Figures 1 – 12. Next, these parts are machined to obtain the dimensions and tolerances given in the machining drawings. After the dimensional controls, the parts of the submersible pump are assembled together and so, the prototype is produced. Also, for the tests to be performed by using a VHS type electric motor, the test setup mentioned in Chapter 4 is designed and manufactured.

CHAPTER 3

CFD ANALYSES AND RESULTS

3.1 General Information on CFD Analyses and Software

The hydraulic characteristics of two nonclog type sewage pumps are investigated by numerical experimentation in this study. Steps and results of these studies are discussed below in two cases; “case 1” and “case 2”. The nonclog pump that is studied in case 1 is a previous design of Layne Bowler Pump Company Inc. and has a single blade impeller. In case 2, the nonclog pump, whose design, construction and performance evaluation are the subjects of this thesis, is studied.

In order to obtain the characteristic curves, the CFD (Computational Fluid Dynamics) software is run for different sets of boundary conditions, which correspond to different points on the characteristic curves of the pumps.

CFD softwares calculate the values of unknowns in 6 equations; conservation of mass, momentum equations in three principle directions, energy and turbulence equations. This is done by an iterative solution based on initial assumptions of unknowns. Therefore, sufficient number of iterations must be made in order to obtain a converged and reliable solution. In this frame, the configuration of the computer used in numerical experimentation is a primary factor determining the time required for the solution. In this study, a Pentium 4, 3.2 GHz, computer that has 2 GB memory is used for numerical experimentation.

CFdesign 7.0 is the software employed for numerical experimentation of the designed pump. The program “uses finite element method primarily because of its flexibility in modelling any geometrical shape”, [24]. The solver algorithm of the software is based on SIMPLE-R technique, [24]. Also, an automatic mesh

generator, which has the ability of using quadrilateral, triangular, tetrahedral, hexahedral, wedge or pyramid elements, is embedded in the software, [24]. Constant eddy viscosity, k-epsilon and RNG turbulence models are available for solving turbulent flows, [25]. In both cases of this study, k-epsilon turbulence model, being the default one, is employed. Because, constant eddy viscosity model is recommended for lower speed turbulent flows and some buoyancy flows; and RNG turbulence model is recommended for separated flows and their reattachment cases, [25]. Whereas, k-epsilon model is “typically more accurate than the constant eddy viscosity” and although it is “not as resource intensive as the RNG model, still gives good results”, [25].

3.2 Steps of the Analyses

The same analysis procedure is followed in numerical experimentations of both case 1 and case 2. This common procedure is explained below in detail.

3.2.1 Preparation of Solid Models

CFD software requires model of the fluid volume, together with the boundary conditions assigned on it, in order to solve the system. To obtain the fluid volume, firstly, impeller, volute, base, shaft and lower mechanical seal pair of the pumps are modelled using Mechanical Desktop 2006 program.

Then, the solid models are assembled together. Since the “rotating reference frame” method has to be used, “rotating regions” that surround all the rotating parts in the systems are created. When the solid models are transferred to the CFD program, the intersecting volumes are cut by each other with a boolean operation. On this basis, closing the inlets and outlets of the pumps by two plugs, the cavities inside the solid models are defined to be separate volumes. Actually, these cavities formed the model of the fluid volume inside the pumps. The plugs also simulate the fluid volumes at the inlet and exit of the pumps.

3.2.2 Meshing

“Prior to running a CFD design analysis, the geometry has to be broken up into small, manageable pieces called elements. The corner of each element is called a node, and it is each node that a calculation is performed”, [25]. Increasing the number of elements leads to a better solution with more reliable results until complete mesh independence is attained. However, time and computer memory required for the solution increase at the same time. Therefore, determination of the element sizes, and so the number of elements for a fixed control volume, is an optimisation. Another important factor to consider while determining the element sizes is that, the regions, in which large gradients of unknown variables are expected, require a dense mesh. Similarly, obtaining a finer mesh at the regions that are to be investigated particularly may be advantageous.

Considering the points mentioned above, the control volumes are broken up to elements, whose sizes vary from 7 to 20 mm depending on the region they are situated in. The mesh is generated automatically after the determined element sizes are entered to the program. For the boundary layer meshing, default values of “number of layers” and “thickness factor”, being 3 and 0.45 respectively, are used, [25]. This means that, the software generates 3 layers of elements in the vicinity of walls into a gap having a height of 0.45 times the original element size assigned to that region, [25].

3.2.3 Definition of Boundary Conditions

After finishing the meshing step, numerical analyses of the pumps are continued with the definition of boundary conditions. Static pressures of fluid at the inlet of both pumps are defined to be zero gage, in other words atmospheric pressure. Then, static pressure of fluid at the exit of the pump is defined for different operating points on the head - flow rate characteristic curve of the pumps. Finally, the rotational speeds of the impellers are defined.

3.3 Analysis and Results of Case 1

The study is started by preparation of solid models, being volute, impeller, base, shaft, lower mechanical seal pair, rotating region and the plugs. These solid models are shown in Figures 3.1-3.

The control volume to be analysed is obtained by assembling these solid models together as it can be seen on the exploded view of the assembly (Figure 3.4). The final form that simulates actual system is given in Figure 3.5.

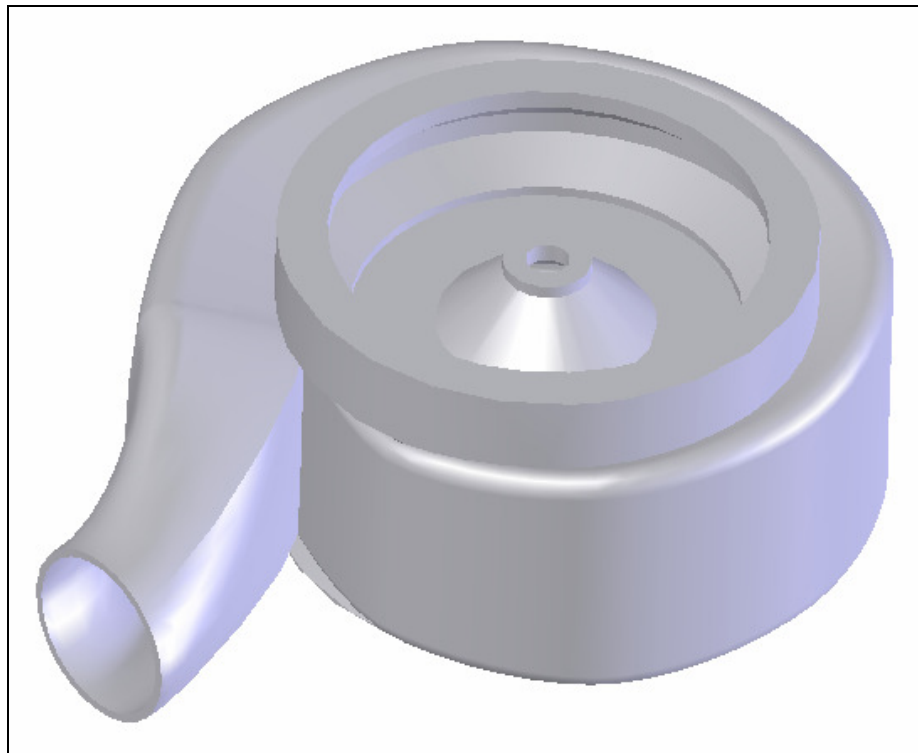


Figure 3.1 – Solid model of the volute (case 1)

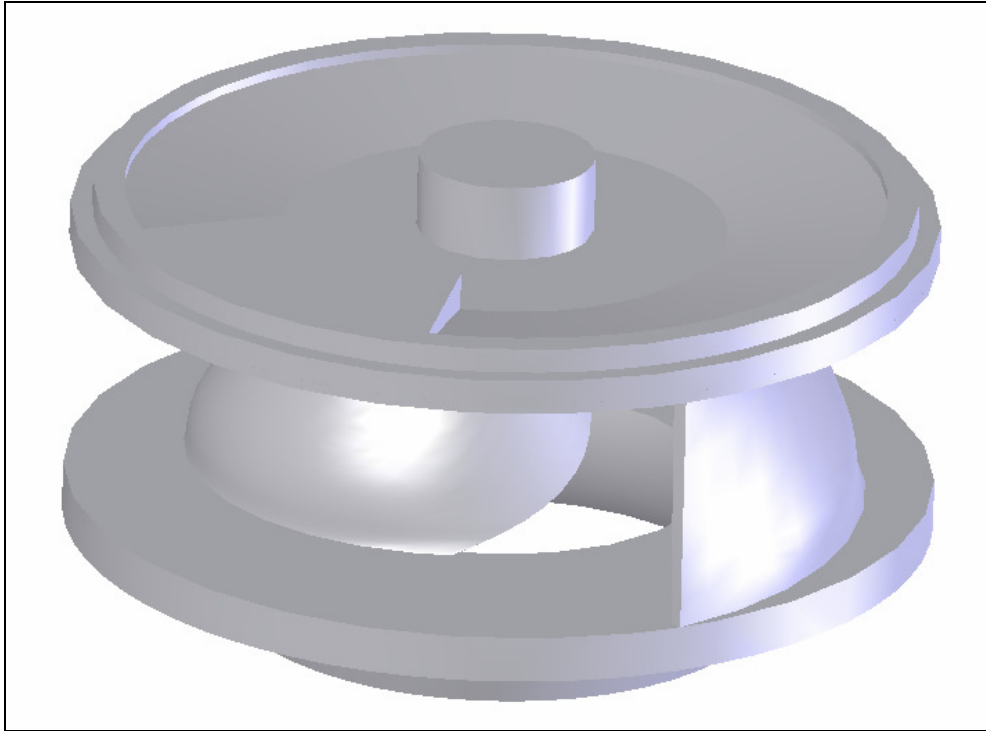


Figure 3.2 – Solid model of the impeller (case 1)

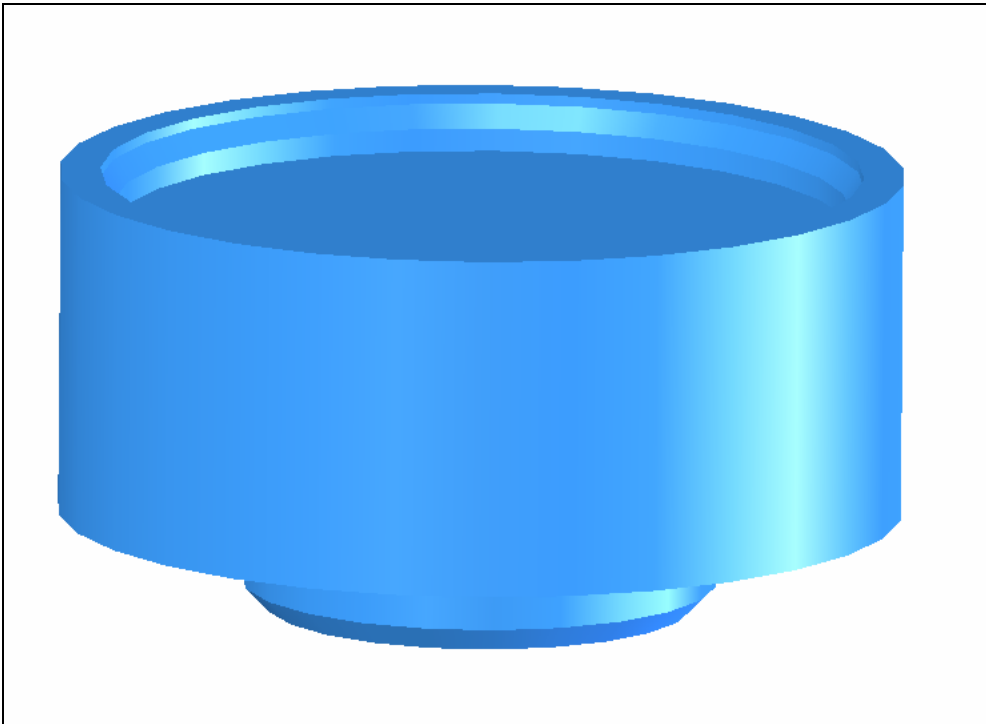


Figure 3.3 – Solid model of rotating region (case 1)

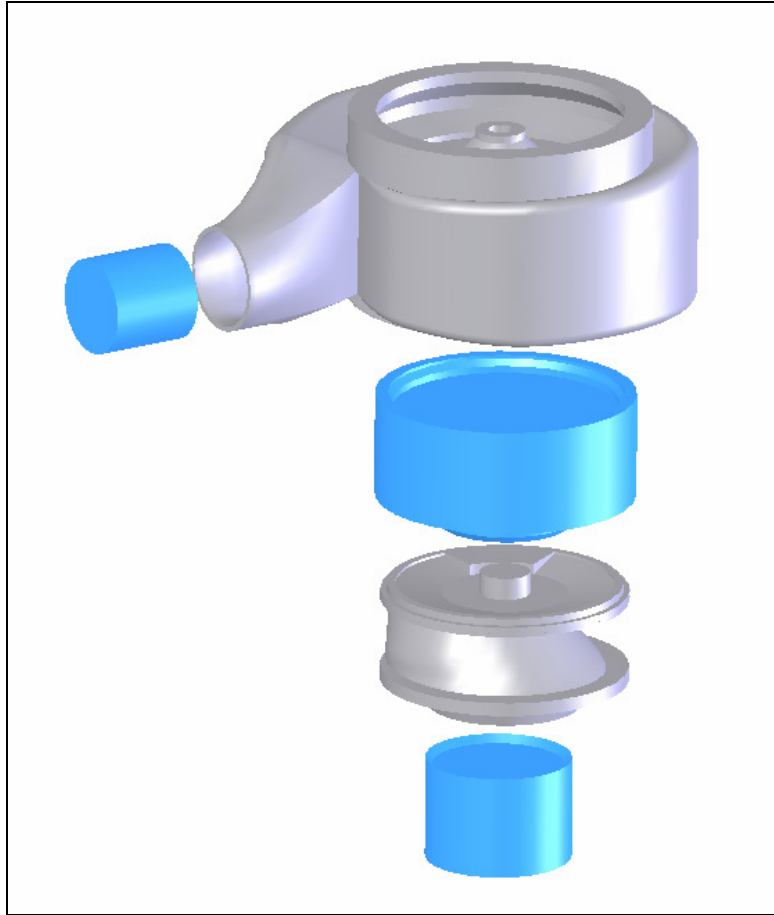


Figure 3.4 – Exploded view of solid model assembly (case 1)

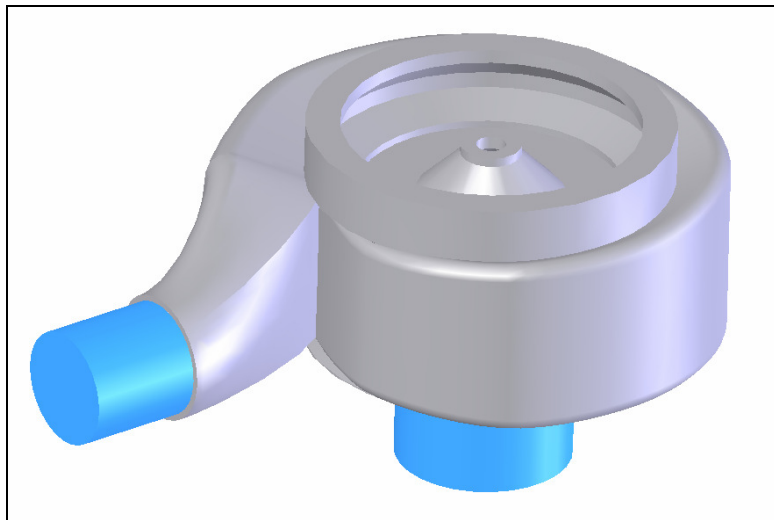


Figure 3.5 – Final view of solid model assembly (case 1)

After transferring the solid model assembly to the CFD program, fluid volumes and impeller volume are meshed. As a result of the meshing process, about 970000 fluid and 163000 solid elements are generated, which correspond to node numbers of about 241000 and 24000, respectively. To give a more physical sense of the mesh used, some views of the meshed control volume are given in Figures 3.6-8.

CFD analysis of case 1 is made at a single operating point that is near to the best efficiency point of the pump. Firstly, a static pressure that corresponds to a head of 27.6 m is defined to the far end of the outlet plug. The lateral surfaces of the inlet and outlet plugs are defined as wall. At the lower surface of the inlet plug, static pressure is assigned to be zero gage. Finally, a rotating speed of 1450 rpm is assigned to the rotating region and the solution is started.

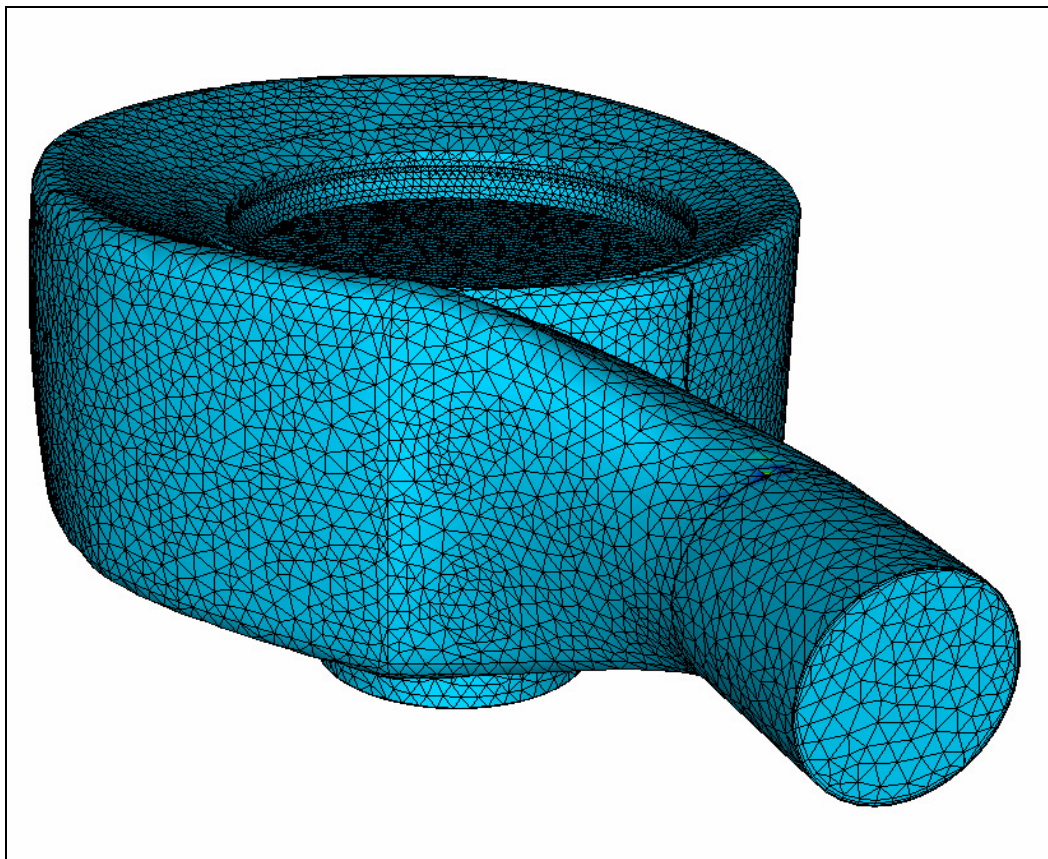


Figure 3.6 – Mesh used in the solution (view-1) (case 1)

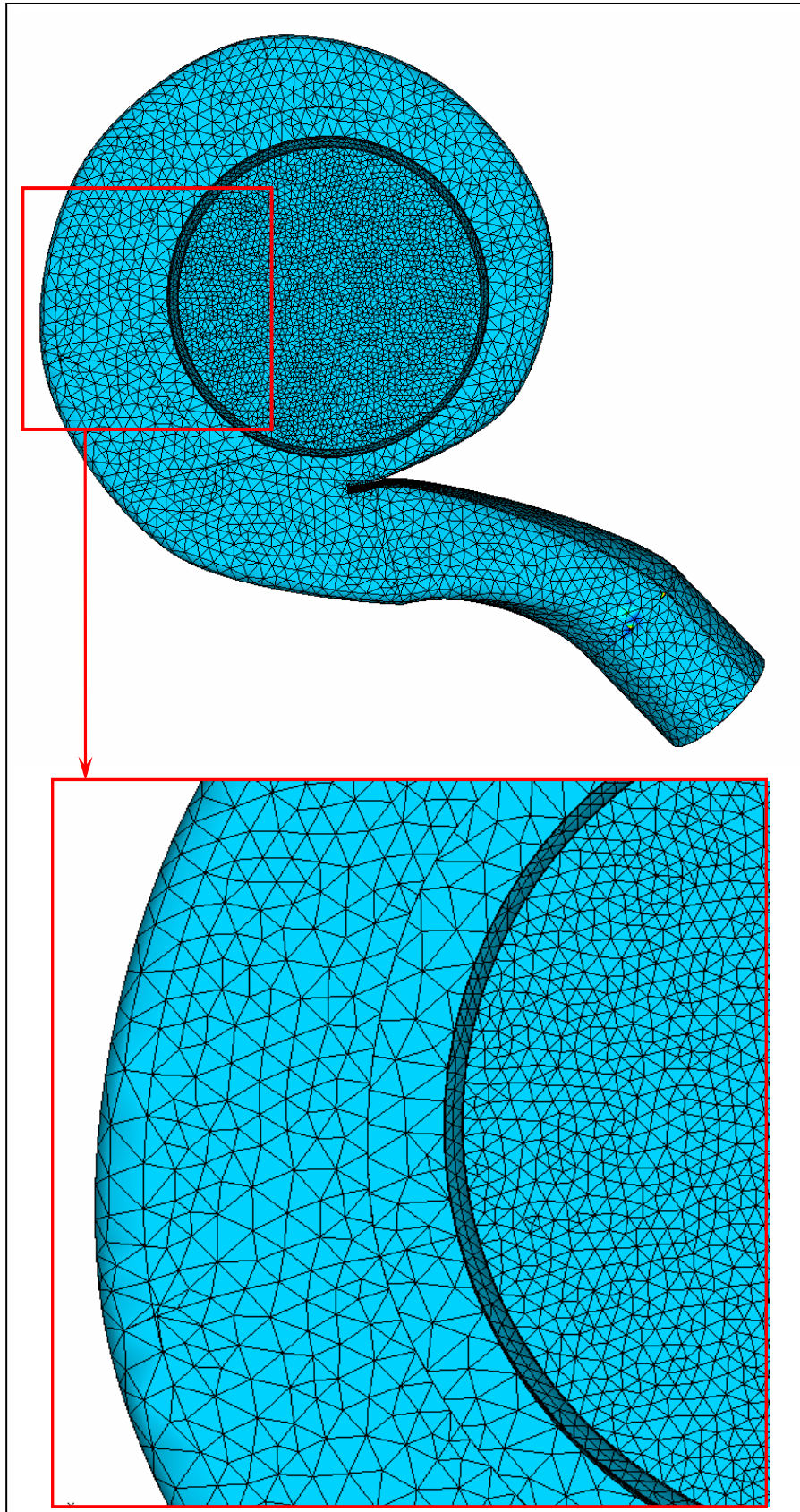


Figure 3.7 – Mesh used in the solution (view-2) (case 1)

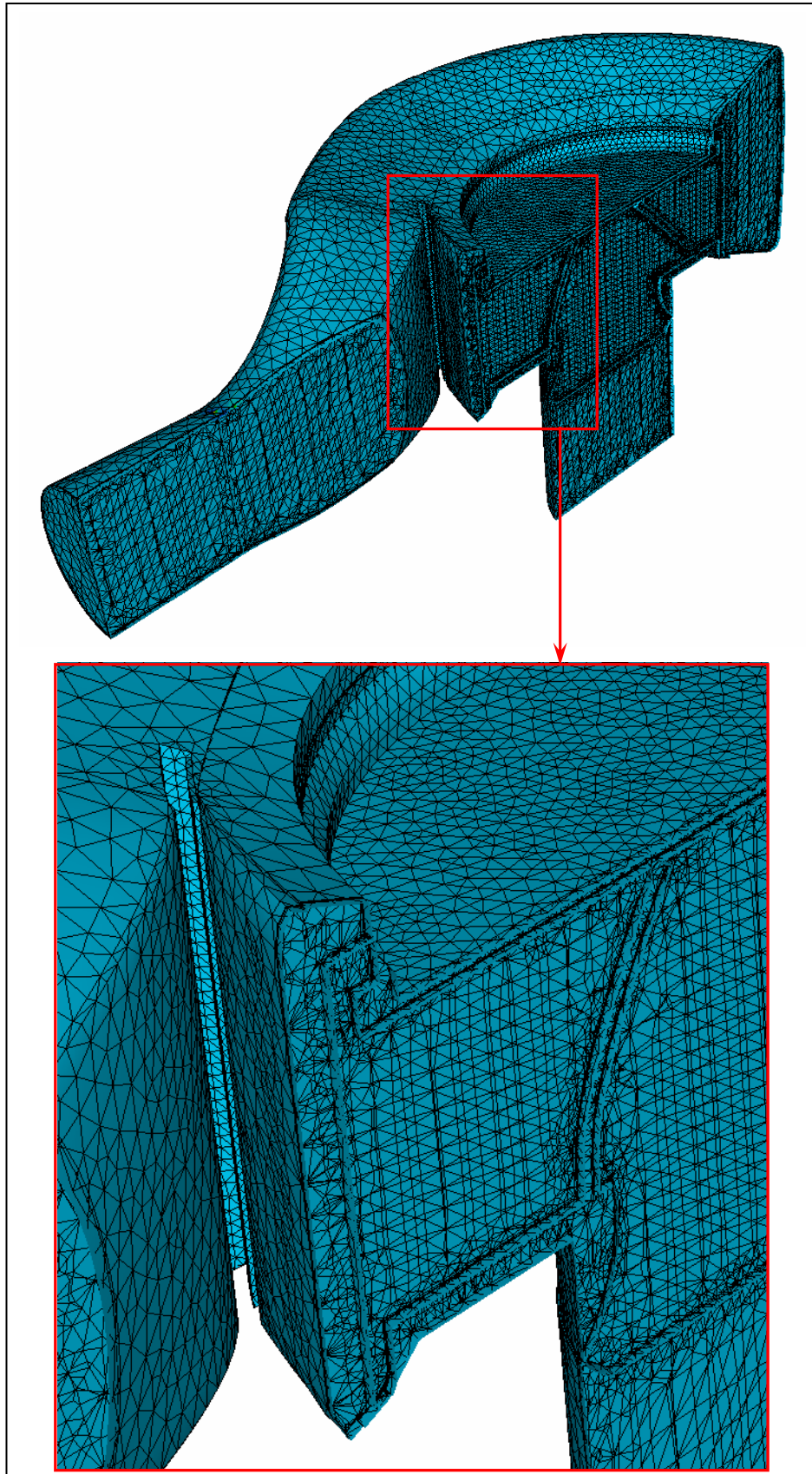


Figure 3.8 – Mesh used in the solution (view-3) (case 1)

The solver is run for 1470 time steps, which correspond to approximately 12.3 revolutions of the impeller. Solution lasted about 113 hours.

Convergence monitor of the solution is given in Figure 3.9. Although the velocity and pressure residuals satisfied the convergence criteria given in Reference Manual [24], at about 800 time steps, the program is kept running in order to observe the differences in pressure and flow rate values of the pump between successive time steps. Since the observed differences are quite small, the solution is accepted to be converged. The intervals between successive peaks of the pressure and velocity residuals on the convergence monitor correspond to one revolution of the impeller.

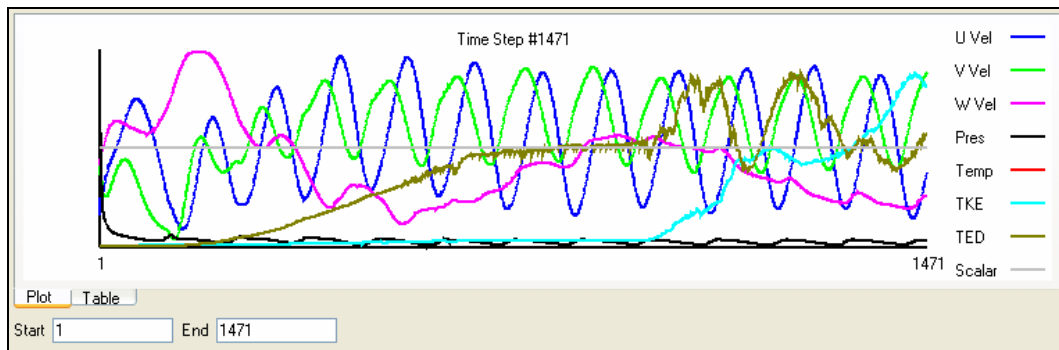


Figure 3.9 – Convergence monitor (case 1)

The details of the solution showing flow characteristics inside the pump are given in Figures 3.10-14. In Figure 3.10, absolute velocity vectors on a vertical cut plane coincident with the axis of rotation are given. The gaps between the sealing surfaces of impeller, volute and suction flange are closed in this solution for the sake of simplicity. Therefore, the leakage of pumping fluid through the cavities above and below the impeller is restrained in this analysis. In this respect, volumetric efficiency is not considered in case 1. The distribution of velocity vectors points out the nonuniformity of flow at the inlet of impeller on both sides of rotation axis, in Figure 3.10. This nonuniformity is a result of usage of single blade impeller.

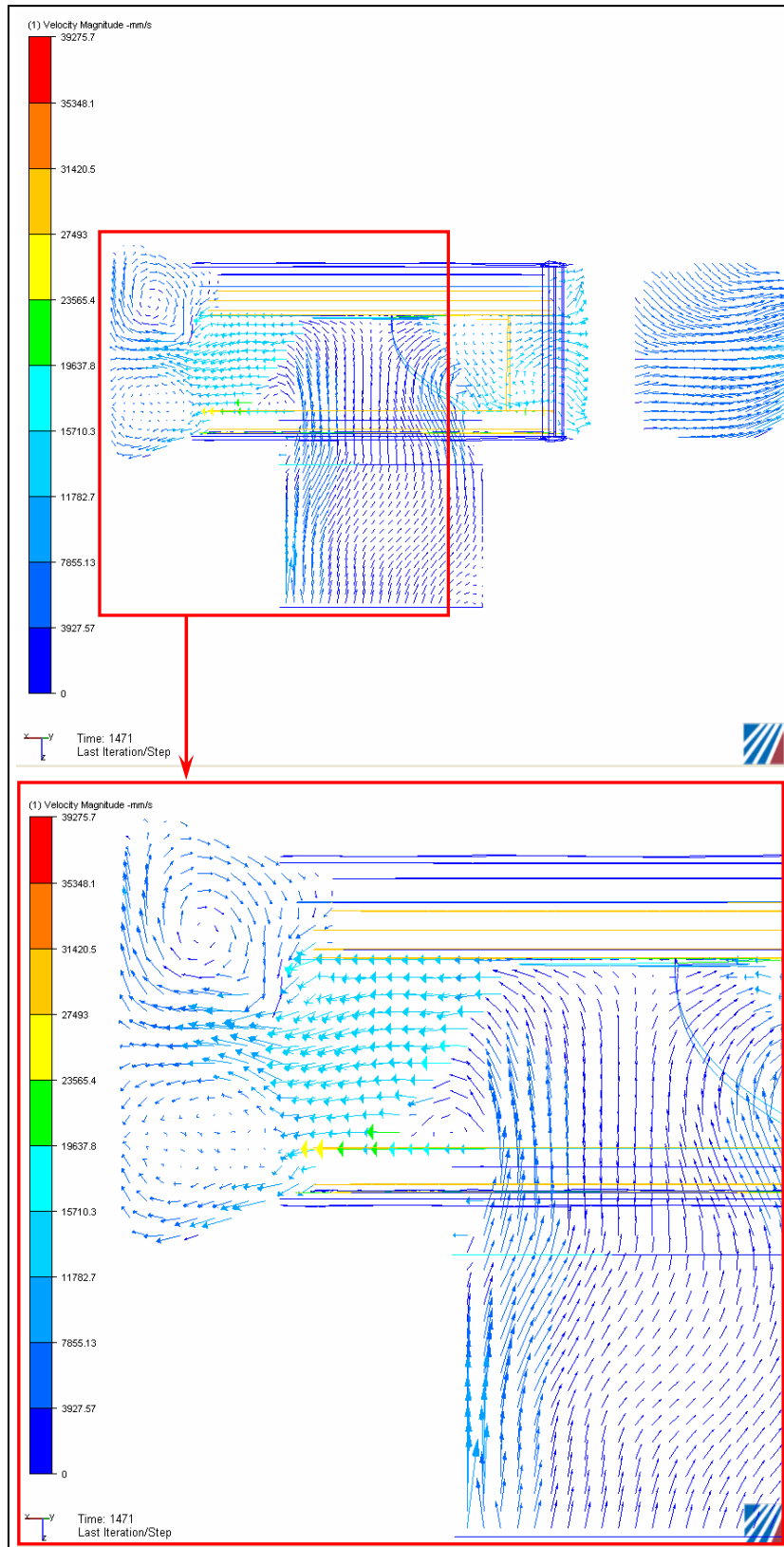


Figure 3.10 – Absolute velocity vectors inside the pump on a vertical cut plane coincident with the axis of rotation (case 1)

Another important point to discuss in Figure 3.10 is the vector characteristics in the volute. As it is stated in the design of volute, the volute area has to be increased for nonclog pumps in most cases for the sake of handling solid particles. For the volutes, which have large divergence angles, increase in the volute area results in significantly high volutes when compared with the height of the impeller. As a result, fluid entering the volute directs through the regions at the upper and lower walls of the volute. This motion is observed in Figure 3.10, since the divergence angle of the volute analysed in case 1 is large.

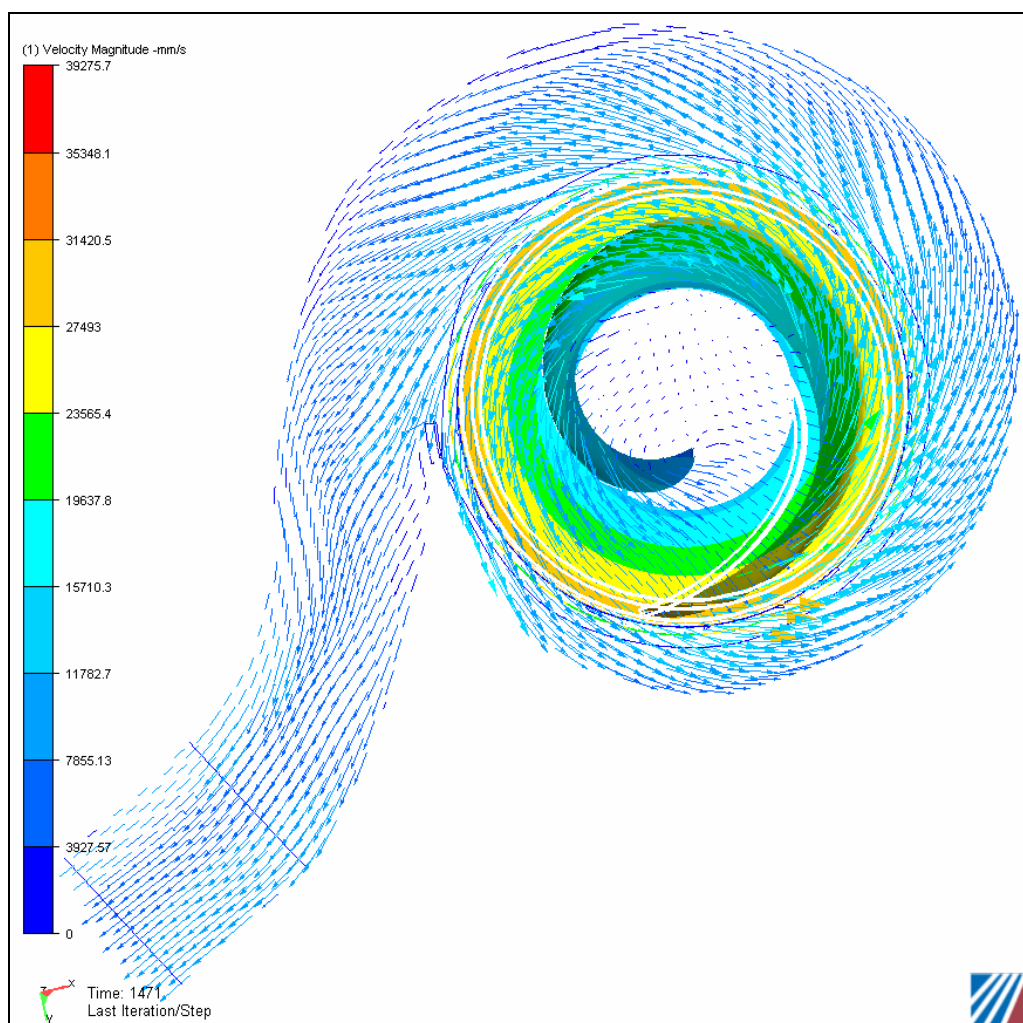


Figure 3.11 – Absolute velocity vectors inside the pump on cut plane perpendicular to the axis of rotation and coincident to the midplane between the hub and shroud (case 1)

Absolute velocity vectors on a cutplane perpendicular to the axis of rotation and coincident to the midplane between the hub and shroud of the impeller are given in Figure 3.11. A slight distortion in the velocity vectors is observed in the vicinity of tongue in Figure 3.11.

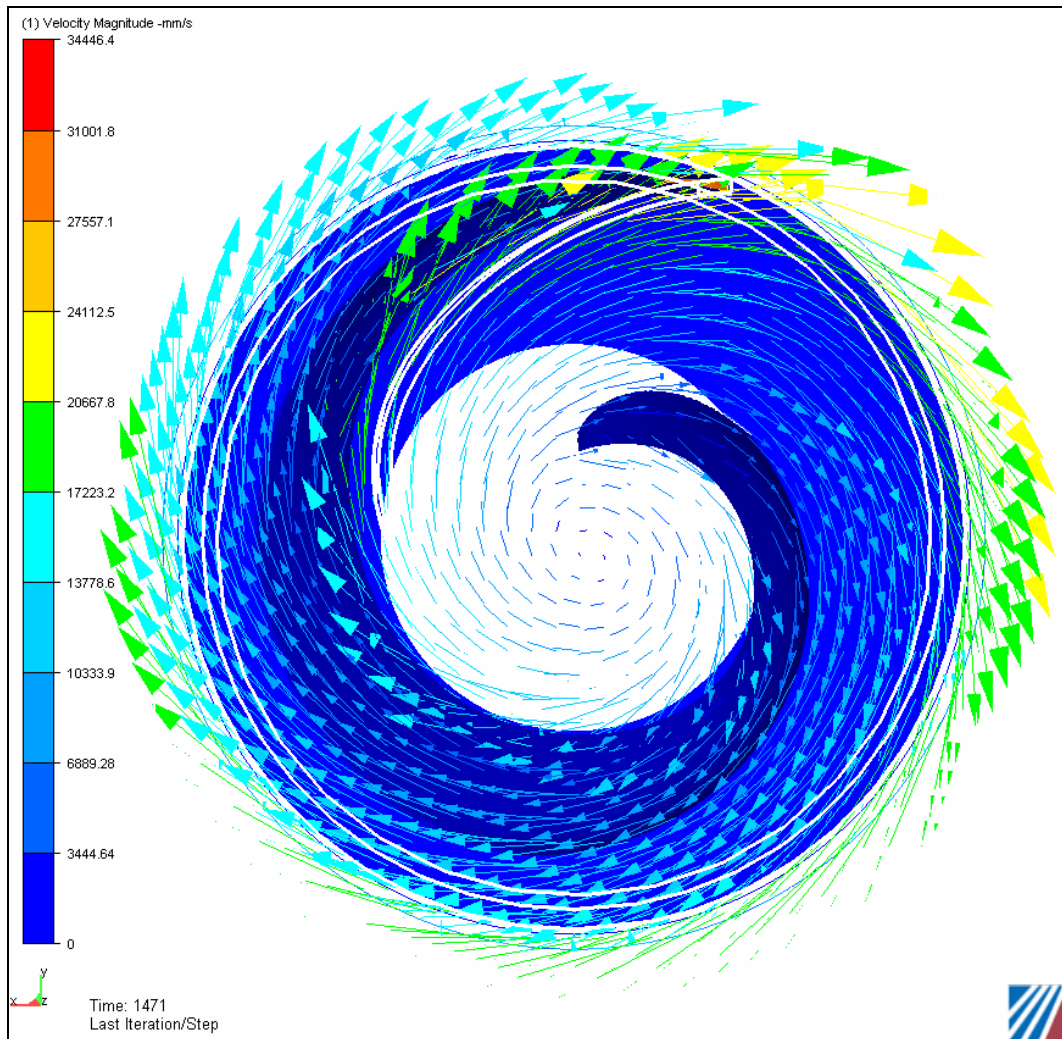


Figure 3.12 – Relative velocity vectors on the midplane of the impeller (view 1) (case 1)

Relative velocity vectors on the midplane of the impeller are given in Figures 3.12 and 3.13. A smooth and uniform change in the directions and magnitudes of the

velocity vectors is observed in these figures. Also, on the basis of CFD analysis results, it can be said that the flow does not separate from the blade surface for the pump considered in case 1.

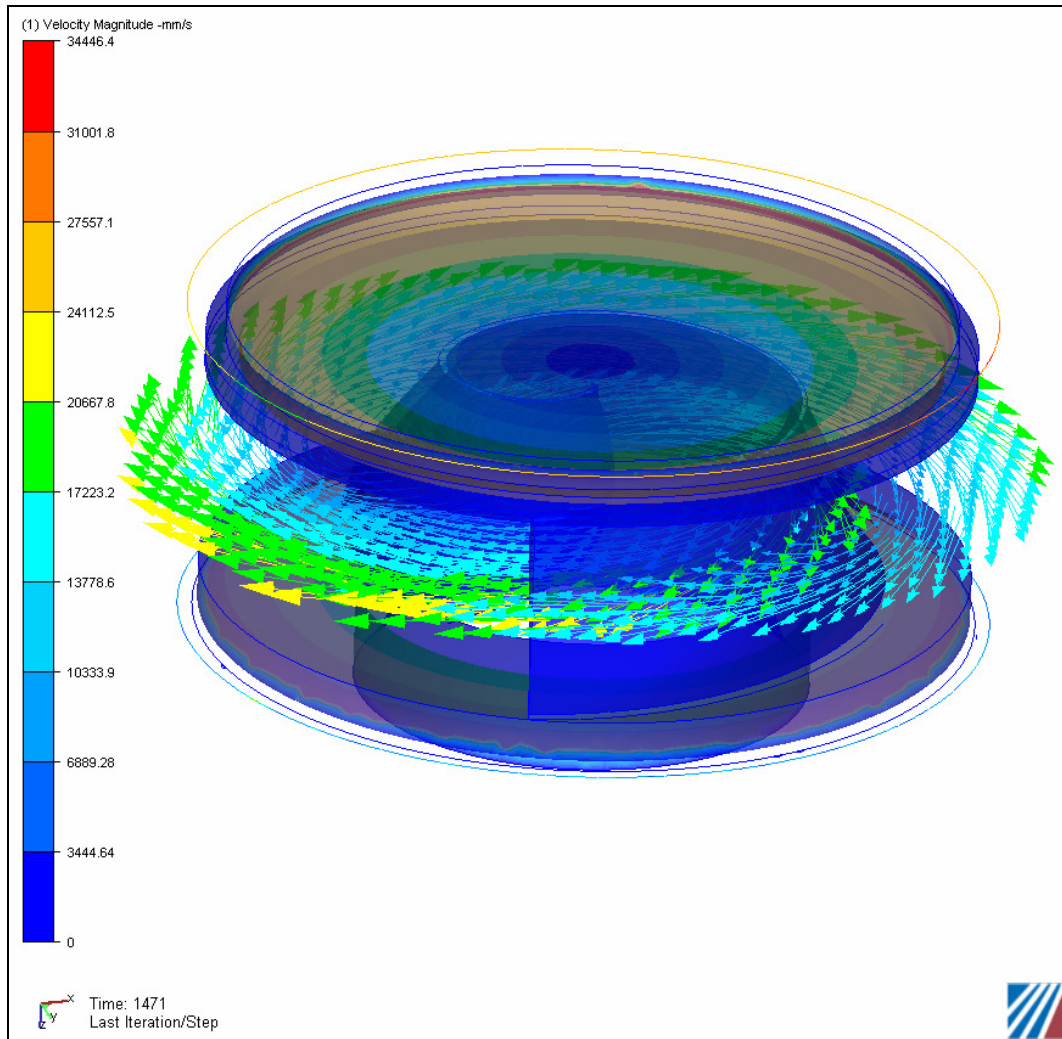


Figure 3.13 – Relative velocity vectors on the midplane of the impeller (view 2) (case 1)

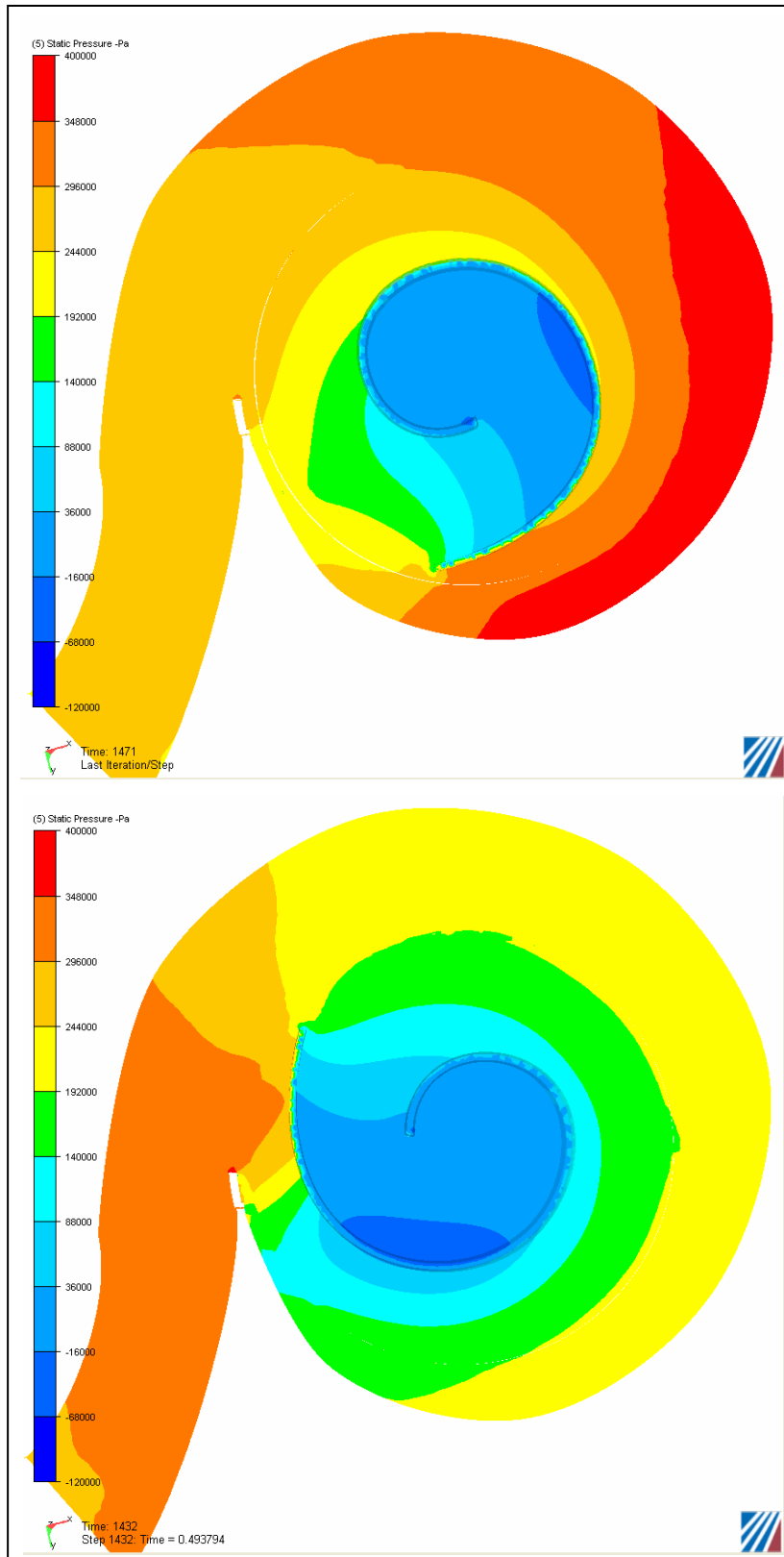


Figure 3.14 – Static pressure distribution in the pump for different positions of impeller blades (case 1)

Figure 3.14 shows the static pressure distribution in the pump for different positions of impeller blade. The significant difference between two distributions pointed out the nonuniformity of the flow in the pump caused by single blade impeller.

As a result, the pump is calculated to deliver a flow rate of 138.4 l/s against a head of 30.5 m with a hydraulic efficiency of 74%. Comparison of the result of CFD analysis and the characteristics obtained by testing the pump is given in Chapter 5.

3.4 Analysis and Results of Case 2

As soon as the design procedure given in Chapter 2 was finished, hydraulic characteristic of the designed pump is investigated by numerical experimentation. Following the procedure mentioned above, firstly the necessary solid models are prepared (Figures 3.15-18).



Figure 3.15 – Solid model of the volute (case 2)

At this stage, a different approach in determining the form of inlet plug is used when compared with case 1. Instead of extending the pump inlet geometry up to a sufficient height to form the plug, the base and the inlet section of the pump is completely submerged into a large volume of fluid. In other words, the inlet plug used in the analysis of case 2 is much more larger than the previous one. Obviously, the latter approach is closer to the actual system. However, obtaining a more realistic control volume in a CFD analysis is a matter of optimising the element or node number and therefore, it is limited with the memory of the computer employed.

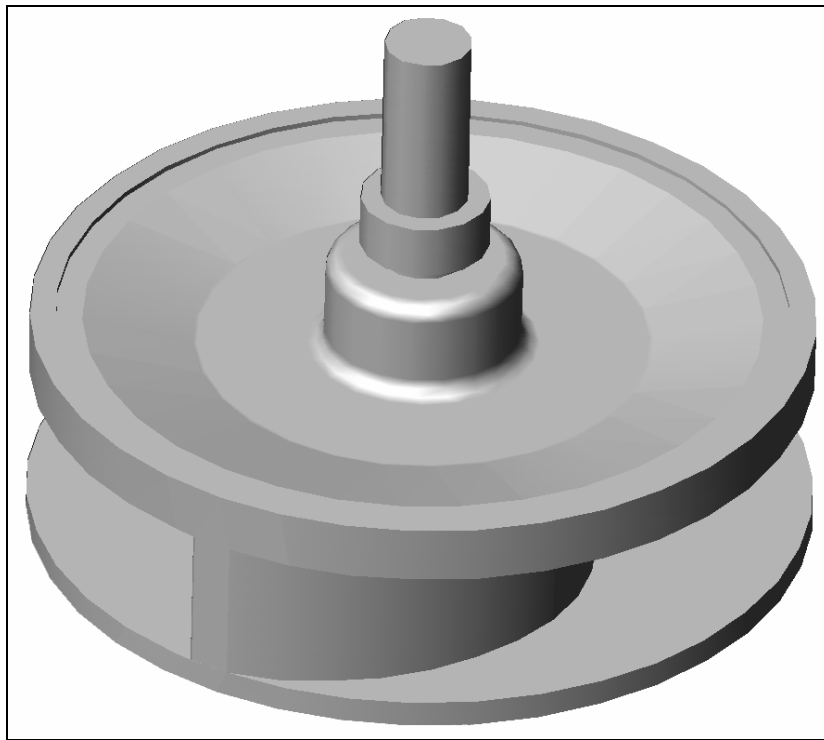


Figure 3.16 – Solid model of the impeller attached to the shaft together with mechanical seal pair (case 2)

Assembling the solid models together, a physical model of the actual system is obtained. Exploded and final views of solid model assembly are given in Figures 3.19 and 3.20, respectively.

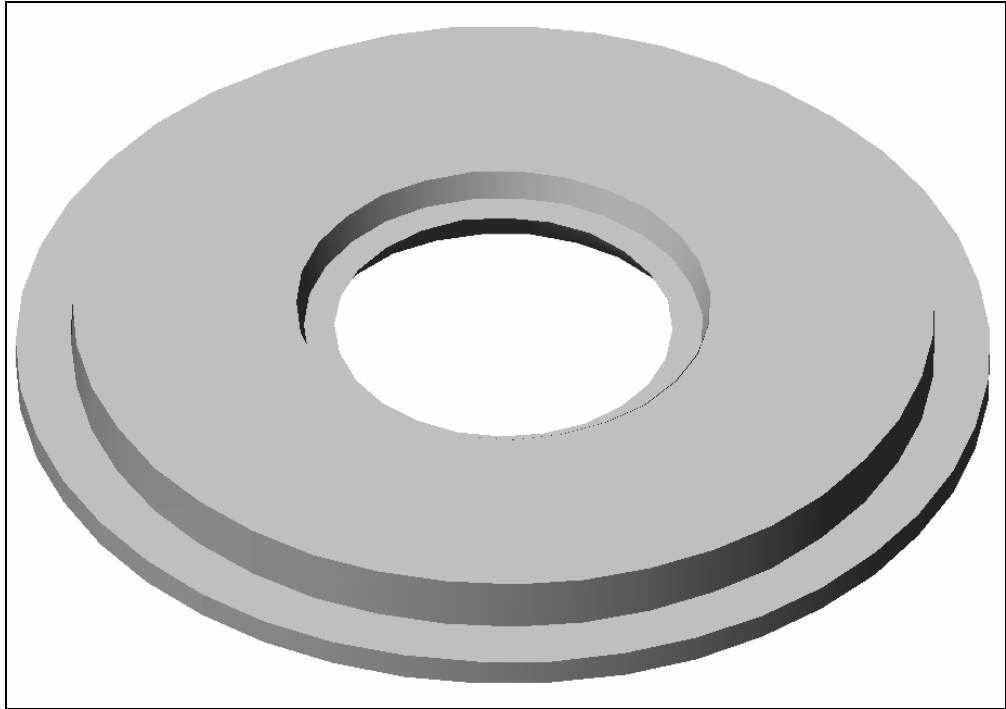


Figure 3.17 – Solid model of suction flange of the base (case 2)

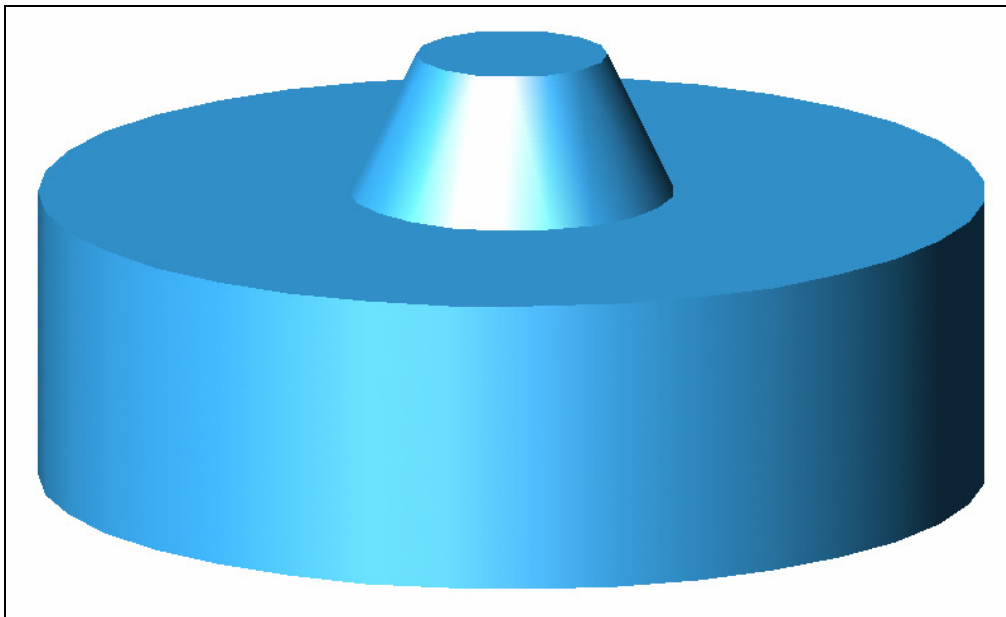


Figure 3.18 – Solid model of rotating region (case 2)

The solid model assembly is then transferred to the CFD program and meshed considering the important points mentioned under “Meshing” topic. The control volume is divided into about 2.1 million elements, which correspond to a node number of about 475000. More specifically, about 1.7 million fluid and 0.4 million solid elements are generated, which correspond to about 412000 and 63000 nodes, respectively. Some views of the meshed control volume are given in Figures 3.21-23, in order to give an idea about the dense of the mesh used.

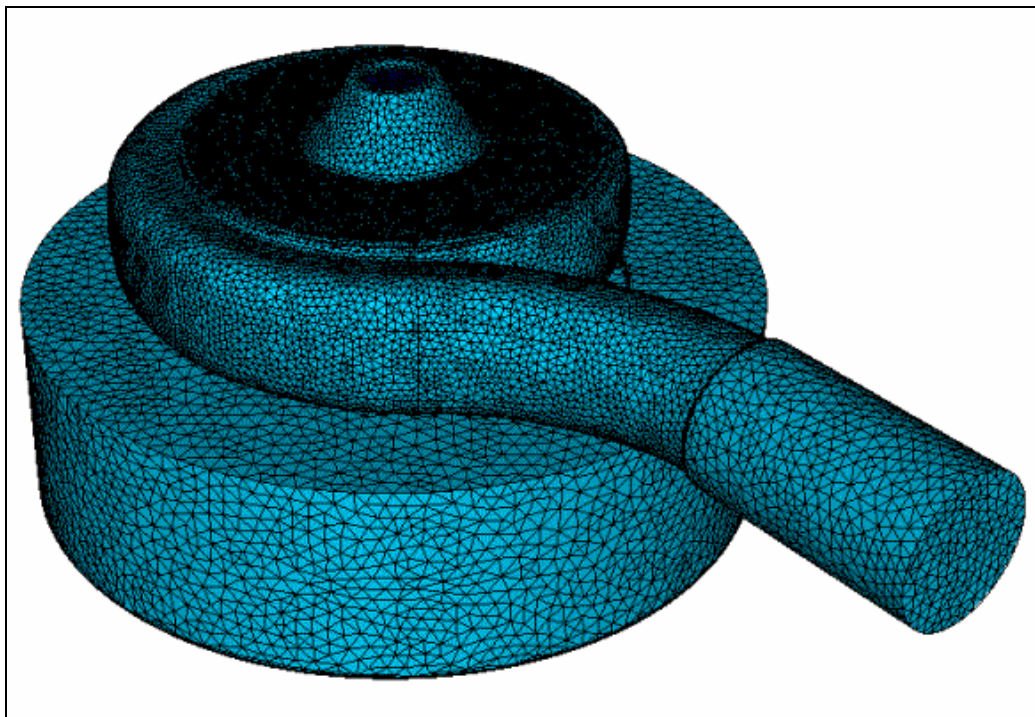


Figure 3.21 – Mesh used in the solution (view-1) (case 2)

Coming to the definition of boundary conditions step, static pressure head of fluid at the far end of outlet plug is defined to be 8, 16, 20, 23, 26 and 30 m for 6 different operating points. Boundary condition on the lateral surface of the outlet plug is defined as slip symmetry. The lower surface of inlet plug is defined to be wall since the pump is to be placed on the ground in the actual case. At the lateral surface of inlet plug, static pressure is assigned to be zero gage.

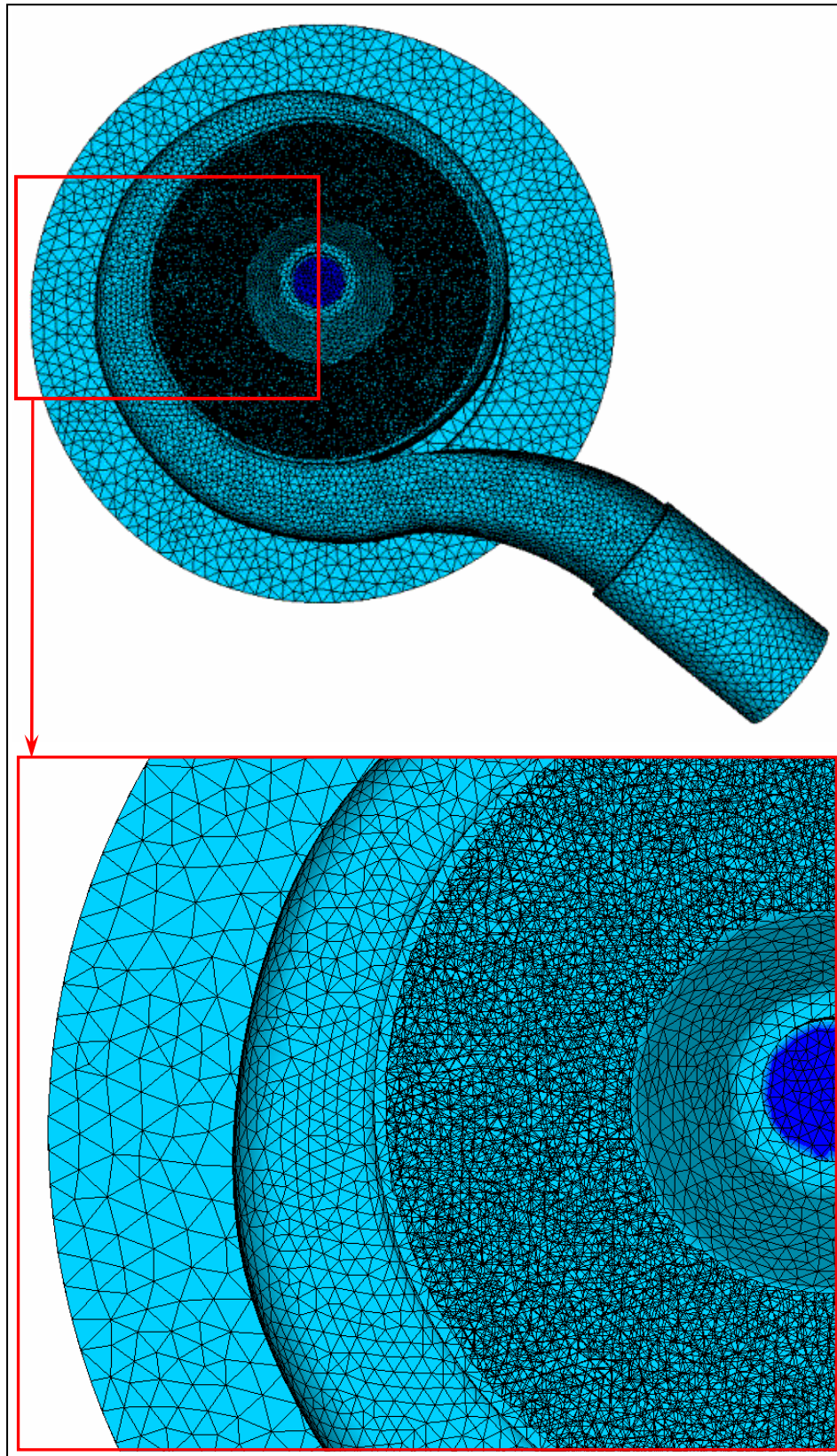


Figure 3.22 – Mesh used in the solution (view-2) (case 2)

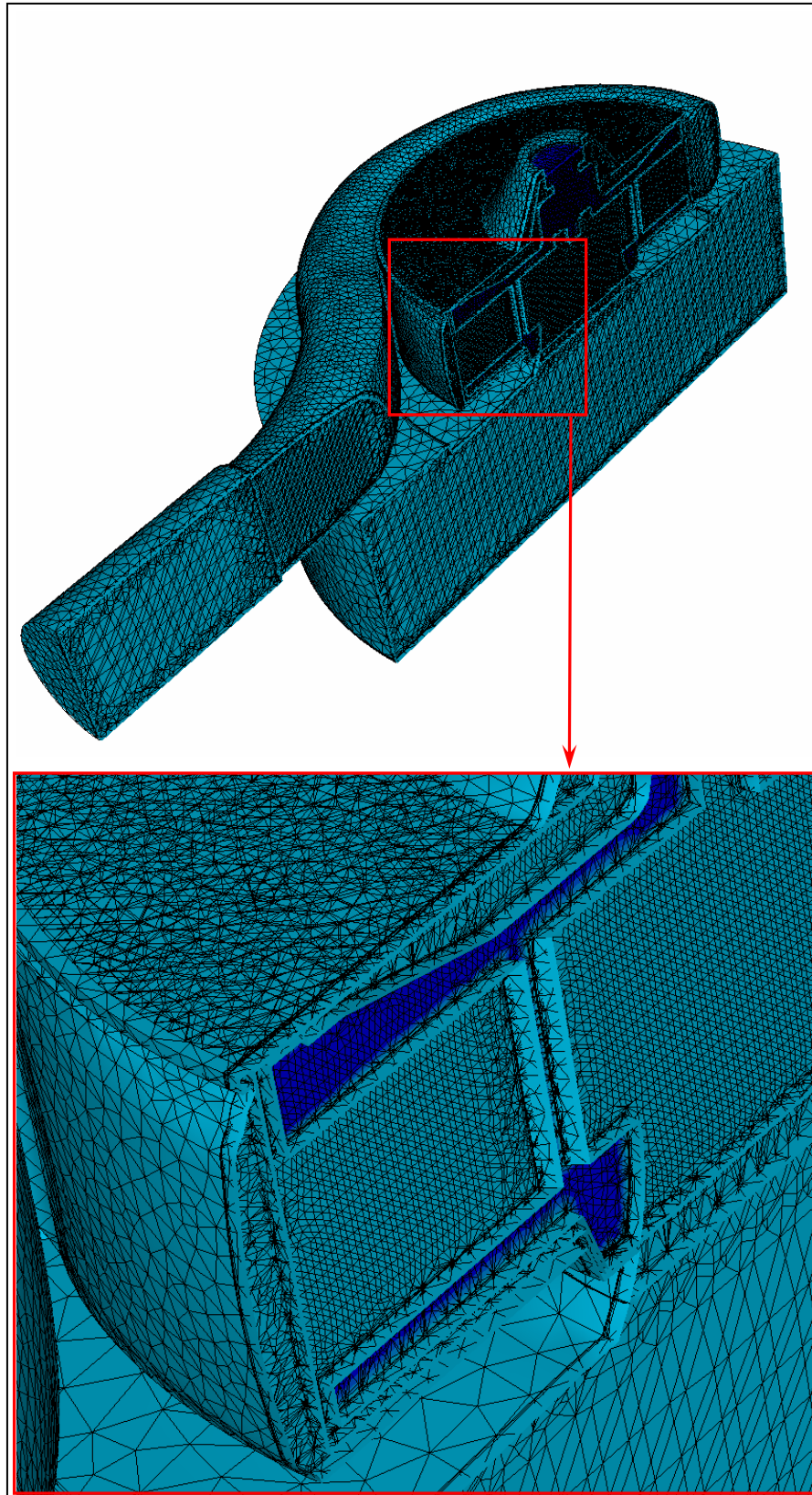


Figure 3.23 – Mesh used in the solution (view-3) (case 2)

In the first few trials for solving this system, static pressures are defined to both the lateral and upper surfaces of the inlet plug. However, the solution is diverged. Recommendation of the technical support of the CFD program is not to define static pressure as boundary condition on the adjacent surfaces. On the other hand, wall effects on the upper side of the inlet plug are not desired since this situation is far from the actual system. Therefore, slip symmetry is defined to the upper surface of inlet plug, and so converged solutions are attained. Finally, the rotational speed of the rotating region is defined to be 1000 rpm and the solver is run.

For each operating point, the convergence of the solution is attained at approximately 800 time steps, which correspond to about 6.7 revolutions of the impeller, considering 3° of rotation between successive time steps. Solution at each operating point lasted about 94 hours.

A sample convergence monitor is given in Figure 3.24. Although there are continuous oscillations in the residuals, the minimum, maximum and average values of them asymptote to a single value as it is stated as the indicator of convergence in Reference [24]. Each period between successive peaks on the pressure residual in Figure 3.24 corresponds to one revolution of the impeller. Details of the solution attained for the boundary conditions that correspond to the best efficiency point of the pump are given in Figures 3.25-3.30.

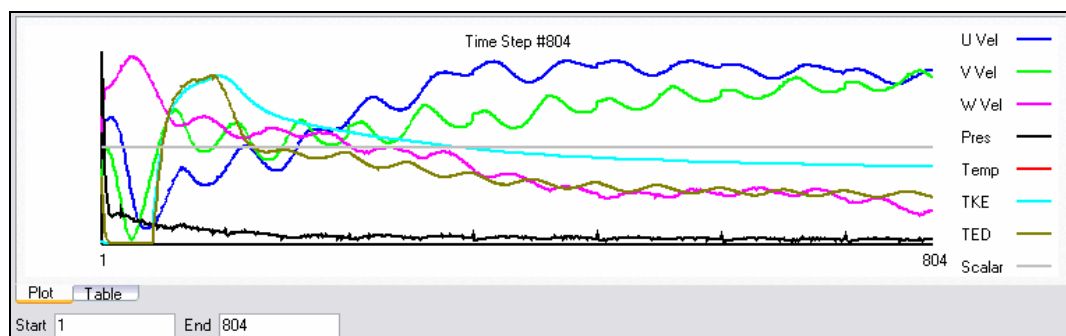


Figure 3.24 – Sample convergence monitor (case 2)

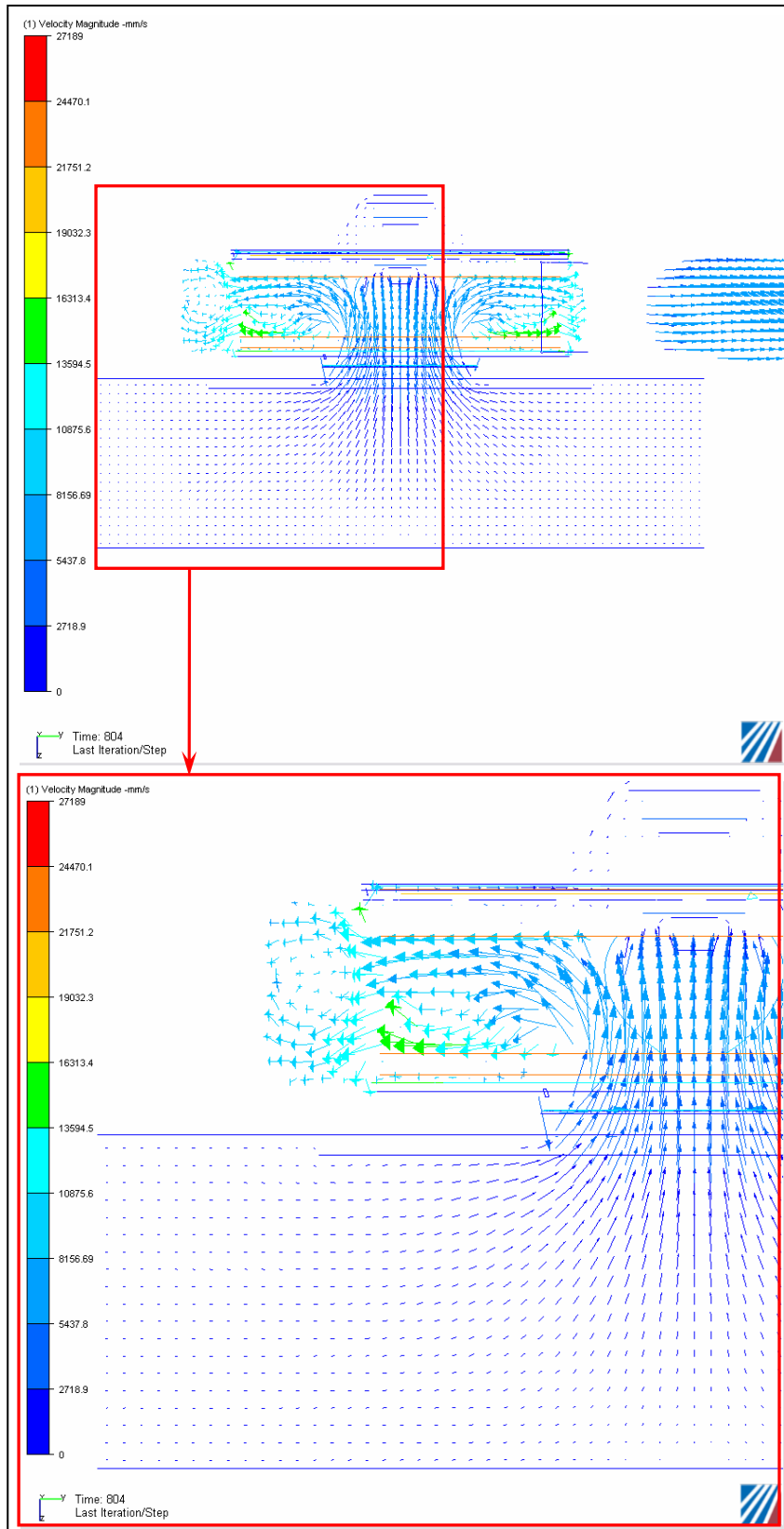


Figure 3.25 – Absolute velocity vectors inside the pump on a vertical cut plane coincident with the axis of rotation (case 2)

Figure 3.25 shows the absolute velocity vectors of pumping fluid in the control volume. The view is obtained on a vertical cut plane coincident with the axis of rotation. An important point to mention in this figure is the directional nonuniformity of the velocity vectors at the entrance of the impeller, immediately after an almost uniform and smooth distribution at the pump inlet. Obviously, the reason of this situation is using two parallel discs as hub and shroud profiles of the impeller, instead of smoothly bended profiles from the inlet to the exit. However, this situation was already taken into account at the design step for the simplicity of manufacturing. Therefore, it is not an unexpected result. Figure 3.25 also indicates a significant point of the analyse; different from most of the CFD analyses regarding with the flow inside the pumps, clearance between the sealing surfaces of the impeller and suction flange is not plugged. Instead, the actual system is simulated and backflow of the fluid from the exit to the inlet of the impeller through the clearance is observed. In other words, together with the hydraulic efficiency, the volumetric efficiency is also considered in this CFD analysis.

Figure 3.26 shows the absolute velocity vectors on a cutplane perpendicular to the axis of rotation and coincident to the midplane between the hub and shroud of the impeller. A significant discontinuity or nonuniformity on the velocity vectors is not encountered at the best efficiency point of the pump. The velocity vectors in the vicinity of the tongue, being one of the most critical locations of the pump, also point out a flow free of problems. Also, it can be seen that bending of the outlet guide is smooth enough to prevent any possible vortices in the flow due to bending.

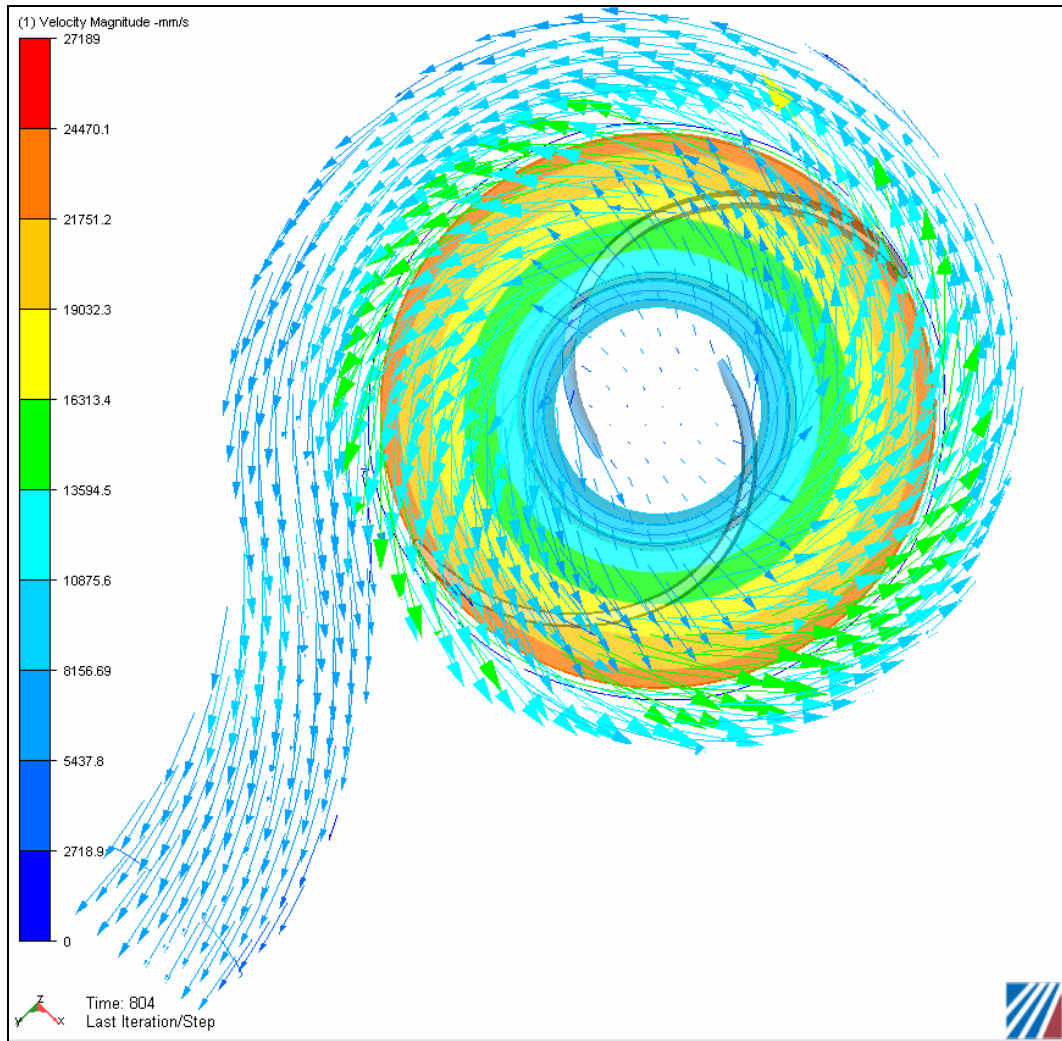


Figure 3.26 – Absolute velocity vectors inside the pump on cut plane perpendicular to the axis of rotation and coincident to the midplane between the hub and shroud (case 2)

The relative velocity vectors on the midplane of the impeller are shown in Figures 3.27 and 3.28. Obtaining the blade profile with “two-arc method”, [9], is more risky when compared with the other methods in the sense of flow separation on the blade surfaces. Because, the smoothness of the profile is left solely to the designer in this method. However no flow separations are seen in the results of CFD analysis (Figures 3.27 and 3.28).

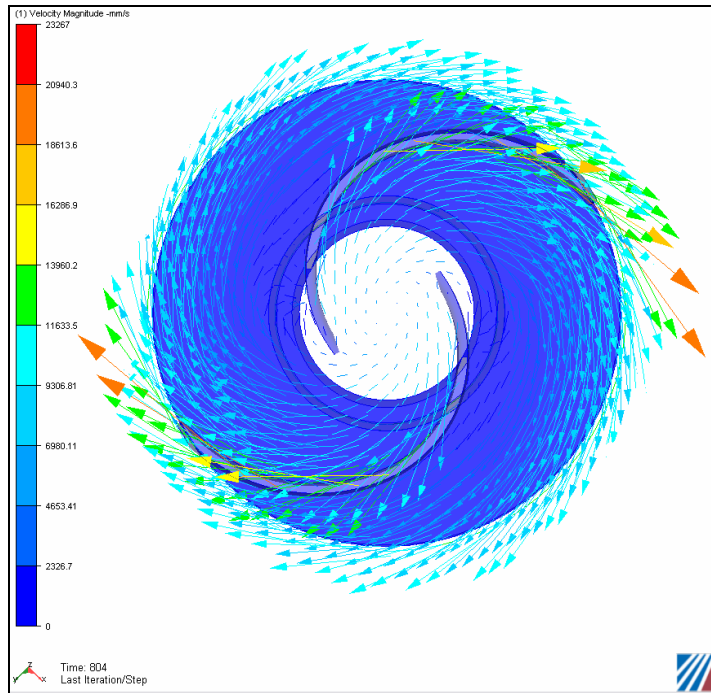


Figure 3.27 – Relative velocity vectors on the midplane of the impeller (view 1) (case 2)

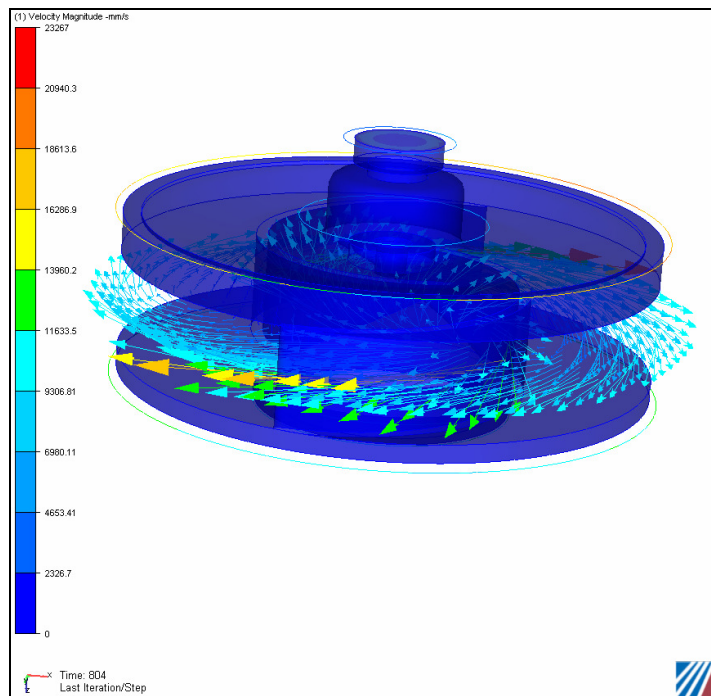


Figure 3.28 – Relative velocity vectors on the midplane of the impeller (view 2) (case 2)

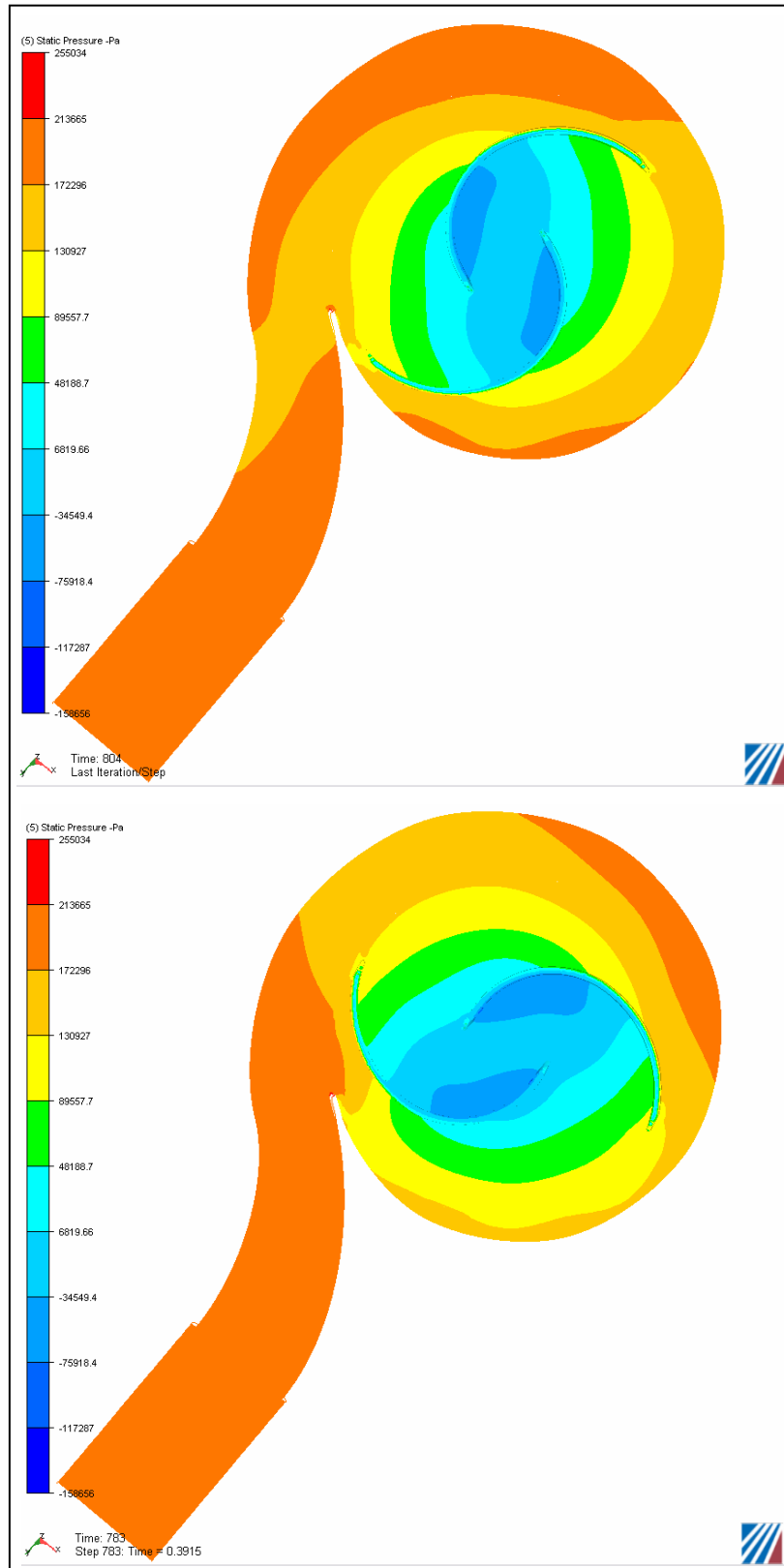


Figure 3.29 – Static pressure distribution in the pump for different positions of impeller blades (case 2)

The static pressure distribution of the flow inside the pump is given in Figure 3.29 for two different positions of the impeller blades relative to the tongue. Since the impeller has two blades, the static pressure distribution inside the pump varies significantly depending on the positions of blades. Eventhough the flow passages between the blades are quite wide, the pressure increase through impeller is observed to be quite uniform in the results of CFD analysis.

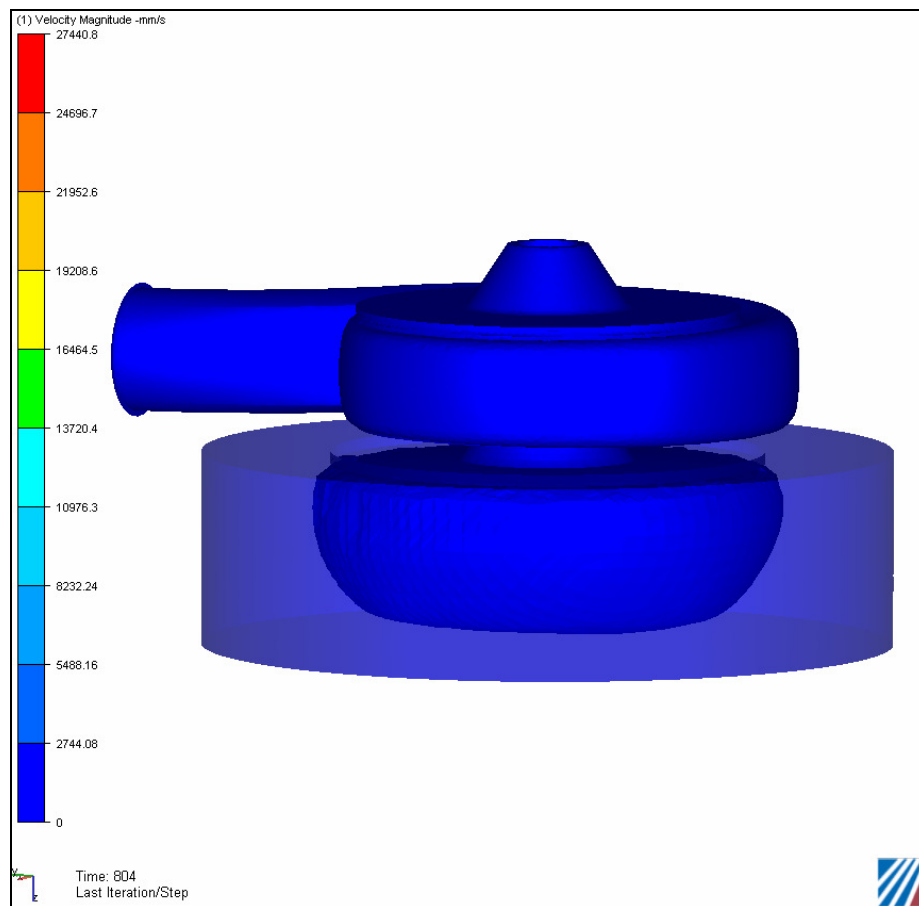


Figure 3.30 – Isosurface formed by the fluid having an absolute velocity of 0.3 m/s (case 2)

In Figure 3.30, isosurface formed by the fluid having an absolute velocity of 0.3 m/s is shown by the colour dark blue. The transparent cylindrical region is the suction domain (inlet plug). The shape of the isosurface indicates that a uniform suction is

attained in the CFD analysis. Also, size of the isosurface points out that, the diameter of the suction domain used in the analysis is large enough to simulate the actual system considering the regions having absolute velocities lower than 0.3 m/s as ineffective on the solution of the system.

Solving the system for 6 sets of boundary conditions, 6 operating points of the pump are obtained. Head versus flow rate and efficiency versus flow rate characteristic curves of the pump that are obtained by the CFD analysis are given in Figure 3.31.

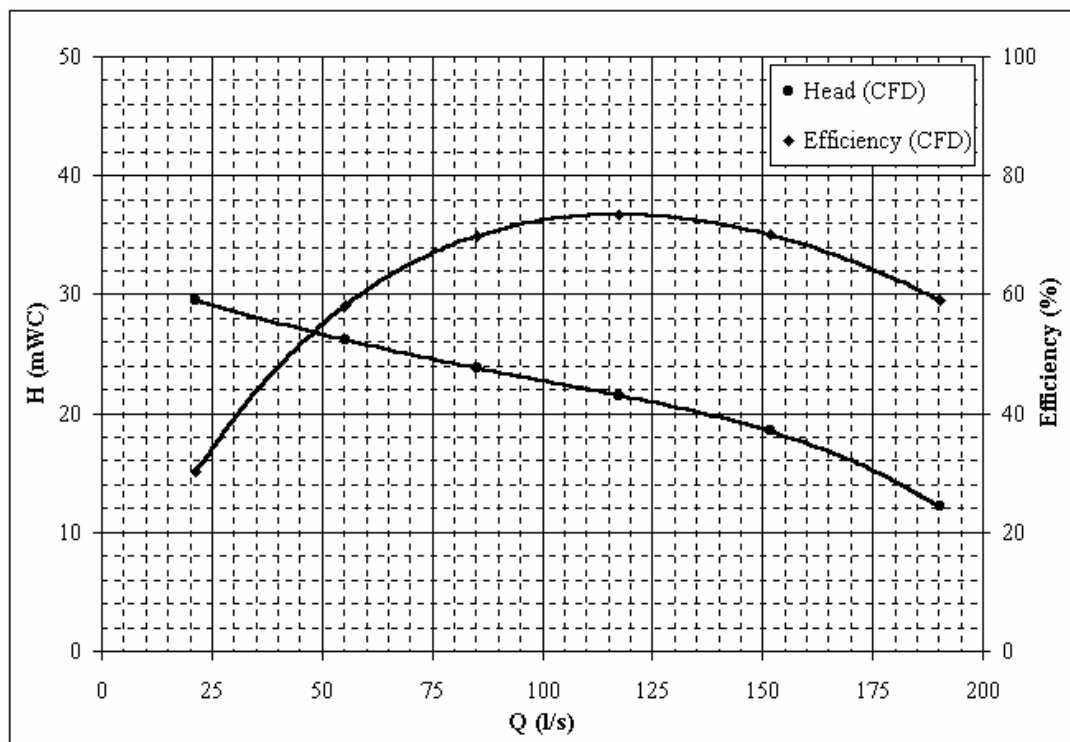


Figure 3.31 – Head versus flow rate and efficiency versus flow rate curves of the pump that are obtained by CFD analysis (case 2)

The efficiency values obtained by the CFD analysis include volumetric efficiency together with the hydraulic efficiency. Therefore, the only factor, which is not

considered in the CFD analysis to affect the overall efficiency, is the mechanical losses in the system. However, the calculated efficiency of the pump is too high to be explained with the negligence of hydraulic losses. Since the efficiency calculations in CFD analyses are based on the value of total torque exerted on the surfaces of rotating parts, the reason for such high values of efficiency may be due to miscalculation of total torque by the solver. Calculated pump characteristics are compared with the test results in Chapter 5.

CHAPTER 4

EXPERIMENTAL SETUP AND PROCEDURE

4.1 Test Stand

The pump tests, whose results are given and discussed in this study, are performed in the test stand of Layne Bowler Pump Company Inc. (Figure 4.1). Being accredited by Turkish Standards Institute in February 2005, test stand has measurement traceability to national standards.

Pump to be tested is carried and mounted to the well by using a crane, which has a capacity of 5 tons. There are three wells in the stand, which are opened to a pool having a depth of 9.6 m and a diameter of 3 m. A discharge pipe for each well, having butterfly type of vanes is present. Each discharge pipe has short intermediate pipes whose diameters are reduced at one end, in order to have flexibility in testing pumps of different discharge diameters with any of the discharge pipes. This reduction in the diameter is made by taking the flow rate limitations for each pipe diameter into consideration.

Whole testing system is controlled by the technical person, who is responsible from the test, by the help of control panel in the test control room. The control panel is connected to the main electric panel in order to start or stop the electric motor that drives the pump. It also has connections with the actuators of butterfly vanes that provide joystick control of outlet pressure of the pump to be tested. The stand has a maximum limit of 250 kW as input power to the motor. Apart from frequency control drive, four individual electric panels are present. They are used for input power ranges of 0-11 kW, 0-37 kW, 11-110 kW and 37-250 kW.

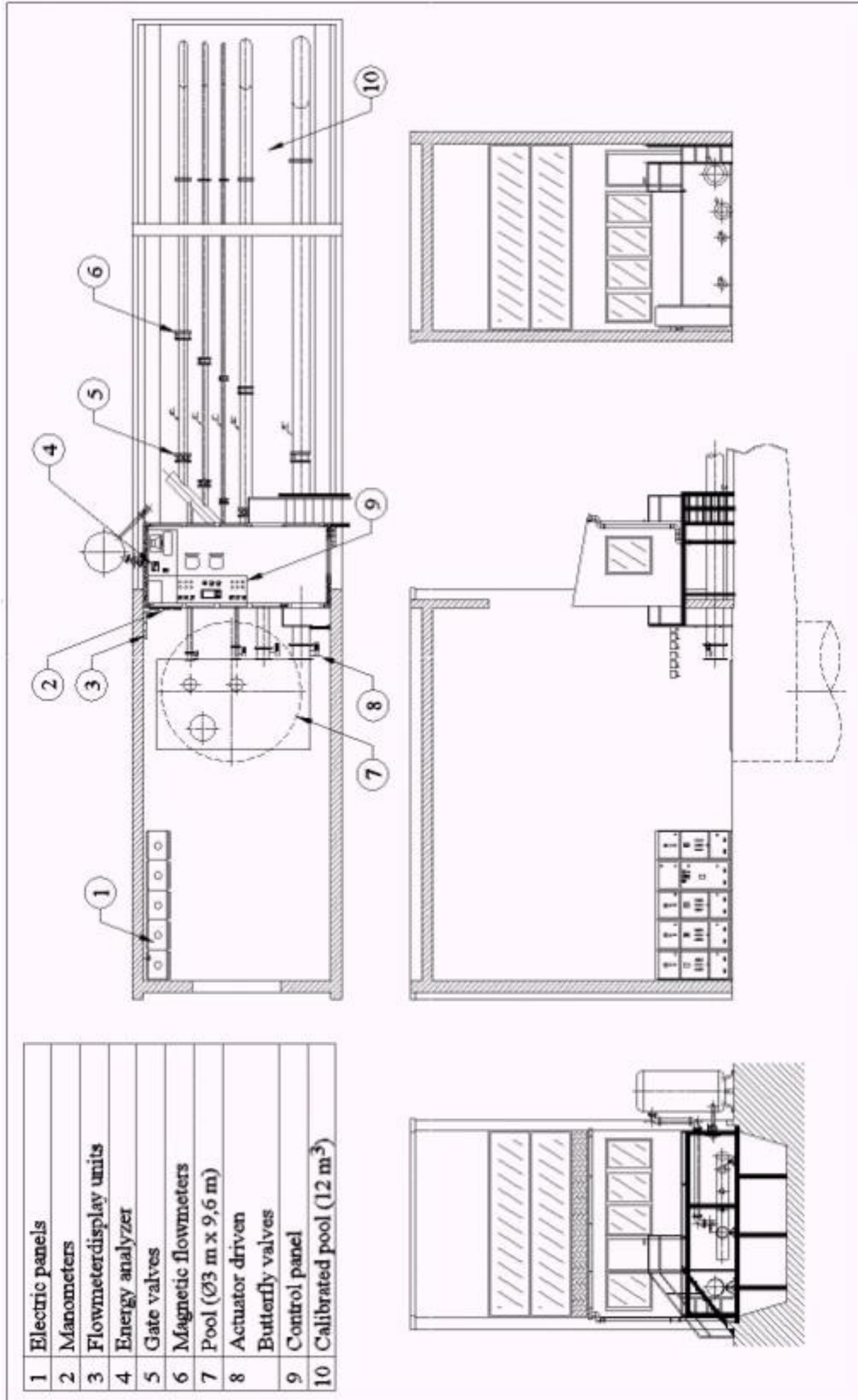


Figure 4.1 – Test Stand

With the frequency control unit, pumps up to 90 kW of motor input power can be tested at any alternative current frequency lower than 50 Hz. except for the cases that the limitation on the torque required to run the pump is exceeded. However, such cases can only be faced when high capacity pumps having large impellers are being tested. An energy analyser of maximum capacity 1000 A measures the electrical variables on the line driving the motor. There are 11 manometers, which are capable of measuring pressures up to 40 bars. The flow rate of the pump to be tested is measured by electromagnetic flowmeters that are mounted on different outlet pipes of diameters DN80, DN125, DN200, DN300 and DN450. Four of them are connected to each other by a gate type vane and collector system in order to be used in parallel arrangement. This system is capable of measuring flow rates up to 900 l/s. All the measuring instruments used in pump tests are being calibrated periodically.

The pump tests are made by using clean cold water as working fluid, although the pump is a special one, which is designed and manufactured to be used in sewage pumping. This is also the case recommended in the regarding standard, [26]. The standard describes the term “clean cold water” as water having maximum values of 40°C in temperature, 1.75×10^{-6} m²/s in kinematic viscosity, 1050 kg/m³ in density, 2.5 kg/m³ in non-absorbing solid particles and 50 kg/m³ in dissolved solid particles. The limitation on the solved gas content is set to the saturation value for the temperature and pressure of the fluid in the pump, [26]. Satisfying these limitations, the test results are acceptable for pumps that are used for pressurizing fluids having a maximum kinematic viscosity of 10×10^{-6} m²/s, maximum non-absorbing solid particles of 5 kg/m³ and a density varying from 450 to 2000 kg/m³, [26]. Since these limitations are also the design limitations of the pumps, that are declared when describing guarantee conditions, clean cold water can be used as working fluid of the pumps during performance tests. Another reason for using clean cold water is to have a reference test standard in nonclog pumps that are used for pressurizing a large variety of fluids in the sense of density, kinematic viscosity, size and shapes of

the particles included, homogeneity, etc. This is due to the difficulties in classifying the working fluid.

4.2 Test Setups

Two different test setups are used in this study. In the first one, the pump is driven by a VHS (vertical hollow shaft) electric motor. The second one is used to determine the final performance characteristics of the submersible pump.

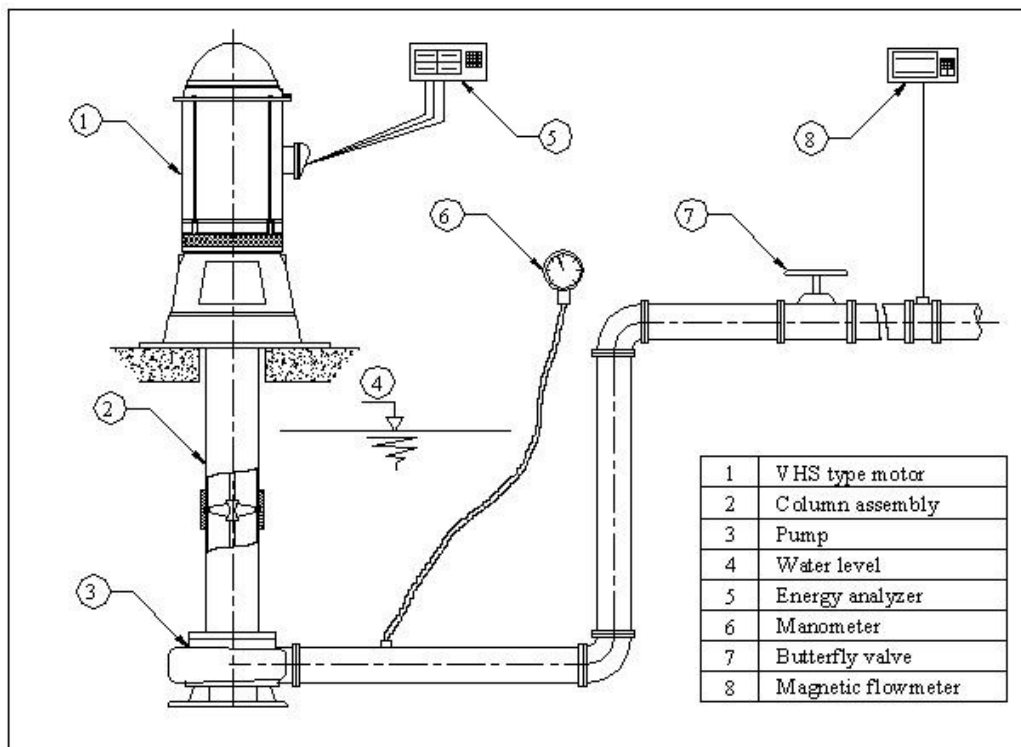


Figure 4.2 – Test setup-1

In test setup-1, a VHS motor is used to drive the pump, Figure 4.2. The motor is mounted on a discharge head, which is placed at the ground level. The power is transmitted from the electric motor to the pump by means of a water lubricated column assembly. In this respect, the system is similar to the one that is used in

water lubricated vertical turbine lineshaft pumps. Headshaft that passes through the interior cavity of the electric motor is connected to the motor by means of an adjusting nut and a key. Different from the vertical turbine pumps, this nut is not used for adjusting the vertical clearance of the pump. It only transmits the power to the headshaft. By couplings, headshaft, lineshaft and pumpshaft are connected to each other when sequenced from top to bottom.

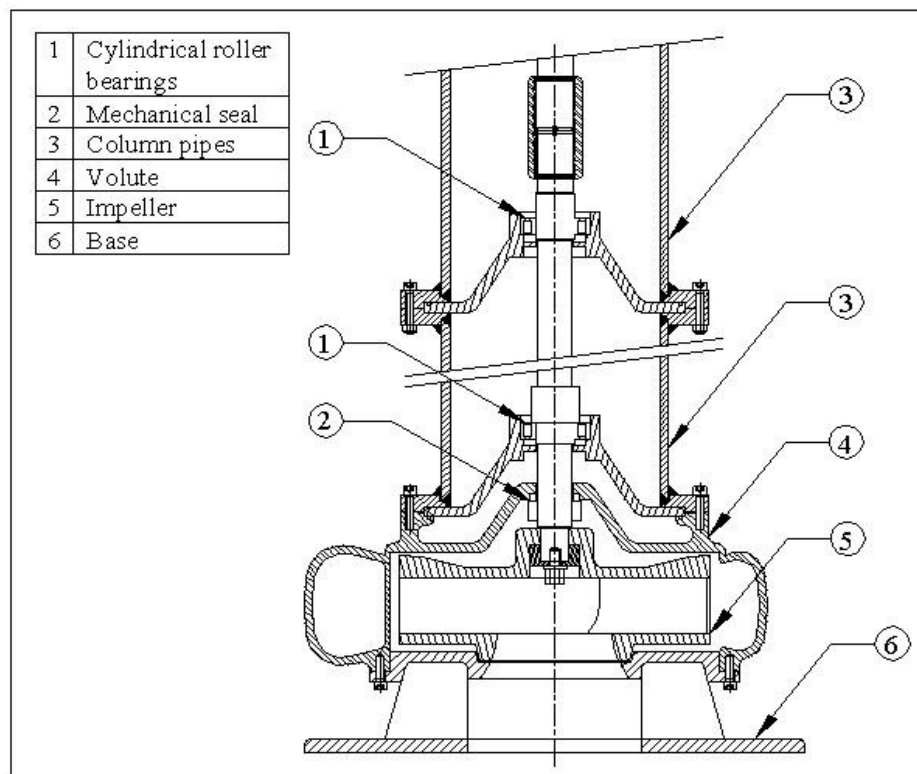


Figure 4.3 – Cross-sectional view of lower part of test setup-1

Inside the discharge head, a stuffing box assembly is located in order to prevent water to pass to the motor side as a result of the rotation of the shaft. The rotating system is fixed to the axis of rotation at 5 points; one inside the motor, one at the stuffing box and three inside the column assembly. Two bronze bushings are used at the stuffing box and column assembly. At the two axis fixing points near to the pump, two cylindrical roller bearings are used since their radial tolerance is less

than the bronze bushings (Figure 4.2). This bearing arrangement is changed for the inner structure of submersible pump as it is given in Chapter 2. Inside the volute, on top of the impeller, a mechanical seal pair is employed in order to prevent pumped fluid pass into the column pipes (Figure 4.3). Eventhough, the column pipes are filled with water from the discharge head before starting the pump, since the bronze bushings require water as working media in order to cool down. The mechanical seal pair used in the pump also prevents the water filled in the column pipes to leak, which would probably result in failure of the shaft due to overheating. In this respect, the column pipes are used to have a water column around the bushings and to carry the weight of the stationary components.

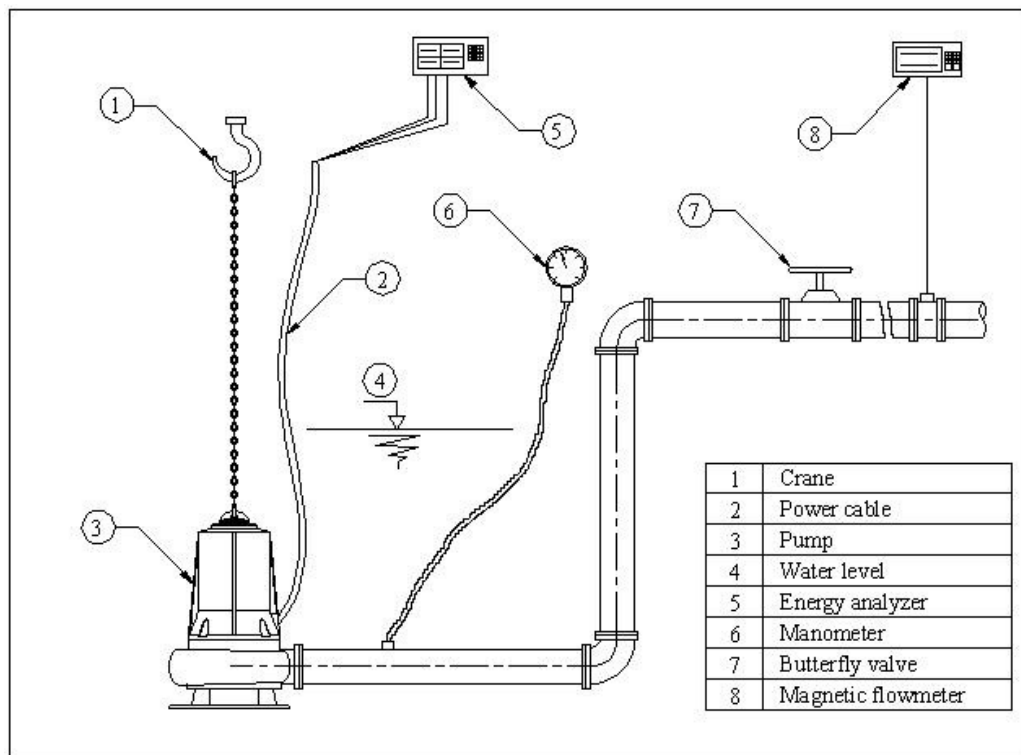


Figure 4.4 – Test setup-2

In the second test setup, the final form of the pump, having both the motor and the hydraulic components together in the same compact structure, is submerged into the

pool and connected to the discharge pipe (Figure 4.4). Except the power transmission system from the motor to the hydraulic components, the setup is the same as the previous one.

Obviously, the mechanical loss in the test setup-1 is higher when compared with test setup-2. In this manner, the pump performances obtained from the tests that are performed by using the first test setup are not quantitatively valuable. For this reason, in the discussions regarding the pump performance concept, these test results are used only for comparing purposes. Also, since the power transmission mechanisms are totally different, these tests do not give an idea about the problems that can occur in the actual case. Because, even though there are nonclog pumps having a working mechanism like the one used in test setup-1, the target product was decided to be a submersible pump. Still, there are some reasons for using such a test setup instead of testing the actual product.

Firstly, using test setup-1, different pumps of different sizes are tested with the same structure, same electric motor and same conditions that make hydraulic comparison among these pumps possible. Due to the easiness of coupling the hydraulic part to the testing system, the tests can be performed very quickly.

The second advantage of test setup-1 is that, standard VHS electric motor can be employed to drive the pump. Designing and manufacturing the motors of the submersible pumps are beyond the scope of this study. Therefore, using the main dimensions of a suitable V1 (norm) electric motor, special motors are ordered from a motor manufacturer to be used in the casings that are designed and manufactured specifically for these pumps, as stated in Chapter 2. However, ordering a special motor for a new pump, whose exact power consumption characteristic cannot be known, is not a preferable case due to economical reasons. Moreover, manufacturing a special motor, especially for the first time, requires more time when compared with the standard production. In this frame, driving the pumps, that

are newly being developed, by a standard VHS electric motor reduces the time required to finish the study.

Finally, using a test setup that enables the pump to be driven by a VHS electric motor, the problems regarding to submersible working of the electric motor are eliminated for the hydraulic development stage, due to the dry installation of the motor. Therefore, studying solely on the hydraulic characteristics of the pumps became possible by using test setup-1.

Once the hydraulic performance of the pump was tested and the required changes were made, submersible pump, being the actual product, is tested in order to investigate any possible leakage or mechanical problems.

In both setups used, the exit of the pump is connected to the discharge pipe. Exit pressure of the pump is measured on the discharge pipe by a manometer, whose range is suitable for the pressure reading. The length of the straight pipe portion between the pump exit and pressure reading location is set to be more than 2 times the nominal diameter of the pipe, as it is stated in the related standard [26]. The flowmeter is placed on the discharge pipe at such a location that, there are straight pipe portions free of any obstacles for the flow, like elbows, valves etc., at the upstream and downstream of the flowmeter, having lengths of at least 5 and 3 times the nominal diameter of it, respectively (Figure 4.1). These straight pipes are required for having a uniform flow through the flowmeter and correct measurement. Since the flowmeter can only be used in full line flow, a gooseneck is placed at the end of the pipe. The water that exits the discharge pipe is directed back to the pool that the pump is submerged in, with an inclination of 6 %. Since not only the hydraulic, but also performance characteristics of the pump is dealt, the electrical variables are measured by the energy analyser. In this way, wire to water efficiency of the pump can be calculated, as it is explained below.

4.3 Test Procedure and Calculations

Procedure followed in the pump performance tests and calculations made with the data collected during the tests are given below.

4.3.1 Test Procedure

During the pump tests performed in the content of this study, the procedure given below is followed.

1. The pump is assembled and prepared for the test. If a special problem on the pump is to be observed, the required preparation is made, like painting the close surfaces of impeller, volute and suction flange, while observing a possible rubbing problem.
2. If the pump is to be driven by VHS electric motor, test setup-1 is assembled and the column pipe is filled with water.
3. The motor is connected to the electric panel whose capacity limits are suitable for the expected power consumption of the test system.
4. If the submersible pump is to be tested, direction of rotation is checked by starting and stopping the pump instantaneously before submerging it. If required, the electrical connections are reversed in the sense of phase sequences in order to reverse the direction of rotation.
5. The pump is submerged to the pool and connected to the discharge pipe.
6. Suitable manometer and flowmeter are chosen according to the maximum expected head and flow rate of the pump, respectively. The chosen manometer is connected to the discharge pipe. Required vane adjustments

are made in order to direct the flow through the collector pipe to the chosen flowmeter.

7. If the pump is to be driven by VHS electric motor, direction of rotation is checked as it is stated in step 4. For tests that are performed using setup-2, direction of rotation can be checked after submerging the pump, since the headshaft is in sight providing the determination of direction of rotation by eye. In this way, the mechanical seal pair is protected from dry working, which may cause in failure of these parts.
8. The pump is started. If frequency converter is used in order to operate the pump at a speed other than standard motor speeds, the frequency is adjusted and the working speed is recorded.
9. Nominal discharge pipe diameter at pressure reading location is recorded.
10. For a number of data points that is sufficient to inspect the hydraulic and power consumption characteristics of the pump, following data recording procedure is repeated: Exit pressure of the pump is fixed to the desired value by adjusting the butterfly valve. No reading is taken for a while that is sufficient for the system to reach equilibrium. The flow rate that pump delivers and the power given to the electric motor are recorded. Vertical distance between the manometer and the water surface is measured.
11. The pump is stopped.

4.3.2 Processing the Test Data and Calculations

Data obtained from the test results are processed and used in the calculations in the following manner to obtain informative results on the characteristics of the pumps tested.

As it is stated above in the introduction of test stand, all the measuring devices used in pump tests are periodically being calibrated by authorized institutions. Using the calibration results that are stated in calibration reports, a formula, which has the data read as input variable and gives the corresponding real value as output, is driven for each instrument used for data measurement during the pump test. Each recorded data is subjected to the calibration formula of the measuring instrument. Then the calculations are made as it is stated in the regarding standard [26], as follows.

In order to find the total head of the pump tested, firstly, the fluid velocity at the pressure reading location is calculated. This is made simply by dividing the flow rate by the cross-sectional area. The cross-sectional area is calculated by using the nominal diameter of the discharge pipe that was recorded during the test. In order to calculate the total head of the pump, vertical distance between the manometer and the water level, which was measured during the test, is added on the dynamic head at the discharge pipe. The distance added is the sum of two vertical distances; from water level to the pressure reading location and from this point to the manometer level. The preceding one came from the Bernoulli equation that is written on the streamline from the water level, where the velocity is assumed to be zero, to the discharge pipe. The latter one is added due to the pressure difference between the top and bottom ends of the water column in the hose, connecting manometer to the discharge pipe, Figures 4.2 and 4.4. Then the variation of the total pump head with changing flow rate is drawn on the graph in order to inspect the hydraulic characteristic of the pump tested.

The electrical power that is measured by the energy analyser is the total power given to the test system, including electrical losses through the wire, in the frequency converter if used, in the electric motor, and mechanical losses in the electric motor, through the power transmission system and the power that pump consumes during operation. Therefore, efficiency calculated by using the measured power represents the total efficiency of the test system, not that of the pump.

To calculate the system efficiency, the output of the system, being the hydraulic output of the pump, is divided by the input of the system, being the power measured. In order to calculate pump efficiency, the total efficiency of the system is to be divided by the efficiencies of the remaining units in the system. The electrical loss in the wire is neglected due to the usage of a short wire that has a rather large cross-sectional area and as a result having a wire loss that is not even comparable with the uncertainty of the test system. If the frequency converter was used in the test, its efficiency, which is a function of the output frequency of the instrument, is found by using the technical data taken from the manufacturer. Dividing the system efficiency with frequency converter efficiency, the instrument is taken out of consideration. If the test was performed by using test setup-1, the efficiency values of VHS type electric motor, which depend on the loading of the motor, are taken from the manufacturer's catalogue [27] and used to calculate the efficiency of the pump together with the power transmission system, being the column assembly. Since the same column assembly is used in the tests performed by using setup-1, the calculated efficiency is informative in the sense of comparison only. However, being the final product, submersible pump tests are different. Since both the wire and the motor are parts of the product, their losses are not taken into consideration and the measured power is used in the efficiency calculations.

The pump tests performed in the content of this study satisfy the limits of class – 2 experiments given in the related standard, [26], with respect to the uncertainty in measurements. A sample calculation of uncertainty for a submersible pump test is given in Appendix B.

CHAPTER 5

RESULTS AND CONCLUSION

In this thesis, a nonclog type submersible sewage pump is designed and manufactured in Layne Bowler Pump Company Inc. Also, CFD analyses of the designed pump and a nonclog type sewage pump of Layne Bowler are made. Both pumps are tested and the comparison of results of actual tests and CFD analyses are given below. Moreover, a similitude analysis of the designed pump based on the rotational speed is made and the results are discussed in the following part. Conclusions drawn during the study are also mentioned in this chapter.

Being special duty pumps, design procedure of nonclog type submersible pumps differs from the standard centrifugal pump design methods. However, the design methodologies of nonclog pumps are mostly developed by the manufacturer firms and a recommended procedure on nonclog pump design is not encountered in the literature.

A nonclog pump, which can deliver 100 l/s against a head of 24 m with a rotational speed of 1000 rpm and capable of handling solid particles up to a diameter of 80 mm, is aimed to be designed in this study. The design procedure followed is given in Chapter 2 together with the important considerations that differ nonclog pump design from the standard centrifugal pump design methods.

The maximum diameter of solid particles to be handled is a design parameter for nonclog pumps. Determination of impeller breadth and number of blades mainly depend on the purpose of maximization of the passage areas instead of hydraulic purposes. On this basis, the formula used for checking the assumed value of blade number in Reference [9] may not be considered as an indispensable approach.

The semi-empirical formula given for Pfleiderer's correction factor check in Reference [9] does not hold for the designed nonclog pump, since the convergence of the assumed and calculated values of C_p can only be achieved for an impeller diameter, several times larger than the one used in the pump. The slip factor approach given in Reference [28] is also not applicable for the pump designed, since the head and efficiency values of the pump that are obtained by the performance test, does not agree with the ones calculated by using the given formulas. Therefore, making a good estimation of C_p , based on the experiences on previous designs may be an important advantage in the design of nonclog pumps.

Depending on the diameter of the solid particles to be handled by the pump, areas of the volute cross-sections may be increased. In such cases, having a small angle of divergence may be useful to avoid excessive volute heights.

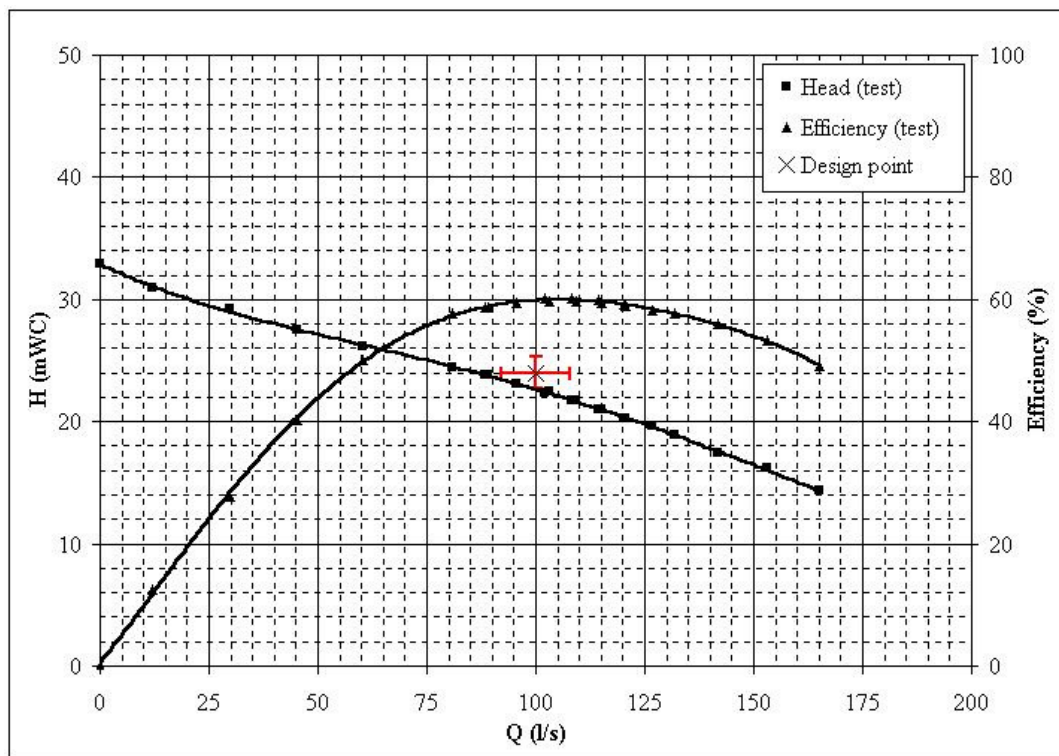


Figure 5.1 – Head versus flow rate and efficiency versus flow rate curves that are obtained by testing the designed nonclog type submersible sewage pump

Head versus flow rate and efficiency versus flow rate curves that are obtained by testing the designed nonclog type submersible sewage pump are given together with the design point in Figure 5.1.

As it is stated in Chapter 2, both the impeller outlet area and throat area of the designed nonclog pump are enlarged with respect to a standard centrifugal pump, in order to satisfy the required passage area throughout the pump. However, the enlargement of impeller outlet area is more than the enlargement of throat area. Therefore, defining a variable as “area ratio”, [29], being outlet area of the impeller divided by throat area, the pump can be said to have a high area ratio with respect to standard centrifugal pumps. For a pump having backward curved impeller blades, a high area ratio results in high head and flow coefficients with a small inclination on the head versus flow rate curve, [29]. Also, the head versus flow rate characteristics of the nonclog type sewage pumps in the market are observed to be almost linear in the catalogues of the manufacturers, [3], [7] and [8]. In this frame, the head characteristic of the designed pump is found to be in agreement with the expectations. On the other hand, the efficiency characteristic of a pump having a high area ratio is given to be wider on the flow rate axis in Reference [29]. Considering this, the efficiency characteristic of the designed submersible pump is found to be in the expected form.

Head versus flow rate curve of the designed submersible pump is found to be passing below the design point as it can be seen in Figure 5.1. Also, the best efficiency point of the pump corresponds to a higher flow rate than the design value. However, the deviation of the head characteristic from the design point lies within the limits determined by the related standard, [26], for class – 2 acceptance tolerances, being $\pm 8\%$ in flow rate and $\pm 5\%$ in head. The cross, indicating the tolerance band corresponding to design point is also shown in Figure 5.1.

Although efficiency of a sewage pump is not a primary consideration for rating the satisfaction of the design, a submersible pump efficiency of 60 % can be introduced to be good in the respect of competing with the alternatives in the market.

Comparison of results of the performance test and CFD analysis for case 1 is given in Figure 5.2. In order to make a comparison between the results of actual and numerical experiments, the values of motor, mechanical and volumetric efficiencies has to be estimated. Using the value given in manufacturers catalogue, [19], the motor efficiency is assumed to be 90%. The mechanical efficiency is assumed to be 94% due to usage of two mechanical seal pairs together with one ball and one roller bearing to support the shaft. Also, an estimation of volumetric efficiency, being 93% is made, since, the gaps between the sealing surfaces of impeller, volute and suction flange are closed in this solution for the sake of simplicity. Therefore, the efficiency curve given in Figure 5.2 refers to the hydraulic efficiency of the pump.

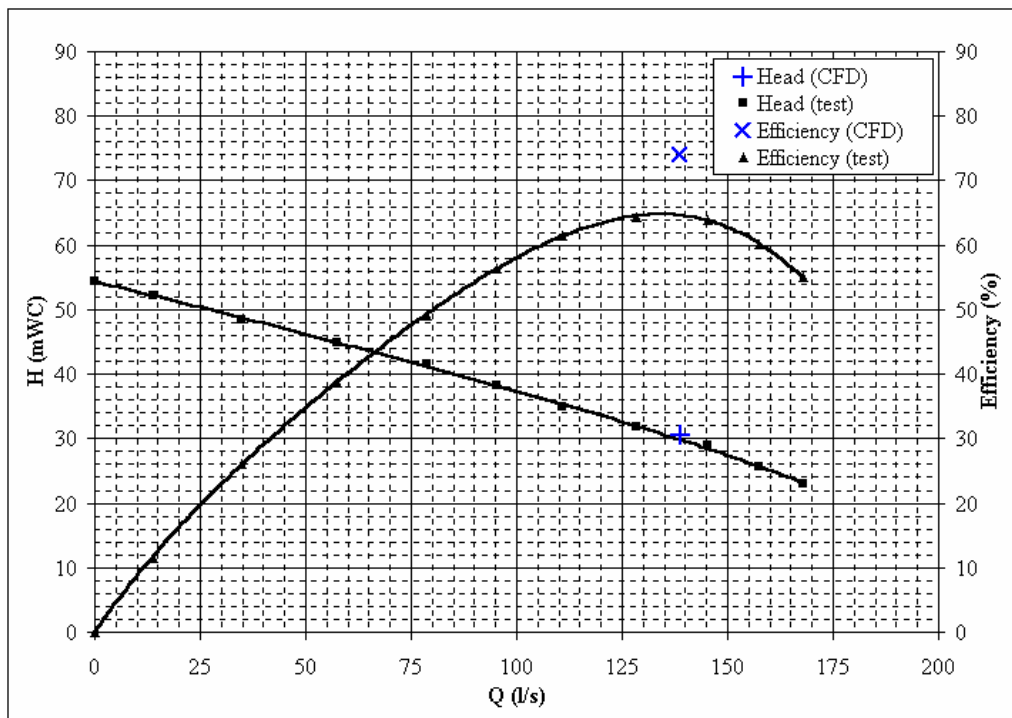


Figure 5.2 – Comparison of results of the performance test and CFD analysis for case 1

On the basis of these estimations, the resultant operating point of case 1 obtained by the CFD analysis can be said to be in agreement with the head characteristic of the pump, which is obtained by the performance test. However, the efficiency calculated for the same operating point is approximately 9% higher than the efficiency obtained by testing the pump. It is difficult to explain such a high deviation by wrong estimations of the efficiency values. In this frame, the encountered deviation may be related to a possible miscalculation of torque by the solver.

Figure 5.3 shows the comparison of pump characteristic curves obtained by performance test and CFD analysis of case 2. Similar to the comparison made for case 1, motor and mechanical efficiencies are estimated for case 2. However, since the gaps between the sealing surfaces of impeller, volute and suction flange are not closed in the CFD analysis of case 2, the results of the actual and numerical experiments are comparable with each other in the sense of volumetric efficiency. The estimation of motor efficiency, being 92%, is based on the value given in manufacturers catalogue, [19]. Due to the similarity of mechanical structures used in submersible pumps of case 1 and case 2 analyses, the value of mechanical efficiency for case 2 is estimated to be the same with the one estimated in case 1, being 94%. In this frame, the efficiency curves given in Figure 5.3 stand for combined efficiency characteristics of hydraulic and volumetric efficiencies.

As it can be seen in Figure 5.3, the head versus flow rate curve found by the CFD analysis of case 2, is in a close agreement with the curve obtained by testing the pump in the majority of characteristic curve including the best efficiency point. Therefore, results of the CFD analysis can be described as highly reliable in the sense of head characteristic for case 2. Coming to the efficiency curves, the calculated best efficiency point lies on a flow rate value approximately 10% higher than the one found by testing the pump. Also, similar to case 1, the calculated efficiency values are found to be approximately 4% higher than the measured values. This deviation points out a probable miscalculation of torque by the solver,

once more. Nevertheless, both efficiency curves resembles the same characteristic with a preserved shift in between, up to the flow rate value that the head characteristic curves start to separate from each other.

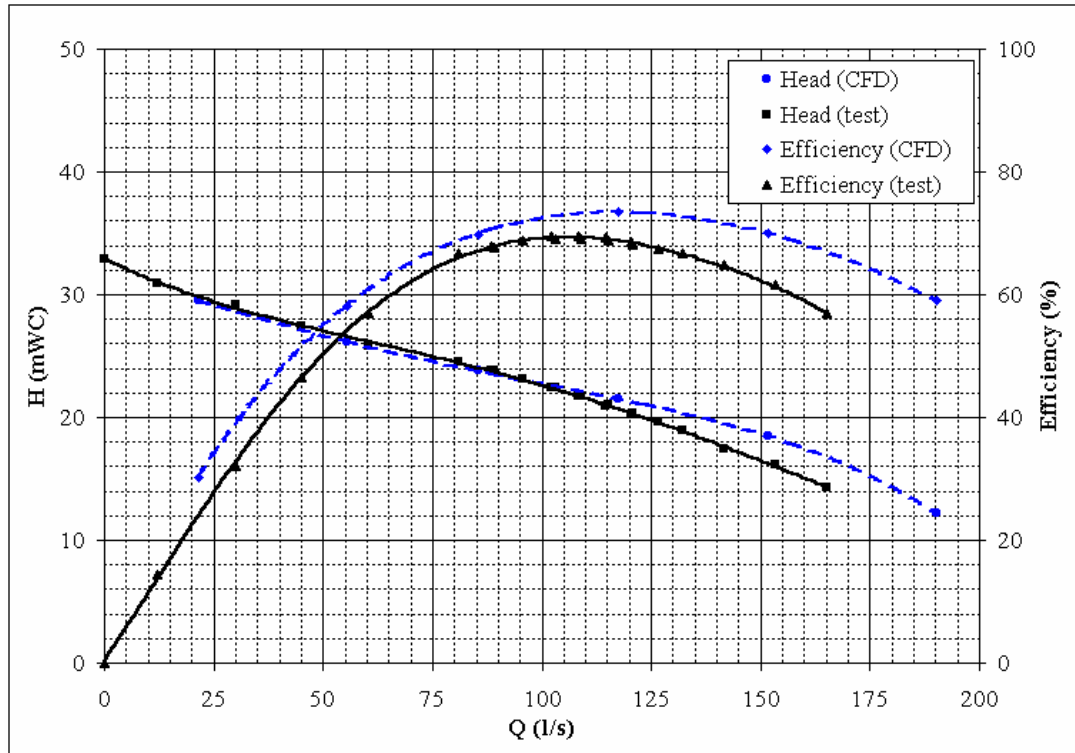


Figure 5.3 – Comparison of pump characteristic curves obtained by performance test and CFD analysis of case 2

In the presence of discussions on the results of CFD analyses mentioned above, numerical experimentation of nonclog pumps can be described as a quite useful tool to predict the characteristic curves or possible problems to occur in the pump without manufacturing the pump. However, the conclusions to be drawn from the results of the CFD analyses are strongly dependent on the experience of numerical experimentation, which assigns verification of CFD analysis results with actual tests as compulsory.

Rotational speed of the designed nonclog type submersible sewage pump is 1000 rpm. However, the pump is also driven by frequency converter at 750 rpm in order to investigate similitude based on the rotational speed. Then, the theoretical head characteristic of the pump at 750 rpm is calculated from the test results obtained at rotational speed of 1000 rpm using the formulas of similarity. Figure 5.4 shows both the measured and calculated head characteristics of the designed pump for 750 rpm of rotational speed.

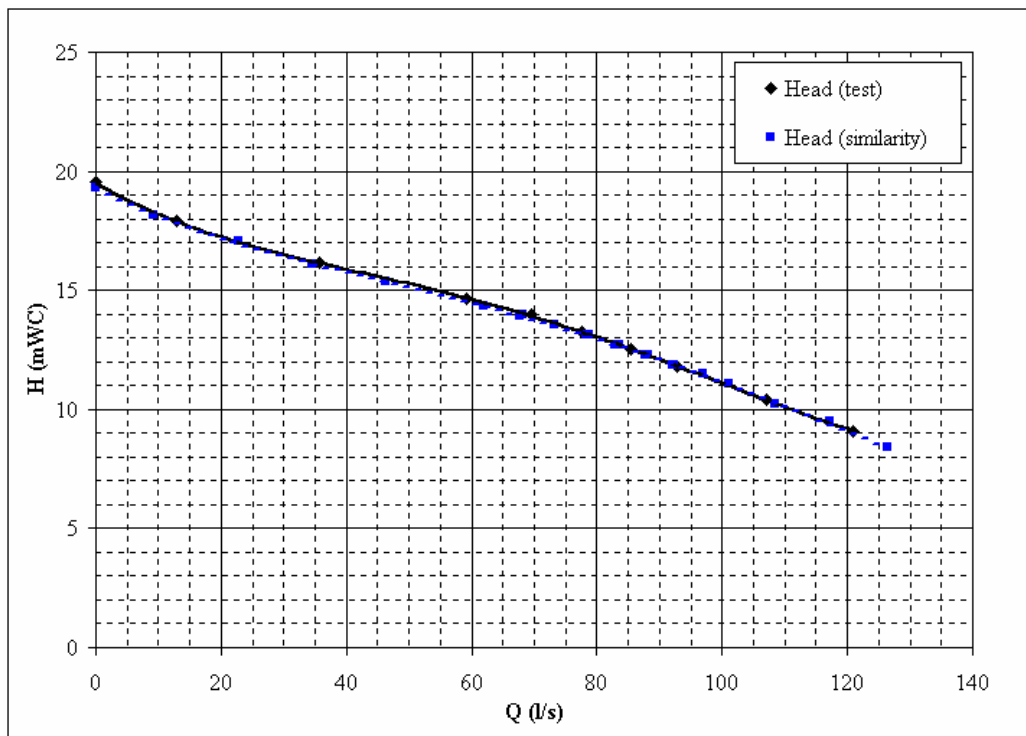


Figure 5.4 – Comparison of head versus flow rate curves of the designed pump that are obtained by performance test and similarity formulas at a rotational speed of 750 rpm

Head versus flow rate curves of the designed pump that are obtained by performance test and similarity formulas at a rotational speed of 750 rpm are found to be matching each other.

In conclusion, despite the significant demand on nonclog type submersible sewage pumps, a design methodology for these pumps is not encountered in the literature. Therefore, the manufacturers tend to develop their own empirical based methodologies. On the other hand, numerical experimentations, being useful tools in pump development, require verification with actual test results. In this frame, design and development of the nonclog type sewage pumps are mainly dependent on experience and know-how.

REFERENCES

1. Jon Schladweiler, Arizona Water & Pollution Control Association (2005) [On-line]: <http://www.sewerhistory.org/articles/compon/pumps.htm>
2. Centrifugal Pump Lexicon (1990) KSB, Germany.
3. General Catalogue (2003) Faggiolati Pumps S.p.A., Italy.
4. Technical Brochure 50 Hz. Flygt Submersible Pumps, Mixers and Hydroturbine Generators, ITT Flygt, Sweden.
5. Carter, R., Karassik, I. J. and Wright, E. F. (1949) Pump Questions and Answers, McGraw – Hill Book Co., New York.
6. Cronin, R. J., House D. A. and Miller A. C. (2004) “Design Considerations for Nonclog Pumps”, Proceedings of the Twenty-First International Pump Users Symposium, pp. 116-128.
7. Sewlayn Dalgıç Atık Su Pompası Katalođu (2004) Layne Bowler Pompa Sanayi ve Ticaret A. Ş., Ankara.
8. Small and Mid-Range Submersible Sewage Pumps Catalogue, ITT Flygt, Sweden.
9. Lazarkiewicz, S. and Troskolanski, A. T. (1965) Impeller Pumps, Pergamon Press Ltd., Oxford.
10. Üçer, A. Ş. (1982) Turbomachinery, Class Notes (ME – METU), Ankara.
11. Spring, H. (1996) Pump Design Code Manual.
12. Döner Rijit Elemanların Balans Niteliđi, TS 2576 (1977) Türk Standardları Enstitüsü, Ankara.
13. Lobanoff, V. S. and Ross, R. R. (1992) Centrifugal Pumps – Design and Application, Gulf Publishing Co., Houston.
14. Kreila 4.0 Program Help Document.
15. Kasai, T. (1966) “Hydraulic Design of Centrifugal Pump Impellers Based on the Specific Speed”, Pump Design Testing and Operation, Her Majesty’s Stationery Office, Edinburg, pp. 51-60.

16. Stepanoff, A. J. (1957) Flow Pumps Design, and Application, John Wiley & Sons Inc., U.S.A.
17. Pompalar – Dalgıç – Pis Su İçin, TS 12599 (1999) Türk Standardları Enstitüsü, Ankara.
18. Shigley, J. E. and Mischke, C.R. (2001) Mechanical Engineering Design, McGraw – Hill Book Co., Singapore.
19. Norm Elektrik Motorları (Tip NM) Kataloğu (2005) Elsan Elektrik San. ve Tic. A. Ş., Ankara.
20. Ball Bearings, Roller Bearings, Housings, Accessories Catalogue (1999) FAG Rolling Bearings, Germany.
21. Promak Mekanik Salmastraları – 5 Kataloğu (2005) İstanbul.
22. O’ring – Nutring – Packing Hidrolik Sızdırmazlık Elemanları Kataloğu, Cayak Lastik ve Plastik San. ve Tic. A. Ş., İstanbul.
23. Beer, F. P. and Johnston, Jr. E. R. (1985) Mechanics of Materials, McGraw – Hill Book Co., Singapore.
24. Reference Manual cfdesign Technical Reference Version 7.0 (2004) Blue Ridge Numerics, Inc., Charlottesville.
25. cfdesign User’s Guide Version 7.0 (2004) Blue Ridge Numerics, Inc., Charlottesville.
26. Rotodinamik Pompalar – Hidrolik Performans Kabul Deneyleri – Sınıf 1 ve Sınıf 2, TS EN ISO 9906 (2002) Türk Standardları Enstitüsü, Ankara.
27. Dik Delik Milli Derin Kuyu Pompa Motorları (VHS) Kataloğu (2005) Elsan Elektrik San. ve Tic. A. Ş., Ankara.
28. Tuzson J., (2000) Centrifugal Pump Design, John Wiley & Sons Inc., Canada.
29. Anderson, H. H. (1986) Submersible Pumps and Their Applications, The Trade & Technical Press Limited, England.

APPENDIX A

SAMPLE PATTERN, CORE BOX, CORE AND CAST PART PHOTOGRAPHS OF THE SUBMERSIBLE PUMP



Figure A.1 – Photograph of impeller pattern



Figure A.2 – Photograph of volute core box



Figure A.3 – Photograph of volute core



Figure A.4 – Photograph of volute pattern



Figure A.5 – Photograph of motor core box



Figure A.6 – Photograph of motor pattern



Figure A.7 – Photograph of top cover pattern



Figure A.8 – Photograph of oil case cover pattern



Figure A.9 – Photograph of base pattern



Figure A.10 – Photograph of impeller before machining



Figure A.11 – Photograph of volute before machining



Figure A.12 – Photograph of motor case before machining

APPENDIX B

SAMPLE UNCERTAINTY CALCULATION

The uncertainty analyses of the submersible pump tests performed in this study are based on the regarding standard, being TS EN ISO 9906, [26]. A sample of the calculations made is given below.

The minimum number of readings to be taken for an operating point is given as 3, in the regarding standard, [26]. Therefore, 5 sets of readings are taken for each operating point, during the test. The following calculations are made for the best efficiency point of the submersible pump. The readings taken are given below:

Table B.1 – Test data for the best efficiency point

Reading Number	H _m (m)	Q (l/s)	H _{dyn} (m)	P (kW)
1	17.90	102.9	2.806	37.76
2	17.95	102.9	2.805	37.52
3	17.90	102.8	2.810	37.78
4	17.85	102.7	2.808	37.68
5	17.90	102.9	2.805	37.76

The total uncertainty of a measurement, U_T , is composed of random and systematic uncertainties, U_R and U_S respectively; and can be calculated as, [26]:

$$U_T = \sqrt{U_R^2 + U_S^2} \quad (\text{B.1})$$

Random uncertainty of a measurement is defined to be two times the standard deviation of it, in the regarding standard, [26]. Therefore, to obtain random uncertainty of each measurement, firstly, their standard deviations, s , are calculated:

$$s = \sqrt{\frac{(x_1 - \bar{x})^2 + (x_2 - \bar{x})^2 + \dots + (x_n - \bar{x})^2}{n}} \quad (\text{B.2})$$

Where, x_1, x_2, \dots, x_n being values, \bar{x} being average and n being number of the readings. In this respect, random uncertainty values for each reading are calculated and tabulated in Table B.2:

Table B.2 – Values of random uncertainty for each reading

H_m (%)	Q (%)	H_{dyn} (%)	P (%)
0.36	0.16	0.14	0.51

Systematic uncertainty depends on the sensitivity of instrument or the method used for measuring, and can not be reduced by repeating the measurements, [26]. Using the calibration reports of the measuring instruments, the systematic uncertainties of each measurement are found as follows:

Table B.3 – Values of systematic uncertainty for each reading

H_m (%)	Q (%)	H_{dyn} (%)	P (%)
2.85	0.70	0.01	1.33

Knowing the random and systematic uncertainty values for each reading, the total uncertainties are calculated using Equation (B.1) and tabulated below:

Table B.4 – Values of total uncertainty for each reading

H _m (%)	Q (%)	H _{dyn} (%)	P (%)
2.87	0.72	0.14	1.42

The total head of the submersible pump, H_t, is calculated using the formula:

$$H_t = H_m + H_{dyn} + \frac{v_{pf}^2}{2g} \quad (B.4)$$

Where, H_m is the manometric head and H_{dyn} is the dynamic water level, designating the vertical distance between the manometer level and water level while the pump is operating. The term g is used for gravitational acceleration and v_{pf} is the velocity of pumped fluid at the outlet pipe cross-section, where pressure reading is taken. Variable v_{pf} is calculated as follows:

$$v_{pf} = \frac{Q}{A_{op}} \quad (B.5)$$

The term A_{op} in Equation (B.5) designates the cross-sectional area of the outlet pipe at the pressure reading location. Cross-sectional area corresponding to nominal diameter of the outlet pipe is 0.018 m². Then, the total uncertainty of v_{pf}, U_{T_vpf}, is calculated using the formula below:

$$U_{T_vpf} = \frac{1}{A_{op}} \cdot U_{T_Q} \quad (B.6)$$

Where U_{T_Q} designates the total uncertainty of flow rate. Substituting the values into Equation (B.6):

$$U_{T_{v_{pf}}} = \frac{1}{0.018} \times 0.0007$$

$$U_{T_{v_{pf}}} = \pm 0.04 \text{ m/s}$$

Dividing the result by the nominal value of v_{pf} total uncertainty of the velocity of pumping fluid is found to be 0.72 %. The total uncertainty of total head, $U_{T_{H_t}}$, is then calculated by the formula:

$$U_{T_{H_t}} = \sqrt{U_{T_{H_m}}^2 + U_{T_{H_{dyn}}}^2 + \left(\frac{V_{pf}}{g} \cdot U_{T_{v_{pf}}}\right)^2} \quad (\text{B.7})$$

Substituting the absolute values of total uncertainties into Equation (B.7):

$$U_{T_{H_t}} = \sqrt{0.51^2 + 0.004^2 + \left(\frac{5.82}{9.81} \times 0.04\right)^2}$$

$$U_{T_{H_t}} = \pm 0.51 \text{ m}$$

Dividing the result by the nominal value of H_t , total uncertainty of the total head is found to be 2.29 %.

The wire to water efficiency of the submersible pump, η_{sp} , is calculated using the formula:

$$\eta_{sp} = \frac{\rho g Q H_t}{P} \quad (\text{B.8})$$

The total uncertainty values of all variables, except the density of the pumping fluid, ρ , in Equation (B.8) are determined. The density of the pumping fluid is assumed to be constant throughout the pumping process. Then, the density is obtained by simply dividing the mass of an amount of pumping fluid, whose volume is measured by a graded cylinder:

$$\rho = \frac{m}{V} \quad (\text{B.9})$$

A volume, V , of 1 ± 0.01 litre of pumping fluid is measured to have a mass, m , of 1 ± 0.0025 kg. On this basis, the total uncertainty of fluid density, $U_{T-\rho}$, is calculated using the formula below:

$$U_{T-\rho} = \sqrt{\left(\frac{1}{V} \cdot U_{T-m}\right)^2 + (m U_{T-V})^2} \quad (\text{B.10})$$

Substituting the values into Equation (B.10):

$$U_{T-\rho} = \sqrt{\left(\frac{1}{1 \times 10^{-3}} \times 2.5 \times 10^{-3}\right)^2 + (1 \times 1 \times 10^{-5})^2}$$

$$U_{T-\rho} = \pm 2.5 \text{ kg/m}^3$$

This value corresponds to $\pm 0.25\%$ of uncertainty in density of the pumping fluid. Efficiency formula for the tested submersible pump is given in Equation (B.8). Using this formula, Equation (B.11) is derived in order to calculate the total uncertainty of the submersible pump efficiency, $U_{T-\eta_{sp}}$, [26]:

$$U_{T-\eta_{sp}} = \left[\left(\frac{gQH_t}{P} \cdot U_{T-\rho} \right)^2 + \left(\frac{\rho g H_t}{P} \cdot U_{T-Q} \right)^2 + \left(\frac{\rho g Q}{P} \cdot U_{T-H_t} \right)^2 + \left(-\frac{\rho g Q H_t}{P^2} \cdot U_{T-P} \right)^2 \right]^{1/2} \quad (\text{B.11})$$

Substituting the values into Equation (B.11):

$$U_{T-\eta_{sp}} = \left[\left(\frac{9.81 \times 0.1028 \times 22.43}{37700} \times 2.5 \right)^2 + \left(\frac{1000 \times 9.81 \times 22.43}{37700} \times 0.0007 \right)^2 + \left(\frac{1000 \times 9.81 \times 0.1028}{37700} \times 0.51 \right)^2 + \left(-\frac{1000 \times 9.81 \times 0.1028 \times 22.43}{37700^2} \times 0.54 \right)^2 \right]^{1/2}$$

$$U_{T-\eta_{sp}} = \pm 1.45 \%$$

As it can be seen on Table B.5, the total uncertainties of measured and calculated variables for this sample test point, satisfy the limitations for class-2 experiments given in the regarding standard, [26]:

Table B.5 – Comparison of total uncertainty percentages and their limits in the regarding standard, [26]

Parameters	Class – 1 Limits	Class – 2 Limits	Calculated Uncertainties
Flow Rate, Q (%)	± 2.0	± 3.5	± 0.72
Total Head, H _t (%)	± 1.5	± 5.5	± 2.29
Power (given to the system), P (%)	± 1.5	± 5.5	± 1.42
Efficiency, η _{sp} (%)	± 2.9	± 6.1	± 2.42